DEVELOPMENT OF MAGNETIC SECTOR MASS SPECTROMETERS FOR ISOTOPIC RATIO ANALYSIS

By
R.K.BHATIA
PHYS01201204015

Bhabha Atomic Research Centre, Mumbai

A thesis submitted to the
Board of Studies in Physical Sciences
In partial fulfillment of requirements
for the Degree of

DOCTOR OF PHILOSOPHY

of

HOMI BHABHA NATIONAL INSTITUTE

September, 2015

Homi Bhabha National Institute[1]

Recommendations of the Viva Voce Committee

As members of the Viva Voce Committee, we certify that we have read the dissertation prepared by R.K.BHATIA entitled "Development of Mass spectrometers for isotopic ratio analysis" and recommend that it may be accepted as fulfilling the thesis requirement for the award of Degree of Doctor of Philosophy.

Chairman – Dr. N.K.Sahoo		**Date:** 6/6/2016
Guide / Convener – Dr. S.K.Gupta		**Date:** 6/6/2016
Co-guide - Dr. S.C.Gadkari		**Date:** 06/06/2016
Examiner – Dr. Kanchan Pande	Kanchan Pande	**Date:** 06/06/2016
Member 1- Dr. M.V.Suryanarayana		**Date:** 06/06/2016
Member 2- Dr. K.G.Bhushan	KGBhushan	**Date:** 06/06/2016

Final approval and acceptance of this thesis is contingent upon the candidate's submission of the final copies of the thesis to HBNI.

I/We hereby certify that I/we have read this thesis prepared under my/our direction and recommend that it may be accepted as fulfilling the thesis requirement.

Date: 6/6/2016

Place: Mumbai

Co-guide **Guide**

---

[1] This page is to be included only for final submission after successful completion of viva voce.

STATEMENT BY AUTHOR

This dissertation has been submitted in partial fulfillment of requirements for an advanced degree at Homi Bhabha National Institute (HBNI) and is deposited in the Library to be made available to borrowers under rules of the HBNI.

Brief quotations from this dissertation are allowable without special permission, provided that accurate acknowledgement of source is made. Requests for permission for extended quotation from or reproduction of this manuscript in whole or in part may be granted by the Competent Authority of HBNI when in his or her judgment the proposed use of the material is in the interests of scholarship. In all other instances, however, permission must be obtained from the author.

R.K.BHATIA

DECLARATION

I, hereby declare that the investigation presented in the thesis has been carried out by me. The work is original and has not been submitted earlier as a whole or in part for a degree / diploma at this or any other Institution / University.

R.K.BHATIA

List of Publications arising from the thesis

Journal

1. "Rotation of focal plane of magnetic analyzer in an isotope ratio mass spectrometer using curved shims", Rajender K. Bhatia, Yogesh Kumar, K.Prathap Reddy, V.K.Yadav, E.Ravisankar, T.K.Saha, V.Nataraju, V.K.Handu, *International Journal of Mass Spectrometry*, **2012**, *313*, 36-40.

2. "A Novel Variable dispersion zoom optics for isotope ratio sector field mass spectrometer", Rajender K. Bhatia, Varun K.Yadav, Vilas M. Mahadeshwar, Milind M. Gulhane, E.Ravisankar, T.K.Saha, V.Nataraju, S.K.Gupta, *International Journal of Mass Spectrometry,* **2013***, 339-340,* 39-44

3. "Improved Faraday collector for magnetic sector mass spectrometers", Rajender K. Bhatia, Varun K.Yadav, Yogesh Kumar, Babu R. Gonde, E.Ravisankar, T.K.Saha, V.Nataraju and S.K.Gupta, *International Journal of Mass Spectrometry,* **2015***, 393,* 58-62

Conferences

1. "Development of a Novel Variable Dispersion Zoom Optics for Magnetic Sector Mass Spectrometer" Rajender K Bhatia, Varun K. Yadav, Vilas M Mahadeshwar, Milind M Gulhane, E.Ravisankar, T.K.Saha, V.Nataraju and S.K.Gupta, *12th ISMAS TRICON*, **2013**, 206-207

2. "Experiments on a new Faraday cup design in an in-house built magnetic sector mass spectrometer" R.K.Bhatia, Yogesh Kumar, Varun K Yadav, Rabi Datta, E Ravisankar, T.K.Saha and V. Nataraju, *28th ISMAS-WS*, **2014**, 224-227

3. “Studies on design modifications in a Thermal ionization source for improved sensitivity**”** Arkadip Bhasak, R.K.Bhatia, Varun K Yadav, Madhavi Sharma, Yogesh Kumar, E.Ravisankar and V.Nataraju , *28th ISMAS-WS*, **2014**, 161-165

4. “An electron impact ion source as a switch-over option for TIMS**”** R.K.Bhatia, Babu R Gonde, V.K.Yadav, M.M.Gulhane, E.Ravisankar, T.K.Saha and V.Nataraju, *29th ISMAS international symposium on mass spectrometry*, **2015**, 158-159

Others

1. “Development of TIMS for isotopic ratio analysis of Boron**”** R.K.Bhatia, V.K.Yadav, M.M.Gulhane, Rabi Datta, K.D.Joshi, A.M.Kasbekar, Madhavei Sharma, Meera Murali, M.M.Vilas, E.Ravisankar, M.Gopalakrishna, T.K.Saha, V.Nataraju and S.K.Gupta, *BARC Newsletter*, **2013**, *332*, 19-24

2. “Performance evaluation of indigenous Thermal Ionization Mass Spectrometer for determination of $^{235}U/^{238}U$ atom ratios**”** D.Alamelu, A.R.Parab, K.SasiBhushan, Raju V.Shah, S.Jagdish Kumar, Radhika M.Rao, S.K.Aggarwal, R.K.Bhatia, V.K.Yadav, Madhavi P.Shrma, Puneet Tulsyan, Pradip Chavda, P.Sriniwasan, *BARC Report No. BARC/2014/E/004*, **2014**

R.K.BHATIA

Dedicated to

MY PARENTS

POOJA

KRITI & KARTIK

ACKNOWLEDGEMENTS

At the outset I thank my research guide Dr. S.K.Gupta, Head, Technical Physics Division (TPD) and Associate Director, Physics Group for encouraging me to undertake this research work. I express my sincere gratitude to him for his valuable guidance and support all through. I would like to extend my heartfelt gratitude to Sh. V. Nataraju, Head, Advanced Mass spectrometry Section, TPD for his co-operation and constant support at every stage of my PhD work. I would like to thank Sh. V. K. Handu (former Head, TPD) for showing confidence in me and giving me the opportunity to work for the mass spectrometry development programme of BARC. My sincere gratitude to Sh. V.V.K.Rama Rao and Sh. S.N.Bindal for their support and for introducing me to the field of mass spectrometry. I specially thank Sh. V.K.Yadav (TPD, BARC) for his constant support during all the experimental work related to this PhD. I am also thankful to Sh. E. Ravisankar (Head, MDAS, TPD), Sh. T.K.Saha (Head, DCS, TPD), Sh. Prakash Abichandani (Head, AEIS, TPD), Sh. R.B.Ingole (Head, LMRMSS, TPD) and all other colleagues associated with mass spectrometry programme of TPD for their support. Thanks are also due to all the members of my doctoral committee for their valuable suggestions during meetings and seminars related to my PhD work.

Words are not enough to express my gratitude to my parents for shaping my life in spite of all the difficulties they faced. I thank them for teaching me the value of hard work and struggle. I express sincere gratitude from the bottom of my heart to my wife ‘Pooja’ for the constant and unconditional support during the PhD work. Special thanks to my daughter ‘Kriti’ and son ‘Kartik’ for bearing my absence during late working hours for my PhD related work. Their affection always inspired me to overcome stressful situations and bring my work to successful conclusions. I express my gratitude to all other family members for their constant moral support. Last but not the least, I express sincere gratitude to all my teachers for their blessings and making me capable of working for BARC and completing PhD work.

R.K.BHATIA

CONTENTS

Chapter-1: Introduction

Chapter-2: Thermal Ionisation mass spectrometer

Chapter-3: Ion source design

Chapter-4: Magnet design

Chapter-5: Variable dispersion zoom optics

Chapter – 6: Faraday collector

SYNOPSIS

Mass spectrometry is widely used analytical technique for a variety of applications *viz*. precise isotopic ratio measurement, trace elemental analysis and compositional analysis of materials as well as characterization of bio-organic molecules etc [1]. Mass spectrometers find application in different fields as nuclear, geochronology, biology, material science, pharmaceutical industry, petrochemical industry, hydrology, environmental science, geology, planetary science etc. There are different types of mass spectrometers based on ion source design, analyzer for separation of ions based on charge/mass and detectors [2-4]. A specific design is selected based on the application. To mention a few– magnetic sector based mass spectrometers are used for the precise isotopic ratio measurements [5], a mass spectrometer with high ionization efficiency like inductively coupled plasma [6] or glow discharge mass spectrometer [7] is employed for trace elemental detection, a quadrupole based mass spectrometer is used for the compositional analysis of mixture of gases [8], and for the characterization of bio organic molecules mass spectrometers with soft ionization techniques like matrix assisted laser desorption ionization (MALDI) [9] and electro spray ionization (ESI) are employed [10,11].

The work presented in the thesis is mainly concerned with the developments carried out to improve the performance of a thermal ionization mass spectrometer (TIMS) which is a magnetic sector based mass spectrometer. These would also be useful for most of other magnetic sector based mass spectrometers. TIMS is used for the precise isotopic ratio measurement of elements for application in various fields like nuclear, geochronology, environmental science etc. The magnetic sector analyzer has unique advantage of simultaneous measurements of ions of different mass to charge ratio thereby eliminating possible errors due to fluctuations in the ion beam due to any parametric variations in ion source or analyser. It can be used in combination with variety of ion sources like electron impact ion source, thermal ionization source, inductively coupled plasma source etc. The work incorporates design, development, testing and evaluation of various sub systems of TIMS and studies to improve the performance in terms of precision and sensitivity of TIMS [12]. The thesis has been divided into seven chapters with first two chapter giving general introduction to mass spectrometers and basic design of TIMS used in present studies. Chapters 3 to 6 present studies made for improvement in different components of this basic design and last chapter presents summary of the thesis and scope for further work. The improvements carried out are: (a) ion source design by insertion and modification of electrode plates to improve sensitivity, (b) design modification of magnetic sector analyzer by addition of shims to result in focal plane normal to principal beam axis, (c) development of zoom optics to result in mechanical simplicity of collector system and (d) studies on Faraday cup for improvement in collection efficiency. These will be discussed in later chapters. A summary of different chapters is given in the following.

Chapter-1: Introduction

The chapter gives general introduction to mass spectrometry with historical evolution of various types of mass spectrometric techniques [13]. A mass spectrometer is an analytical instrument which analyse a given material by ionising its neutral particles and then separating the ions as per their mass to charge ratio. It has mainly three parts - ion source, analyser and the detector system. The ion source converts the neutral analyte particles into ions and accelerates them in form of a continuous ion beam or packets of ions depending upon the application. The ions from the ion source are introduced to the analyser which separates them as per their mass to charge ratio followed by the measurements of ion currents corresponding to the separated ions. A mass spectrometer is characterised by its sensitivity, resolution, precision, mass range and selectivity. The chapter includes the introduction to different types of ion sources, analyzers and detectors used in different types of mass spectrometers. The scope of the current research and development has been discussed in the chapter.

Chapter-2 Thermal Ionisation mass spectrometer

Thermal Ionization Mass Spectrometry (TIMS) is a very well recognized and accepted technique for precise isotopic ratio measurements of different elements present in a solid sample [14-19]. The TIMS instrument incorporates a thermal ionization ion source, magnetic field based analyzer and Faraday collectors as detectors. The ionization is achieved by evaporated atoms of material for analysis striking a heated filament with high work function (Rhenium, Tungsten etc). In this chapter general design features of thermal ionization mass spectrometer developed for these studies has been presented. It consists of 12 filament assemblies mounted on a turret, 90° magnetic sector analyzer in stigmatic geometry with magnetic field in 0-1 Tesla range and five Faraday collectors. It has resolution of 400 and sensitivity of 1 ion in 600 atoms of uranium.

Chapter-3: Ion source design

Thermal ionization source consists of a high work function filament heated to high temperature on which thermally evaporated atoms strike and get ionized. The ion source is a vital part of the mass spectrometer which determines its sensitivity and the design aspects of ion source employed in TIMS have been discussed. The ion source is mainly characterized by its ionization efficiency, selectivity, stability and energy spread. After ionization at the filament the ions are extracted out and accelerated by applying electrostatic potentials on different electrodes. The good sensitivity of the mass spectrometer requires that the ions are extracted efficiently from the filament surface and transmitted through the ion source with minimum loss. Secondly the design of the ion source should be optimised in such a way that it can hold high electrostatic potential without any breakdown and with minimum leakage current so as to produce a stable ion current with maximum possible transmission for higher sensitivity.

In present studies, the design has been improved to result in better transmission and thereby sensitivity by simulation studies carried out using SIMION software [20]. Filament assembly has been redesigned using ceramic materials to result in better life and reproducibility of characteristics [21]. Electrical insulation has been optimized to enable application of higher voltages.

Chapter-4: Magnet design

In this chapter theory and design features of magnetic sector analyzer has been discussed [22-27]. The magnetic sector is an important part of a mass spectrometer which is responsible for separation of ions as per their mass to charge (m/q) ratio. In a mass spectrometer, the ions produced in the ion source are accelerated and introduced to magnetic analyser in form of diverging ion beam. The ion beam during its passage through the magnetic sector undergoes deflection and refocuses at different points depending on m/q ratio. The refocusing of the ion beam is characterized by parameters *viz.* resolution, dispersion and magnification. This in turn depend on the geometry of the magnetic sector i.e. radius of curvature, deflection angle and entry and exit angles of ions. In early days of mass spectrometry, normal geometry was used where ion beam entrance and exit in the magnetic sector was normal to the boundaries of the magnetic sector. In this case the distance of object (source slit) from magnet boundary and that of magnet boundary to image position (detector slit) are equal to the radius of curvature of analyzer. The normal geometry is limited in dispersion, resolution and focusing. These limitations were circumvented by stigmatic geometry which uses the ion beam entry and exit angles of 26.5° with respect to entry and exit boundaries of the magnetic sector. Resolution in this geometry is factor of two better than that of normal geometry and focusing is improved. However, in both normal and stigmatic geometry, focal plane of different ions is not normal to principal beam axis. This results in unwieldy mechanical design of collector system. In present investigations, simulation and theoretical studies have been carried out for design of shims to be attached to main magnet so that focal plane becomes normal to principal axis. The results have been verified and shim design has been further optimized experimentally.

Chapter-5: Variable dispersion zoom optics

In TIMS, a multi collector system is required so as to simultaneously focus different isotopes of element under study on different Faraday cups [5, 6, 28-36]. Separation of Faraday cups depends on the element under study and therefore in actual use it becomes necessary to move Faraday cups to different locations depending on isotopic dispersion for the element. A facility to change dispersion of ions by application of electric field in place of mechanical movement has obvious advantages. A variable dispersion zoom optics has been developed that consists of a DC quadrupole, deflection optics and Faraday collectors with fixed positions. The DC quadrupole adjusts the dispersion of the ion beams with different masses in such a way that the ion beams get properly aligned with the respective apertures on the deflection optics which further deflects the ion beams in order to optimize their dispersions while they reach the respective collectors. It has additional advantage of increasing the dispersion of ion beams which provides extra space between the adjacent ion beams so that collector with wider apertures can be used. This has also helped in getting better peak shapes (with more flatness on peak tops) thereby enhancing the performance of the mass spectrometer.

Chapter-6: Faraday collector

The Faraday collector is used for the measurement of the ion beam intensity with minimum detection limit of 10^{-14} A [2-4, 37-38]. Conventionally it consists of mainly three parts- the main collector, secondary electron suppressor (SES) and the entrance slit. All the parts are insulated from each other and the complete assembly is covered with a grounded shield from out side to avoid the collection of any stray ion from the surroundings. The ion beam enters through the entrance slit and hits the main collector which is connected to the electrometer amplifier. The SES suppresses secondary electrons which are generated by the impact of ions on the main collector surface. In present studies improvement in Faraday collector has been carried out by (a) using magnetic field instead of SES to suppress secondary electrons, (b) graphite coating to reduce secondary emission and (c) inclination of base of collector so that secondary electrons hit wall of collector and are not lost.

Chapter-7: Summary

In this chapter results of studies have been summarized and scope of further work has been discussed.

References

[1] Introduction to mass spectrometery by S.K.Aggarwal, H.C.Jain, Indian Society for Mass spectrometry, 1997

[2] Modern isotope ratio mass spectrometry by I.T.Platzner, John Wiley & Sons, 1997

[3] Introduction to mass spectrometry by John Roboz, John Wiley & Sons,1968

[4] Mass spectrometry, Jurgen H. Gross, Springer

[5] Michael E. Wieser, Johannes B. Schwieters, International Journal of Mass Spectrometry 242 (2005) 97–115

[6] J. Sabine Becker, J. Anal. At. Spectrom. 20 (2005) 1173 – 1184

[7] J.W.Coburn, W.W.Harrison, Appl. Spectroscop. Rev. 17, 95 (1981)

[8] Quadrupole Mass Spectrometer and its application, Peter H. Dawson, Elsevier Scientific Publishing Company, Amsterdam (Netherland), 1976

[9] Lame F. Marvin, Matthew A. Roberts, Laurent B.Fay, Clinica Chemica Acta 337(2003)11-21

[10] Shibdas Banerjee and Shyamalava Mazumdar, International Journal of Analytical Chemistry, Vol. 2012, Article ID 282574

[11] Andries P. Bruins, Journal of Chromatography A, 794 (1998) 345-357

[12] R.K.Bhatia, R.Datta, R. Chandak, M.M.Gulhane, P.R.Kasina, A.M.Kasbekar, N.Ved, V.k.Yadav, M.Gopalakrishna, E.Ravisankar, R.K.Saha, V.Nataraju and V.K.Handu, 11th ISMAS-TRICON-2009, 493-495

[13] Simon Maher, Fred P.M.Jjunju and Stephen Taylor, Reviews of Modern Physics, Vol. 87, Jan –March 2015

[14] S.N.Bindal et.al., p 761, 8th ISMAS Symposium 1999

[15] S.K.Aggarwal, A.I.Almaula, P.S.Khodade, A.R.Parab, R.K.Duggal, C.P.Singh, A.S.Rawat, G.Chourasiya, S.A.Chitambar and H.C.Jain, J. Radioanal.Nucl.Chem.-Letters, 87, (1984) , p.169-178.

[16] K.L. Ramakumar, P.S. Khodade, A.R. Parab, S.A. Chitambar, H.C. Jain, J. Radioanal. Nucl. Chem. 107 (1985) 215

[17] Rajender K Bhatia, Pratap Reddy K, Varun K Yadav, V.Nataraju, E.Ravisankar, T.K.Saha,V.K.Handu and S.K.Gupta,14th ISMAS workshop 2011, 195-198

[18] R.K. Bhatia, V.K.Yadav, M.M. Gulhane, Rabi Dutta, Reku Chandak, K.D.Joshi, Meera Murali, A.M. Kasbekar, Vilas Mahadeswar, E.Ravisankar, Ananya Verma, T.K.Saha, V.Nataraju, V.K.Handu and S.K.Gupta,14th ISMAS workshop 2011, 202-205

[19] R.M. Rao, A.R. Parab, K. Sasibhushan, S.K. Aggarwal, International Journal of Mass Spectrometry 273 (2008) 105–110

[20] D.A.Dahl, “SIMION version 7.0”, Idaho National Engineering Laboratory, 2000

[21] E.Ravisankar, R.K.Bhatia, V.V.Katke, A.M.Kori, V.K.Yadav, V.Nataraju and V.K.Handu, Proceedings of 11th ISMAS-TRICON-2009, 419-421

[22] Harald A. Enge, "Deflecting Magnets", pp. 203-263, from Septier, A., The Focusing of Charged Particles, Academic Press, New York, 1967

[23] H.Hintenberger and L.A.König, Advances in Mass Spectrometry, Pergamon Press, New York, 1959, p. 16-35

[24] H.H.Tuithof and A.J.H.Boerboom, International Journal of Mass Spectrometry and Ion Physics, 20 (1976), 107-121

[25] Konig, L.A. and Hinterberger, H., Nuclear Instruments, 3, (1958), 133I.Chavet, Nuclear Instruments and Methods 99(1972), 115-119

[26] V.V.K. Rama Rao, International Journal of Mass Spectrometry, Vol. 145, Issue 1-2, 1995, p.45

[27] R.K.Bhatia, V.V.K.RamaRao, N.Padma and A.D.Kulkarni, *9th ISMAS Symposium 2003*

[28] Rajender K Bhatia, S.N.Bindal and V.K.Handu,13th ISMAS symposium cum workshop 2008, 230-232

[29] Mario Ishihara, United states patent, Patent no. 4998015

[30] Mario Ishihara, United states patent, Patent no. 5118939

[31] Freedman, Philip, Antony, European patent no. EP 0857353B1

[32] Matthew A. Coble et al., Chemical Geology 290 (2011) 75-87

[33] Xiaoping Xia, J. Anal. At. Spectrom. 26 (2011) 1868

[34] J.M. Saxton, International Journal of Mass Spectrometry and Ion Processes 154 (1996) 99-131

[35] N.S. Belshaw et al., International Journal of Mass Spectrometry 181 (1998) 51–58

[36] Simon Turner et al, J. Anal. At. Spectrom. 16 (2001) 612-615

[37] Turner, Haines, Kelsall, United States Patent, Patent no. 5903002

[38] Johannes Schwieters, United States Patent, Patent no. US 6452165 B1

List of figures

List of Tables

Chapter-1

Introduction

Mass spectrometry is highly powerful and useful analytical technique for assaying a material on the basis of mass to charge ratio of the analyte ions [1-4]. When compared with other analytical techniques *viz*. spectroscopy, radio-active emission counting etc., mass spectrometry is more sensitive, precise and selective technique [5]. The technique provides highly valuable information in various fields *viz*. nuclear technology, geochronology, chemistry, biology, planetary science, pharmaceutical industry, petrochemical industry etc. Some of the typical applications of mass spectrometry in different fields are as below:

- Characterization of various materials employed in different stages of nuclear energy generation is executed by the isotopic ratio measurement of various elements by mass spectrometry. For example the reactor fuel (U), the spent fuel (Pu), the activity controlling material (B), moderator (H) and structural materials (Pb) etc. are characterized by their isotopic composition measurement using isotope ratio mass spectrometry. In geochronology the isotopic ratio composition of Sr, Nd, Os, and Pb etc. helps in exploring the nuclear fuel by age determination of various rock samples in a region under investigation.
- In environmental science, mass spectrometry is employed for the trace elemental detection of toxic elements like Pb, As, Hg etc. for the health and safety purpose. The isotopic ratios of various elements like Sr, C, S, O and N etc. are used as signature pertaining to certain region or system. This helps in studying migration of substance from one region / system to another. For example - the ground water studies, crop

production, soil erosion, meteorological studies etc. In planetary science, the isotopic studies of any planetary object are carried out to ascertain its origin of composition.

- The accelerator mass spectrometry [1] is employed for the age determination of various organic or planetary species consisting of long lived radio nuclides e.g. radio isotopes of C, Be, Al and I etc.
- In organic chemistry [4] mass spectrometry is used in the determination of molecular weights, structural and speciation studies of compounds, detection of various drugs in the blood samples of athletes, identification of drugs and their metabolites in human body fluids etc.

1.1 Historical

The mass spectrometry originated with the discovery of electrons and positive rays in vacuum tube by J.J.Thomson in the early part of 20th century. The world's first mass spectrometer called as Thomson parabola spectrograph [2, 6] was invented by J.J.Thomson in 1912. The spectrograph consisted of electric and magnet fields in cross configuration followed by photographic plates. The ions passing through the electromagnetic field generated parabolic images on photographic plate with each parabola corresponding to a given m/q ratio. The spectrograph even though exhibited lower mass resolution, was capable of detecting presence of Neon isotope with mass 22 amu. Later the photographic plate was replaced with Faraday detector preceded by a parabolic slit to transmit ions of particular m/q. The mass spectrum was generated by changing magnetic or electric field. The presence of Neon isotope was further confirmed by another high resolution mass spectrograph developed by Aston. The spectrograph consisted of successive electric and magnetic fields in order to select ions with smaller energy spread resulting into higher resolution. Aston was able to discover many other isotopes and was awarded Noble prize for his pioneering work. Subsequently, Dempster invented mass spectrometer based on magnetic sector with 180° geometry. He developed the sector field theory which is useful even for the present day mass spectrometric development.

Dempster discovered the four isotopes of Zn and most importantly the isotope of Uranium with mass 235 amu. Bleankey took forward the developments of Dempster and mainly worked on electron impact ion source. Subsequently, the design of the electron impact ion source was modified by Bainbridge, Nier, Mattauch and Herzog in 1930s. This ion source helped in studying the organic molecules by generating the spectra of their fragments which were used as fingerprints corresponding to a particular organic molecule. The lower resolution of single focusing instruments led to the need of double focusing instrument which was firstly described by Mattauch and Herzog in 1935. The double focusing instruments were based on the energy focusing of the ions using electrostatic analyzer along with the usual directional focusing by the magnetic sector. Later different geometries of electric and magnetic field were introduced by Bainbrige and Jordan, Neir and Johnson in 1940s. 1950s saw the development of other techniques for higher resolution analysis of large bio-molecules. This includes the development of ion cyclotron resonance mass spectrometer, Fourier transform mass spectrometry etc. The discovery of techniques like electro-spray ionization in 1980s by Fenn and later matrix assisted laser desorption in 1990s proved to be revolutionary for the analysis of bio-organic molecules. These techniques along with time of flight analyser are mostly used for the bio-organic analysis. The evolution of techniques like inductively coupled based plasma ionization and glow discharge mass spectrometry for the trace elemental analysis in 1990s were instrumental in reducing the detection limits to below parts-per-quadrillion (ppq; 1 part in 10^{15}) for some of the elements which were difficult to be detected by other techniques like emission and absorption spectrometry. The key developments in mass spectrometry are enlisted below in chronological order:

- Discovery of **electron impact** ion source by Bleakney in 1929
- First **double focusing mass spectrometer** developed by Mattauch and Herzog in 1934
- Stephens described the concept of **Time of flight mass spectrometry** in 1946
- Introduction of **SIMS** concept in 1940s and first SIMS experiments performed by Herzog and Viehbock in 1949

- In 1949 **ion cyclotron mass spectrometer** was developed by Hipple and co-workers
- The **thermal ionization mass spectrometry** using triple filament assembly developed by Inghram and Chupka in 1953
- The **QMS** and **ion trap** concept was introduced by Paul and Steinweddel in 1953 followed by development of QMS and ion trap in 1956.
- In 1960s QMS gained popularity because of its coupling with gas chromatography
- **MS/MS** techniques were developed during 1960s for the structural information of bio-organic molecules.
- **Fourier transform ion cyclotron resonance (FTICR) mass spectrometer** was a notable high performance mass spectrometer developed during early 1970s
- One of the key developments of 1970s was coupling of **liquid chromatography with MS (LC-MS)** providing very high sensitivity and selectivity for complex mixtures
- Invention of Reflectron based Time of flight mass spectrometer in 1973 revolutionized the mass spectrometry with very high resolution and mass range.
- Highly sensitive and selective techniques like **Accelerator mass spectrometry (AMS) and Resonance ionisation mass spectrometry (RIMS)** were evolved during late 1970s.
- The development of techniques applied to bio molecules like **Electro spray ionization (ESI), Matrix Assisted Laser desorption ionization (MALDI)** during 1980s
- **ICP** technique evolved during 1988-1992 by pioneer work by Houk, Fassel, Gray, Taylor, Walder and Freedman etc.
- In 1990s a new hybrid instrument was developed by combining **quadrupole and TOF (Q-TOF)** providing highly sensitive MS/MS analysis which enabled bio-polymer sequencing in atto mole to femto mole range.
- Last 20 years have seen new development related to biological sciences vis. **Ion mobility mass spectrometry (IMS)** in 1997 and **Orbitrap** in 1999

1.2 Principle

A mass spectrometer consists of mainly three parts: (a) the ion source, (b) analyzer and (c) detector. The analyte material is introduced in the ion source where the neutral atoms/molecules of analyte material undergo ionization. The analyte ions are accelerated and passed through or trapped inside the analyzer where they get separated as per their m/q ratio. The ion current corresponding to respective isotopes are measured using suitable detector and spectrum of ion intensity versus m/q is generated. There are variety of ion sources, analyzers and detectors which are used in different combinations as per the application. A mass spectrometer is characterized by the parameters like resolution, mass range, sensitivity and precision etc. Typical examples of a mass spectrometers are- thermal ionization mass spectrometer (TIMS), electron impact mass spectrometer (EIMS), quadrupole mass spectrometer (QMS), inductively coupled mass spectrometer (ICPMS), resonance ionization mass spectrometer (RIMS), glow discharge mass spectrometer (GDMS), time of flight mass spectrometer (TOFMS), secondary ion mass spectrometer (SIMS), accelerator mass spectrometer (AMS) etc.

The mass spectrometers for inorganic applications are mainly employed for the measurements related to elemental species. The ionization technique is selected based on the effective ionization of the atoms of an element present in the analyte material and the molecular integrity of the analyte species is not important. The main applications covered in this category are – isotopic ratio measurement of an element, compositional analysis of material, trace elemental detection and surface and bulk imaging of the solid materials etc. The mass spectrometers for the isotopic ratio measurements use thermal ionization [1-4] and electron impact ionization techniques [1, 2] for the ionization of the sample and magnetic sector based analyzers for the separation of ions. For trace elemental and compositional studies quadrupole based mass spectrometers are employed with ionization techniques as electron impact (for compositional studies) and inductively coupled plasma ionization [7]. For surface and bulk analysis of solid materials secondary ion mass spectrometry [4, 8] is employed with analyzers as magnetic sector in combination with electrostatic analyzer. SIMS is also used for isotopic ratio measurements.

The organic applications include mass spectrometers with soft ionization techniques [2, 4] so that the integrity of the molecules of organic or bio-organic analyte remains intact. Mostly used techniques are Matrix Assisted Laser Desorption Ionization (MALDI) [4, 9] and Electro Spray Ionization (ESI) [10, 11] with RF quadrupole [12], time of flight [4, 13] and ion trap analyzers [14]. The applications involve the molecular weight measurements, molecular structural characterization and speciation studies of organic compounds etc.

1.3 Ion sources

- Thermal ionization (TI)
- Electron impact / bombardment (EI / EB)
- Inductively Coupled Plasma (ICP)
- Glow Discharge (GD)
- Resonance Ionization (RI)
- Matrix assisted laser desorption ionization (MALDI)
- Electro-spray ionization (ESI)

Above techniques are explained in the following.

1.3.1 Thermal ionization source

In this technique ionization of a given analyte occurs when it is adsorbed on a hot surface of high work function material [1-4]. Source consists of single or plurality of filaments of a high work function material in the form of a ribbon. The solid sample dissolved in acidic medium is deposited on one or two filaments called sample filament. The sample filament is heated electrically under vacuum and the ionization is achieved by surface ionization of the sample vapors on same filament (single filament assembly) or the other filament (double or triple filament assembly) called as ionization filament.

The ionization efficiency is governed by Saha Langmuir equation:

$$\boldsymbol{n^+/n_o = g_i/g_o\,[(1\text{-}r_i)/(1\text{-}r_o)]\,\exp\{(W\text{-}I)/kT\}} \qquad (1.1)$$

where n^+& n_o are the number of positive ions formed and neutral species evaporated, r_i & r_o are reflection coefficients and g_i& g_o are the statistical weights of the ionic and atomic states, W is the work function of the filament, I is the ionization energy of the element, T is the temperature of the surface and k is the Boltzmann constant.

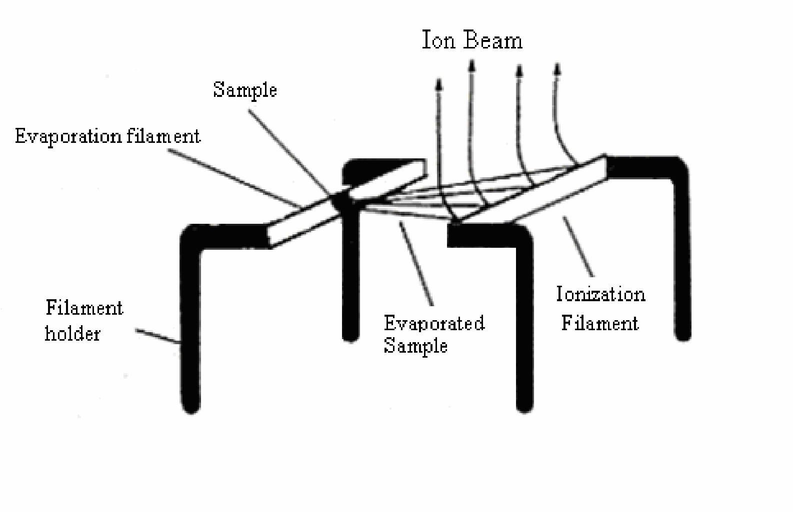

(a)

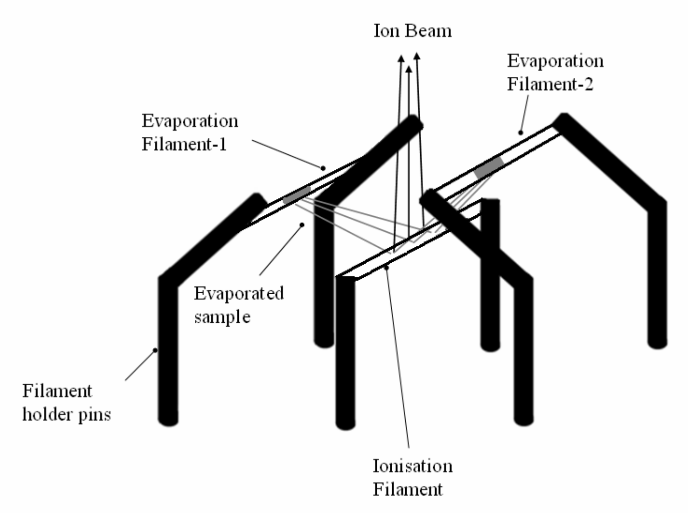

(b)

Fig.1.1: (a) A double filament assembly and (b) a triple filament assembly

The ionization efficiency (β) is defined as the relative number of neutral species converted to ions as follows:

$$\boldsymbol{\beta = n^{+} / N} \tag{1.2}$$

where N is total number of species given as:

$$\boldsymbol{N = n_o + n^{+} + n^{-}}$$

For negligible negative ions: $$\boldsymbol{N \simeq n_o + n^{+}} \tag{1.3}$$

Using equation 1.2 and 1.3:

$$\boldsymbol{\beta = 1/(1+1/\alpha)} \tag{1.4}$$

where $\alpha = n^{+}/n_o$

Equation 1.1 and 1.4 shows that the ionization efficiency has dependence on the parameters *viz.* ionization potential of the analyte species, work function of the filament material and the temperature.

In case of elements with low ionization potential (IP) ($< W$), W-I term in equation 1 is positive which implies that the ionization efficiency increases with reduced temperature. In this case single filament is sufficient for sample deposition as well as ionization. The filament is heated to a temperature just enough for the sufficient vaporization of sample to get the ions in gas phase.

In case of elements with high IP ($>W$), the term W-I becomes negative so that the ionization efficiency increases with the temperature. In this case the sample is required to be heated at much higher temperature for high sensitivity that can lead to evaporation of the sample before sufficient ionization takes place if single filament is used. This leads to the use of multiple filament assembly whereby double or triple filaments are employed to decouple the evaporation and ionization processes. The double filament assembly consists of one sample and one ionization filament facing each other as shown in the Fig. 1.1a. The triple filament assembly incorporates two side filaments and a centre filament as shown in Fig. 1.1b. The de-coupling helps in controlling the evaporation and ionization processes independently and hence optimizing the ionization efficiency. Generally rhenium (Re) filament (single or multiple) is used for ionization because of its high work function (~5.2 eV) and high melting point (3180° C). Other used filament materials are Tungsten, Tantalum and platinum etc.

As the ionization efficiency is dependent on the work function of the filament, there are various techniques used for enhancing the work function for specific element with very high IP (> 7eV). To mention a few techniques - graphite coating of the filament for enhancing ionization of actinides, deposition of silica gel/ phosphoric acidic on the filament before sample loading for Pb, Fe, Cr etc. and resin bead technique to analyse nanograms of U and Pu samples.

Some of the elements (with high IP) exhibit sufficiently high probability of negative ionization which is governed by following equation:

$$n^{-}/n_o = g_i \,/\, g_o\, [(1-r_i)/(1-r_o)]\ \exp\{(W-EA)/kT\} \tag{1.5}$$

Where EA denotes electron affinity and other terms represents same meanings as for eq. 1.1. The elements with high EA produce negative ions in excess than positive ions during thermal ionization and are analysed by negative thermal ionization mass spectrometry (NTIMS) e.g. Osmium (Os), Boron (B) and Rhenium (Re) etc.

The thermal ionization source [1-4] is known for its sensitivity, stability, selectivity and low energy spread (1 – 2 eV). It is used in combination with a magnetic sector analyzer for precise isotopic ratio measurement of elements. It is typically employed for the analysis of elements with IP lower than 7 eV. Special techniques are used for the elements with IP above 7 eV as already mentioned above.

1.3.2 Electron impact /bombardment ion source

The electron impact ion source [1, 2, 15] is used for the ionization of samples in gaseous phase. The ionization is based on the principle of ionization of neutral atoms or molecules of analyte by collision with the energetic electrons. The ionization can take place by following processes. Removal of electrons from outermost orbit of an atom (A) or molecule (M):

$$A + e \rightarrow A^{+} + 2e$$

$$M + e \rightarrow M^{+} + 2e$$

Molecules may also undergo fragmentation along with ionization of one or more fragments.

$$M + e \rightarrow A^{+} + (M\text{-}A)^{0} + 2e$$

The ion source consists of an ionization box (also called as case box) which incorporates tungsten filament for producing electrons and other electrodes *viz*. repeller, trap, electron focus and shield as shown in the Fig. (1.2). A magnetic field in the range of 150 – 200 gauss is also employed in the direction of electron beam to increase the path length of the electrons. This helps in increasing the ionization efficiency of the ion source.

The filament is heated to very high temperature by electrical heating. Electrons are emitted by thermionic emission from the hot filament surface. The emission is governed by Child Langmuir's Law as given below:

$$\boldsymbol{N_e = AT^2 \exp(-\Phi/kT)} \tag{1.6}$$

Where N_e – number of electrons emitted per unit area per unit time from the filament surface, A – Constant (material property), Φ – work function of the filament, k – Boltzman's constant, T – absolute temperature

The thermionically emitted electrons from filament are allowed to enter case box and accelerated to an electrical potential around 50 – 70 eV by applying suitable potentials on various electrodes (Case, Electron focus and trap electrodes). The gas particles are introduced into the ion source in a direction orthogonal to the electron beam in such a way that there is maximum overlap between the particle beam and the electron beam. The electrons undergo inelastic collision with the gas molecules/atoms and ionise them by transferring their kinetic energy to knock out outermost electrons or by breaking the chemical bonds of the molecules. The ion beam intensity (I^{+}) obtained from the ion source is given by following equation.

$$\boldsymbol{I^{+} = \beta\, \Gamma\, L_e\, \sigma\, n_g} \tag{1.7}$$

Where $\boldsymbol{\beta}$ – transmission factor of ion source, $\boldsymbol{\Gamma}$ - electron current (also called as emission current of filament), $\boldsymbol{L_e}$ – path length of electron, $\boldsymbol{\sigma}$ – ionization cross section of gas particle for a given energy of electron, $\boldsymbol{n_g}$ – gas density

The ionization cross section σ is dependent on ionization potential of analyte species and the energy of electron as shown in Fig. 1.3. It is evident from this figure that the ionization is maximum in the range of 50 -100 eV for various analyte samples. In the lower energy region the electrons do not possess sufficient energy for undergoing in-elastic collision with the gas particles. So that, the probability of in-elastic collision (and hence the ionization) increases with kinetic energy in lower energy limits. However with increasing kinetic energy (and hence the speed), the time spent by the electron in the vicinity of analyte molecule also reduces thereby reducing the interaction between the ionizing electron and analyte. This leads to reduced probability of ionization of the analyte molecule. Hence after a certain limit, the ionization probability reduces with the kinetic energy of the electrons. In the intermediate region (50 – 100 eV) the interaction time and the energy of electron are optimum for maximum ionization.

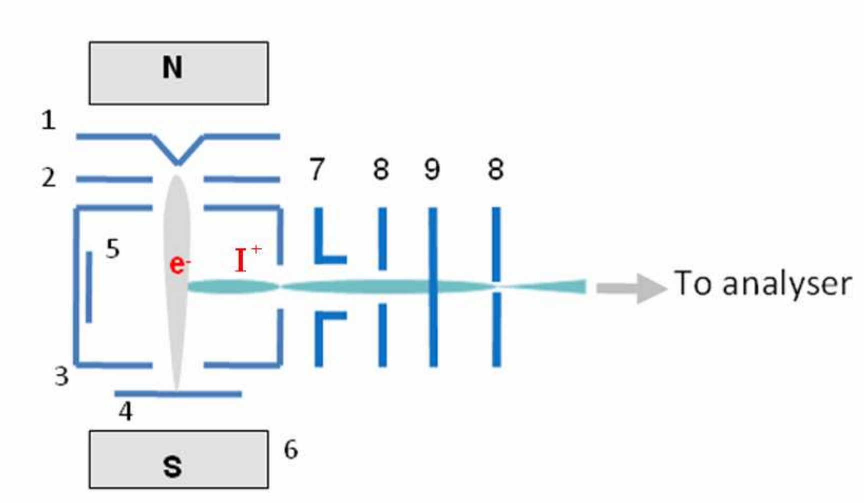

1. Filament 2. Electron focus plate 3. Case Box 4. Trap
5. Repeller 6. Magnet 7. Y plate 8. Ground plates 9. Z plate

Fig.1.2: Schematic of Electron impact ion source

The dependence of σ on energy of electron can also be explained by considering the wave nature of electron. The wave length of the electron is governed by the momentum (and hence kinetic energy) of electron. The maximum overlap between the analyte molecule and the electron is possible when the wave length of electron matches with the size of the molecules (~ 1 Angstrom) that happens for an electron kinetic energy in the range of 50 – 100 eV.

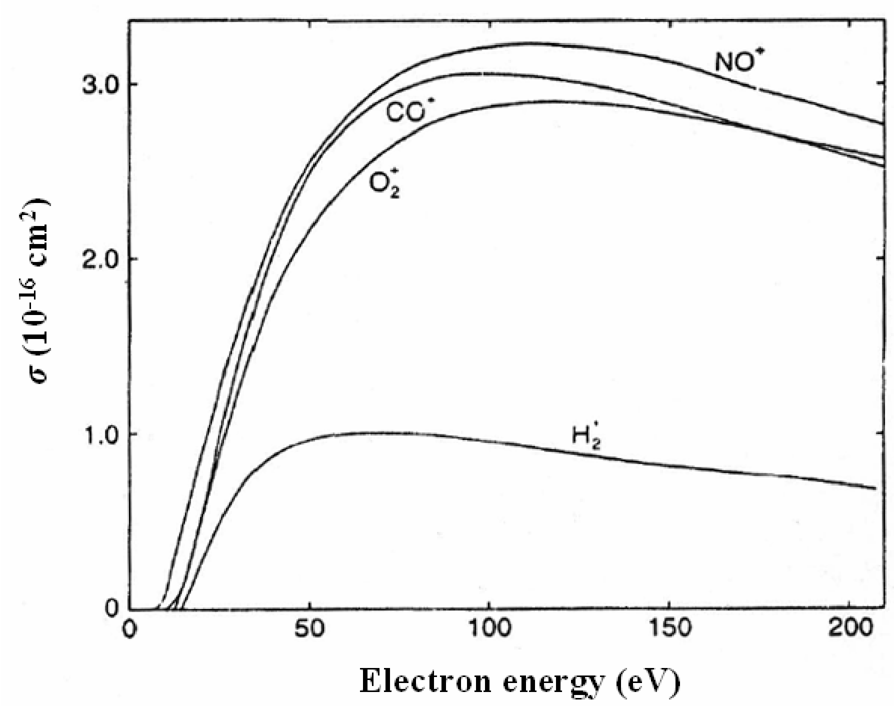

Fig. 1.3: Dependence of ionization cross section on kinetic energy of electron in an EI source

The electron impact ion source is known for its reliability, stability and sensitivity. It is suitable for magnetic sector (for precise isotopic ratio analysis) and quadrupole analyzers (for compositional analysis of gas mixture and organic samples). Subsequent to the ionization in EI source, the ions are accelerated to 5 – 10 keV for a magnetic sector and to 100-200 eV for a radio frequency (RF) quadrupole analyser. The ions exhibit moderate energy spread in the range of 1 – 5 eV and therefore for certain applications may require double focusing (magnetic sector in combination with electrostatic analyser) for high resolution. Being a hard ionization (fragmentation of molecules) technique it is not suitable for bio-organic molecules as the molecular integrity is lost due to fragmentation.

1.3.3 Inductively coupled plasma ion source

The technique exhibits very high ionization efficiency [4, 7] and is employed for the trace elemental detection for more than 90% of the elements in periodic table. The technique is known for very low detection limit (up to 10^{-15} for some of the elements), high sample throughput (number of sample analysed in a given time), very simple sample preparation and sample introduction systems. It is used in combination with RF (radio frequency) quadrupole for trace elemental detection. It can also be coupled with combination of electrostatic analyser and magnetic analyser for precise isotopic ratio measurements. The ionization is based on the evaporation, atomization and ionization of liquid sample by the high temperature (> 8000 K) plasma generated by inductive coupling between the RF field from coil and the electrons present inside the coil.

An ICP source consists of a plasma torch, an RF coil and RF power supply as shown in Fig. 1.4. The plasma torch incorporates three hollow co-axial quartz tubes (with different radii) coupled together. The quartz tube combination is surrounded by water cooled copper excitation coil. Argon gas is introduced in the regions of three tubes separately with different flow rates. In the outer most (region between outer tube and the middle tube) the Ar is introduced at a flow rate of 12 – 15 l/min (plasma flow) to generate plasma and for cooling the outer most tube. An auxiliary flow of ~ 1 l/min is introduced in the mid region and carrier flow of ~ 0.5 l/min is maintained in the inner most tube region. An RF power of 1-1.5 kW with frequency of 27.12 MHz is supplied to the coil. Electrons produced by spark from a Tesla coil get coupled to the RF field (produced by RF coil surrounding the torch) and get energized and ignites intense plasma in the region near to the opening of the torch. A very high temperature of around 8000 K is generated in the central part of the region close to opening of coil and reduces to around 6000 K at a distance of about 30 mm from coil. The sample introduced by the carrier gas gets evaporated, atomized and ionized in the central region of the plasma.

As the ions are produced in atmosphere, the introduction inside the vacuum is achieved by differential pumping using sampler and skimmer cones. The sampler cone with orifice of around 1 mm is placed around 30 mm from the torch. The skimmer cone with orifice of 0.85 mm is placed at a distance of around 6 mm from the sampler cone. Both the cones are made of Nickel because of its high thermal conductivity and oxidation resistance.

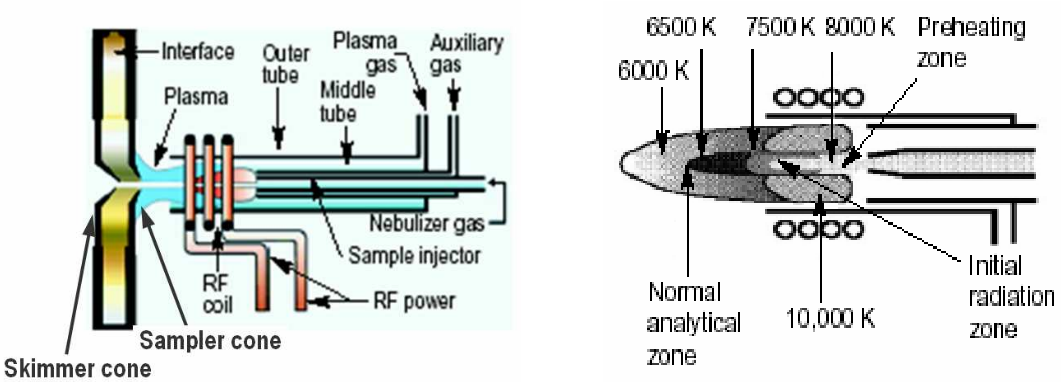

(a) (b)

Fig. 1.4: a) Schematic of ICP b) different temperature zones in plasma

The region between sampler and skimmer cone is evacuated up to 1 – 0.1 torr. The hot gas from plasma while passing through the sampler cone aperture undergoes ultrasonic expansion and gets cooled down within a distance of less than aperture diameter. This leads to freezing the reactions which can change the composition of the plasma gas. The sudden cooling at reduced pressure directs the gas along the axis leading to the free jet formation that is bound radially by shock wave known as barrel shock and terminated by perpendicular shock known as Mach disc. The skimmer cone is placed at a distance before the formation of Mach disc since the Mach disc makes the flow subsonic again which can allow the interaction of plasma gas with background gas particles. The region beyond skimmer cone has high vacuum in the range of 10^{-6} torr and incorporates electrostatic lens followed by mass analyser.

The analyser separates the ions as per mass to charge (m/q) ratio and detected by electron multiplier.

1.3.4 Glow Discharge (GD)

Glow discharge ionization [16] is a powerful analytical technique for the trace elemental detection of the sample in solid form. It is a complementary technique to ICP with advantages of lower detection limit and lower cost of the instrumentation as compared with ICP. However, lower throughput and presence of more matrix effects (as compared with ICP) are the drawbacks of this technique.

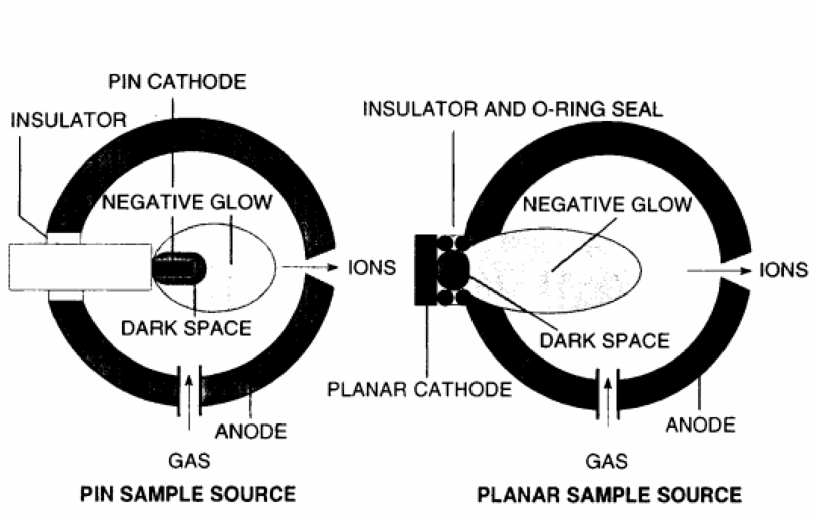

Fig. 1.5: Schematic of the GD ion source with a) Pin cathode b) Planer cathode

The ionization is based on sputtering and ionization of the molecules by Argon ions generated by glow discharge. The glow discharge in the ion source can be obtained by various methods namely direct current (DC) glow discharge, radiofrequency and pulsed mode glow discharge. The mostly employed method is DC glow discharge.

In DC glow discharge, the solid sample in form of disc or pin is used as cathode in the ion source as shown in Fig. 1.5. The plasma is struck between cathode and anode under low pressure atmosphere (0.1 – 10 torr) of Argon gas by applying negative DC voltage (500 volts –

1000 volts) on cathode with respect to anode at ground potential. Different discharge regions are generated as shown in the Fig. 1.6. The cathode is surrounded by a narrow dark space which is extended up to one mean free path away from the cathode surface and hence is free form collision induced excitation and recombination involving electrons. Around 80% of the voltage (between electrodes) falls across this region that leads to the maximum acceleration of electrons and Ar^+ to gain maximum kinetic energy. Beyond this region, the negative glow region prevails. The characteristic glow is provided by the relaxation of the metastable species in this region. The atomization of the sample is provided by sputtering of the cathode by Ar^+ ions generated in negative glow region by impact of stray electrons. The atoms freed by sputtering process get ionized in negative glow region by Penning discharge and collision with free electrons present in this region. The major mode of ionization is Penning discharge i.e. the transfer of energy by metastable Ar atom to the analyte atom. The metastable states of Ar at 11.55 eV and 11.72 eV can afford ionization of most of the elements in periodic table. This along with low cost, inertness and high sputtering yield make it the preferable working gas for GD source. The de-coupling of atomization and ionization processes makes the ionization less dependent on matrix effects. However, the sample should be electrically conducting which otherwise can accumulate static charge affecting the discharge process. The non conducting sample is converted to powder form and a conducting mixture is prepared using conducting binders *viz*. Ag, Cu, Ta etc. Subsequently, the mixture is molded in form of pin or disk to be used as cathode in GD source. However the mixing of conducting binders can lead to diluting the analyte signals and contaminating the sample with extra impurities thereby affecting the analysis adversely. The alternate way is to use RF Glow Discharge. The technique uses same setup as used in dc glow discharge except applying RF voltage (2 kV peak to peak at 13.56 MHz) on the cathode instead of dc voltage. The charging of cathode in first half cycle of the voltage is neutralized by opposite polarity of the other half cycle of RF voltage. This circumvents any accumulation of charge on the time averaged cathode with half of the peak to peak voltage developing across the electrodes.

The pulsed mode of operation is used along with DC or RF glow discharge. This includes the application of high voltage for short duration (micro seconds) which leads to higher peak voltages and peak currents for the same average power. This increases sputtering that leads to the availability of more analyte ions and hence higher sensitivity. This also helps in distinguishing the analyte of interest from interfering ions by using time resolving methods.

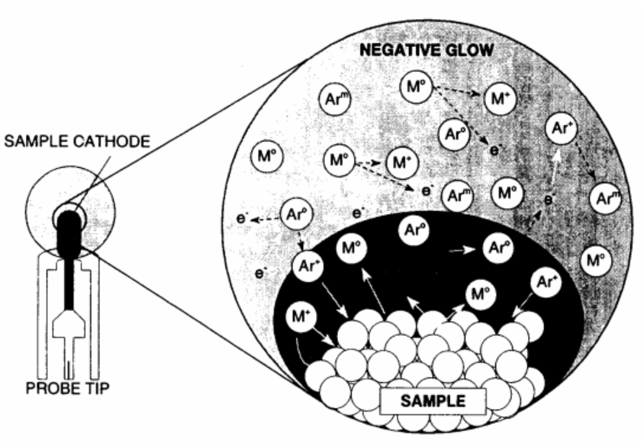

Fig. 1-6: Schematic showing different regions in glow discharge

1.3.5 Resonance Ionization (RI)

It is a highly sensitive analytical technique based on ionization induced by Lasers for sample in gas phase [4, 17-18]. The ultra high sensitivity along with high selectivity make this technique very useful for the detection of very small traces of analyte in a sample by circumventing any isobaric interference from other species present in the sample. It employs tunable laser with small bandwidth in the range of 0.1 to 0.5 cm^{-1} (3 to 15 GHz). The sample atom in gas phase is excited with photon of suitable energy matching with characteristic energy state of the atom. Due to resonance absorption of the photon energy the atom gets excited to the higher energy state and stays there for time of around tens of nanoseconds before de-excitation by photo emission or collision with another atom. During this time, the transfer of energy by another photon can further excite the atom to higher energy state. Conditions can be generated, by which the excitation process can continue till the atom gets ionized. There are certain schemes by which excitation and ionization can take place as shown in Fig. 1.7. Each element has its characteristic ionization potential (I.P.) ranging from 3.89 for Cs to 24.48 eV for He. For *n* photons of frequency *v* the ionization occurs when $n.hv \geq$ I.P. However due to single color multi-photon ionization the selectivity reduces due to non resonant excitation of the closely matching energy states for elements in a given group of periodic table. The non resonant excitation and ionization is the source of noise that is undesirable. For higher selectivity multi-color excitation and ionization process is employed. After excitation of the atom to desired state the ionization can be achieved by different types of processes namely photo-ionization, field ionization and by excitation to auto-ionising states. The photo-ionization is carried out by using photon of suitable frequency usually more than the excitation frequency to achieve saturation i.e. ionization of each atom of the sample under study. In case of field ionization suitable electric field is applied to excite the atom to Rydberg states (high energy states). The pulse of electric field is applied soon after the application of excitation laser pulse. In case of ionization using auto-ionising states, another tunable laser is required to excite the atom to its characteristic auto ionising states present in the ionization continuum. The added advantage with this technique is the additional selectivity during ionization along with the selectivity provided during the excitation process.

The actual scheme adopted for a given analysis depends upon the ionization cross section of element under study and the extent of selectivity required. The necessary and the sufficient condition for the saturation to occur is to transfer the electron to ionization state before the excited state is destroyed by other process. This requires fluence (number of photons per unit area) and the flux (number of photons per unit area per unit time) to be higher than particular values.

Flux condition: $$\sigma_i . F \gg \Gamma_{10} + \beta$$

Fluence condition: $$\sigma_i . F g' T = g' \Phi \sigma_i \gg 1$$

Where σ_i – cross section for photo-ionization of state 1, F – flux of laser photons, Γ_{10} – cross section for stimulated emission, β – rate of decay of state 1 by other processes, $g' = g_1/(g_0 + g_1)$; g_i – statistical weight of i^{th} state, Φ – fluence

The different types of resonance ionization sources (RIS) are – thermal atomization RIS (TARIS), Laser ablation RIS (LARIS), sputter initiated RIS (SIRIS). In case of TARIS, the sample is deposited electrolytically in a high purity filament of Re or Ta. The sample is evaporated by heating the filament at high temperature in a cavity. The laser beam is introduced in the cavity for ionization. The LARIS incorporates ablating atoms from solid sample by imparting laser beam on it. In case of SIRIS the sputtering of solid sample is carried out using energetic ion beams.

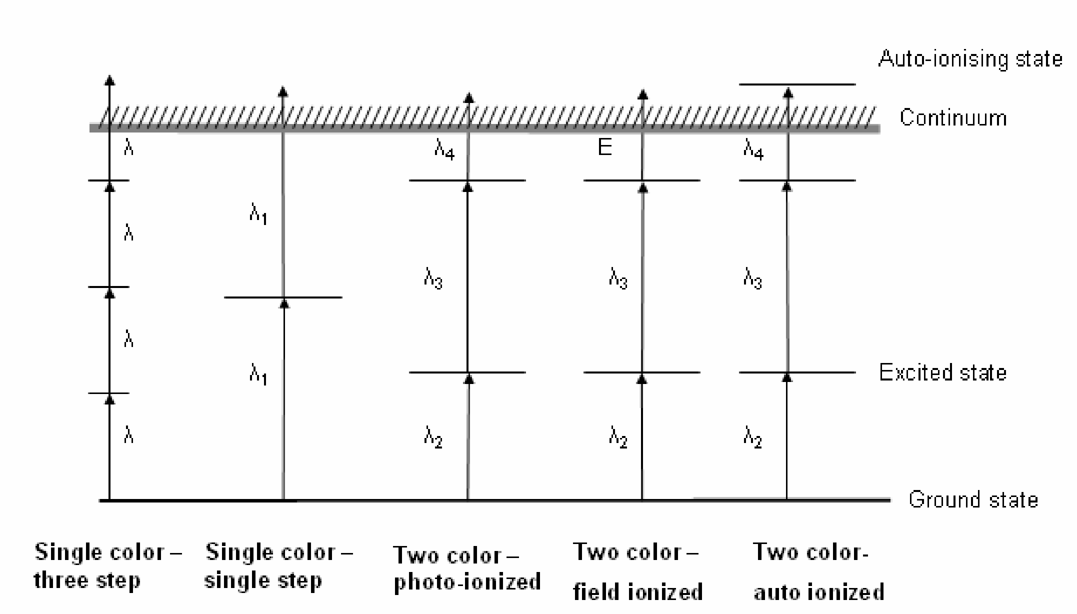

Fig. 1.7: Schemes for excitation and ionization in Resonance Ionization

The most commonly employed laser for RIMS is dye laser pumped by either Nd: YAG laser or XeCl excimer laser. The pulse width is in the range of 2 – 20 nsec with energy in the range of tens of mJ per pulse. The band width is in the range of 0.1 – 0.5 cm^{-1} (3 to 15 GHz). The pumping with Nd:YAG is more useful than excimer laser in the sense that same can be used for ionisation of the excited atoms.

1.3.6 Ion impact induced ionization

This technique is used in secondary ion mass spectrometry and is a versatile analytical technique [4, 8] for the compositional characterization of the surface and bulk of the solid state materials. It includes the measurement of spatial and depth dependent concentration of analyte material in solid matrix by sputtering them with energetic primary ions followed by mass spectrometric measurements of secondary analyte ions using suitable mass analyzers *viz.* magnetic sector, time of flight or quadrupole. There are varieties of primary ion sources and the modes of operation employed in this technique and their selection is dependent on the application.

The material under investigation undergoes bombardment with the energetic primary ion beam (Fig. 1.8) which is selected based on the electrochemical nature of the analyte material. The typically used primary ions for various analyte elements are as given below:

Primary ions	***Type of element /application***
O_2^+	Electropositive element
Cs^+	Electronegative element
O^-	Less conductive material
Ga^+	High lateral resolution

The primary ions sputter out analyte material which consists of positive or negative secondary ions along with the neutral atoms or molecules. The secondary ion current (I_s) can be expressed in terms of charge state (q), primary ion current (I_p), sputtering yields (Y), analyte concentration (C) and transmission of the instrument (T) and ionization cross section (α) as follows:

$$I_s = q \,.\, I_p \,.\, Y \,.\, \alpha \,.\, C \,.\, T$$

Typical values for some of the above parameters are: $Y = 0.1 – 10$, $T = \sim 0.3$, $\alpha = 0.1 – 10^{-6}$. The large variation in α is mainly responsible for the inaccuracy in the quantitative measurements.

Some of the major advantages of SIMS are its very high sensitivity in ppb range and very high depth resolution of the order of 0.1 nm. It can also be used to analyse light elements like H, C, O and N which are generally difficult to be analysed with other techniques.

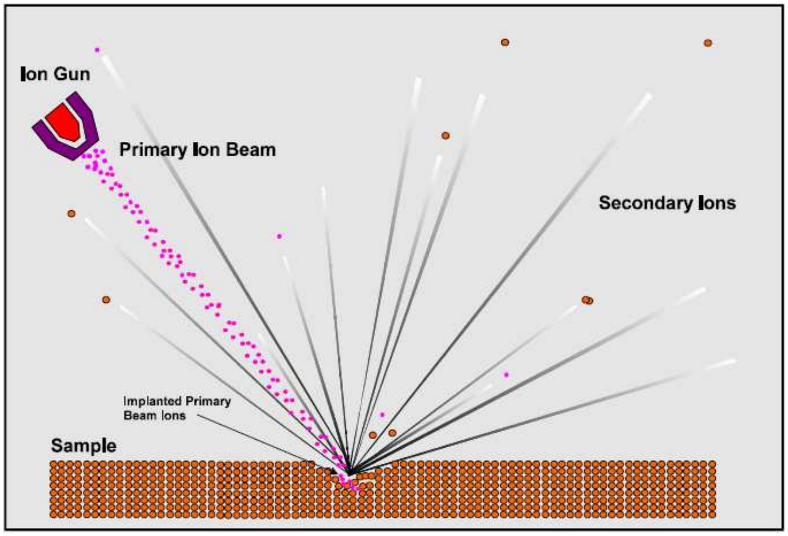

Fig. 1.8: Schematic showing the secondary ionization

The different types of modes for the operation of SIMS are: Static, dynamic, line/ gate scan, mass spectrometry mode, isotope ratio and imaging mode. The static mode is used for the compositional analysis of few top layers of the material. It uses very low primary currents (~nA/cm^2) and ultra high vacuum conditions (10^{-9} – 10^{-10} torr) so that soft desorption of the top layers can take place at very low sputtering rate (~0.1nm/hr). Dynamic mode is used for the depth profile of the material. It uses higher primary currents (~ µA to mA/cm^2) which can generate a sputtering rate of 0.1 nm/s. High sensitivity measurements (sub ppb) with depth resolution of 0.1nm can be carried out in this mode. The line / gate scan provides concentration profiling along a line over the surface of the material. It uses microscope mode for line scan and microprobe mode for gate scan. In case of microscope mode the primary ion beam is focused on very small area of the specimen which is moved to take scan. In case of gate scan the larger area (500 µm x 500 µm) of the specimen is exposed to ion beam whereas the analysis area is defined by electronic gate which is moved to take scan. The mass spectrometry and isotope ratio modes are used for the compositional analysis and isotopic ratio measurements of very small amount of material loaded in the ion source of SIMS. In imaging mode the surface and depth profiling are combined to generate 3d images of the specimen in terms of various concentrations of constituent elements.

1.3.7 Matrix assisted laser desorption ionization (MALDI)

It is a soft ionization technique [4, 9] used for the ionization of bio-organic molecules such as DNA, proteins, peptides, sugars and large organic molecules such as polymers and other macromolecules. It provides very high resolution and mass range in combination with time of flight (TOF) analyser. The ionization is based on absorption of laser energy by matrix and transferring it to analyte for ionizing it with negligible fragmentation.

The ion source consists of laser system with wavelengths ranging from ultraviolet (UV) to infrared (IR) e.g. Nitrogen lasers (337 nm), excimer lasers (193, 248, 308 and 351 nm), Q-switched, frequency tripled and quadrupled Nd: YAG lasers (355 and 266 nm), Er:YAG lasers (2.94 μm) and TEA-CO_2 (10.6 μm) lasers. The laser fluence and irradiance are important parameters to be controlled for the generation of ions. This is achieved by employing optical lens with beam attenuator in the optical path of laser. The laser beam with shorter pulse width in the range of a few nanoseconds and spot size of 100 – 200 μm is preferred. The shorter duration of pulse inhibits the degradation of the sample matrix due to heating and provides high resolution for analysis with TOF. Most of the MALDI instruments use UV nitrogen lasers (337 nm, 3 ns pulse width) whereas IR lasers (with pulse width 6 – 200 ns) are restricted to applications where its deeper penetration offers advantages e.g. for the direct desorption of analytes from sodium dodecyl sulfate gets or thin layer chromatographic plates.

The analyte material is mixed with suitable matrix exhibiting high absorption efficiency for laser employed for the analysis. The mixture of analyte and the matrix is deposited on sample plate and dried to solid form. The laser energy is absorbed by the matrix molecules and transferred to the analyte molecules thereby desorbing them in form of ions.

The matrix to analyte molar ratio is optimised for the generation of ions with lower laser fluence. In case of high molar ratio of matrix to analyte the less availability of analyte molecules requires large fluence for the production of ion. However for lower ratio the efficiency of energy absorption is reduced due to lower concentration of matrix molecules.

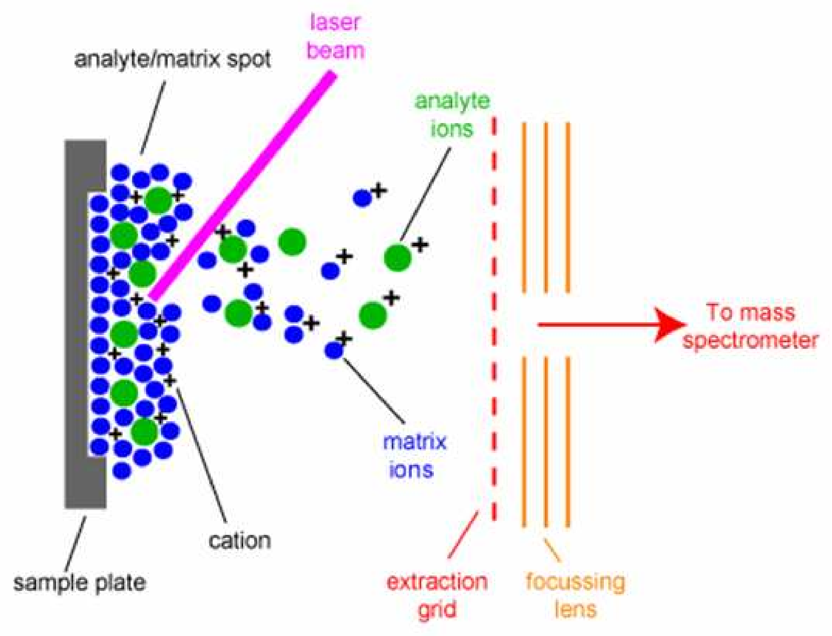

Fig. 1.9: Schematic presentation of ionization process in MALDI

In case of UV-MALDI, matrix is based on some aromatic core with a suitable functional group to achieve desired properties. In case of IR-MALDI, the requirements are not stringent as wavelengths up to 10 μm are easily absorbed by O-H and N-H stretch vibrations or C-O and O-H bending vibrations. Some of the commonly used matrices for UV-MALDI are-picolinic acid (PA), 3 hydroxy picolinic acid (HPA), 3 Amino picolinic acid (APA) for DNA ; 2, 5 hydroxy benzoic acid (DHB) for oligosaccharides; α-cyano-4-hydroxycinnamic acid for peptides and smaller proteins; dimethoxy-4-hydroxycinnamic acid (sinapinic acid) for proteins etc. In general a polar matrix is used for a polar analyte and a non polar analyte is preferably combined with a non polar matrix.

1.3.8 Electro-spray ionization (ESI)

It is a soft ionization technique [10, 11] employed for the analysis of large, non-volatile, chargeable molecules such as proteins and nucleic acid polymers. It incorporates desorption of analyte ions from solution to gas phase. The solution is composed of a volatile solvent and the ionic analyte molecules. It is an alternative technique to MALDI with an added advantage of higher mass range owing to very high charge state achieved with ESI. Moreover, the ionization occurs in atmospheric pressure which circumvents the restriction imposed on the solvent required to make the analyte solution in case of ionization under vacuum.

An ESI ion source consists of hypodermic needle held at a voltage of 3 – 4 kV with respect to a surrounding cylindrical electrode (Fig. 1.10). The dilute sample solution is pumped through the needle at a flow rate of 5 – 20 μl min^{-1}. The solution is electro- sprayed out of the needle in the form of aerosol and expands into counter current stream of dry nitrogen gas that helps in evaporation of the volatile solvent from the aerosol droplets. With the evaporation of the volatile solvent from the large droplets, the charge density increases thereby increasing the electrostatic repulsion among charged molecules in the droplets leading to the coulomb fission of the droplets into molecular ions. A small portion of the sprayed material enters the aperture of a short capillary (0.2 mm diameter) that interfaces the atmospheric pressure region to the first pumping stage (~1 mbar). In this region, the rate of dessolvation of aerosol is increased and most of the gas is pumped out. The analyte ions are further taken by the skimmer cone and passed to the high vacuum portion where by complete dessolvation of the droplets occur and the molecular ions of analyte are available for the further analysis using mass analyse and detector.

The conventional ESI ion source has some limitations in terms of limited flow rate, volatility and polarity of the solvent thereby restricting its use as liquid chromatography (LC) MS interface. These limitations are circumvented in different types of modified ESI sources. Some of them are: pneumatically assisted ESI, ultrasonic nebulizer and nano-Electrospray. In case of pneumatically assisted ESI larger flow rates up to 10-200 μl min^{-1} can be handled. The ultrasonic nebulizer handles flow rates of 50 - 100 μl min^{-1}. The nano electro spray produces droplets of size less than 200 nm (much smaller than 1 – 2 μm as produced by conventional ESI) and allows for high polarity solvents such as pure water with smaller consumption of sample as compared with conventional ESI.

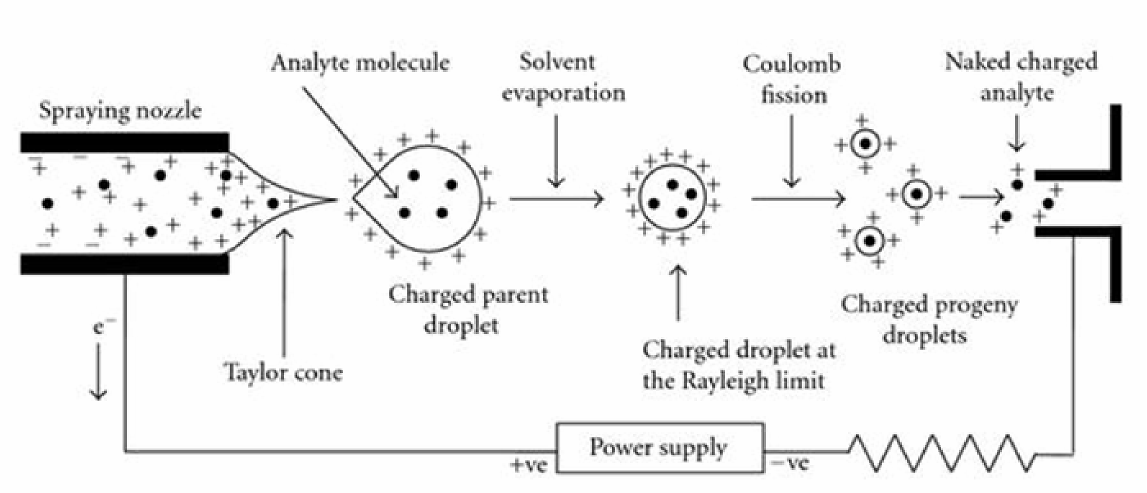

Fig. 1.10: Schematic showing the ionization mechanism in ESI source

1.4 Analyzers

1.4.1 Magnetic Sector

The magnetic sector analyser [19-23] is employed in mass spectrometers used for the precise isotopic ratio measurements of the analyte elements. It is a prime component of the mass spectrometer that decides the resolution and overall foot print of the instrument. It exhibits unique feature of passing ions (within given mass range) simultaneously thereby making provision for their simultaneous collection on different collectors of multi-collector system which increases the precision of given analysis. The separation of ions with different m/q ratio is achieved due to different Lorentz forces applied by the magnetic field on the analyte ions with different m/q ratio. The ion traverses a circular path of radius (*r*) which is related to mass '*m*' and charge '*q*' of the analyte ion by following equation.

$$m/q = (B^2 . r^2 / 2V) \tag{1.8}$$

Where *B* is the magnetic field in the magnetic analyser and *V* is the accelerating potential of the analyte ion.

The ions produced in the ion source of a mass spectrometer are accelerated by an accelerating potential of 5 – 10 kV in the ion source and introduced to magnetic analyser in form of diverging ion beam. The ion beam undergoes deflection and separation (as per m/q) during its passage through the magnetic sector and after leaving the magnetic field it re-focuses at a location dependent on the geometry of the magnetic sector as shown in the Fig. 1.11. The magnetic sector geometry is characterized by parameters: radius of curvature, deflection angle and entry/ exit angles of ion beam with respect to entry/ exit boundary of the magnetic field. The system parameters like resolution, dispersion and magnification are decided by the geometry of the magnetic sector.

The dispersion is defined as the separation between the ions of two different masses (say m and $m + \Delta m$) at the refocusing points of the respective ion beams. It is given by the product of relative mass difference $\Delta m/m$ (between given ion beams) and the dispersion factor (d) as shown in equation below.

$$\boldsymbol{D_m = d \,.\, \Delta m/m} \tag{1.9}$$

The dispersion factor d is dependent on the geometry of the magnetic sector. For example in normal geometry the value of d is one. However in case of stigmatic geometry it is two i.e. double of that for normal geometry.

In early development period of mass spectrometry, normal geometry was employed where ion beam entrance and exit in the magnetic sector was normal to the boundaries of the magnetic sector i.e. entry and exit angles were 0° as shown in Fig. 1.11. In this case the distances of object (source slit) and image (detector slit) from entry and exit boundary of magnetic sector respectively are equal to the radius of curvature of the analyser. The normal geometry provides limited dispersion and resolution. The focusing of the ions occur in a plane (median plane) orthogonal to the magnetic field so that the ions diverging in the plane parallel to magnetic field are not collected by the detector which leads to loss of sensitivity of the mass spectrometer. These limitations were circumvented by extended geometry or stigmatic geometry.

In case of stigmatic geometry the ion beam entry and exit from the boundary of magnetic sector are inclined at some specific angles. In case of symmetric stigmatic geometry the entry and exit angles are 26.5° with respect to normal at entry and exit boundaries of the magnetic sector as shown in Fig. 1.12. In this case, the object and image points of ion beam (with respect to entrance and exit boundary of magnetic sector respectively) are located at distance equal to double the radius of curvature of magnetic sector. The dispersion and hence resolution for this geometry also become double of those in case of normal geometry. Moreover, the stigmatic geometry also provides focusing of the ion beam in a plane along the magnetic field along with the focusing in median plane and the re-focusing points for both the planes occur at same location. This results into higher transmission of the magnetic analyser thereby providing higher sensitivity of MS.

The magnification is defined as the ratio of cross sectional width of ion beam at refocusing point to that at the source point. In case of symmetric normal and stigmatic geometries it is unity i.e. magnification is not affected by changing geometry from normal to stigmatic as long as it is symmetric.

The resolution of any mass spectrometer is related to the ratio of dispersion to the magnification of the ion beam. As in case of stigmatic geometry dispersion is doubled with same magnification of unity, the resolution also gets doubled. For two adjacent ion beams with masses of ions as m and $m + \Delta m$, resolution conventionally defined as $m/\Delta m$ and is given by:

$$\boldsymbol{R = d \,.\, r \,/\, (W_c + W_i)} \tag{1.10}$$

Where $\boldsymbol{r}$ – radius of curvature of magnetic sector, $\boldsymbol{W_c}$ - the width of detector entry slit, $\boldsymbol{W_i}$ - the width of ion beam cross section, $\boldsymbol{d}$ – dispersion factor.

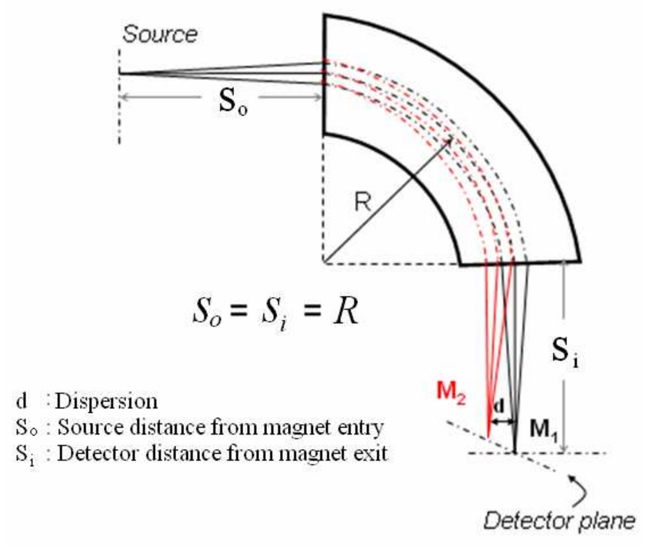

Fig. 1.11: Ion beam focusing in case of normal geometry magnetic sector with 90° deflection angle

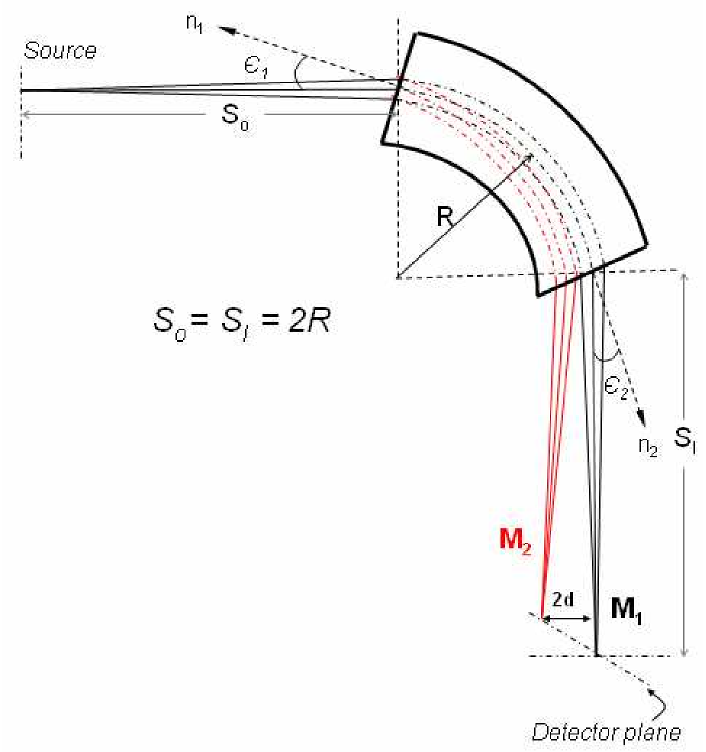

Fig.1.12: Ion beam focusing in case of stigmatic geometry for a 90° deflection angle; the entry angle (ϵ_1) and exit angle (ϵ_2) of the ion beam with respect to entry and exit boundaries of the magnet are 26.5° each

The ion beam width W_i is mainly decided by the source slit width but owing to various factors *viz.* instability in the power supplies related to acceleration and analyser magnetic field, energy spread of ions and in-homogeneity of the magnetic field of magnetic analyser various aberrations are introduced to the focusing of ion beam which increase the cross sectional width of ion beam and hence reduce the resolution of mass spectrometer.

1.4.2 Radio frequency (RF) Quadrupole

The RF quadrupole [12] is widely used analyser in mass spectrometers employed for compositional analysis of materials. Because of its rapid scanning capabilities it has gained importance for gas and liquid chromatography mass spectrometry where fast scanning is required. The advantages of RFQ (radio frequency quadrupole) are: 1) high transmission 2) light weight and compactness 3) more economic than other type of analyzers 4) Low acceleration voltage than magnetic analyser 5) very fast scanning speed. The various applications of RFQ includes: Residual gas analyser for partial pressure measurement, elemental and isotopic analysis in combination with ICP, EI and secondary ion sources, organic analysis in GC and LC chromatography, tandem mass spectrometry for the structural analysis of organic molecules.

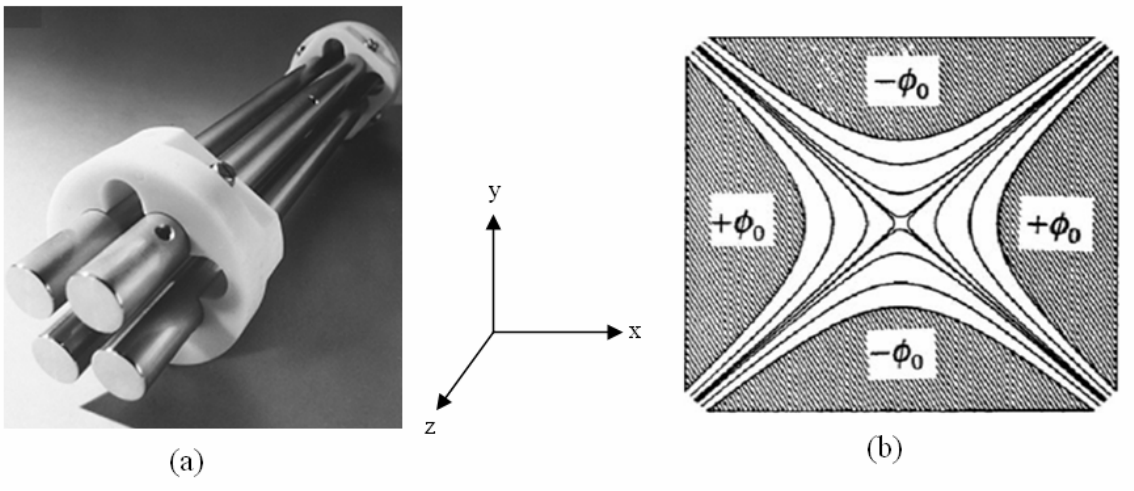

Fig. 1.13: (a) The photograph of Quadrupole (b) the electric field distribution in xy plane

A quadrupole consists of four hyperbolically or cylindrically shaped rods placed parallel to each other on the vertices of square with inter rod distance dependent on the radius of rods as shown in the Fig. 1.13. The pairs of opposite rods are shorted electrically and both the pairs are held at DC and RF potential of opposite polarity. Considering the case when positive DC potential is applied on the rods along *x-z* plane and negative DC potential is applied on rods along *y-z* plane, the electrostatic field is generated in the region between the rods in such a way that the positively charged particles undergo focusing along *x-z* plane and de-focusing along *y-z* plane. The focusing and defocusing of charged particles as produced by DC fields are mass independent. The application of RF potentials on the same sets of rods generates oscillations in the path of charged particles and deviate them from the stable paths traversed in the pure DC field. In *x-z* plane, the RF field will try to deviate the charged particles from focusing and the deviations are more effective for lower masses as compared to higher masses thereby making it a high (mass) pass filter in *x-z* plane. In *y-z* plane the RF field deviates the charged particles from defocusing and here again lower masses are more deviated from the defocusing action thereby making it a low (mass) pass filter along *y-z* plane. The combined effect of focusing and defocusing of charged particles in both the planes (*x-z* and *y-z*) allows only certain mass range to pass through thereby making it a mass filter. The deviations produced by RF field are mass dependent and for given values of DC and RF field charged particles only within particular mass band are allowed to pass through the quadrupole. Hence for charged particles with given charge state, RF quadrupole works as mass filter. The mass scanning is carried out by changing the value of RF and DC potentials while maintaining the same ratio of DC and RF potential.

The field distribution (*Φ*) inside the quadrupole consisting of hyperbolic rods with DC (*U*) and RF (*V*) potentials is given by:

$$\Phi(x,y)=\frac{(x^2-y^2)}{{r_0}^2}\phi_0$$

$$\Phi_0=U+V\cos\omega t$$

Where x and y are the co-ordinates in x and y axis, r_o – radius of inscribed circle in x-y plane with centre at z axis, Φ_o – potential on one pair of rods with respect to other pair, U – DC potential, V – amplitude of RF potential.

The electric field (E) and force (F) at charge particle with charge (e) at any point (x, y) is given by:

$$\vec{E} = -\nabla\Phi(x,y)$$

$$\vec{F} = e\vec{E}$$

The equations of motion (Matheiu's equations) of charged particle are given by:

$$\frac{d^2x}{dt^2} + \frac{2e}{m_i r_0^2}(U + V\cos\omega t)x = 0$$

$$\frac{d^2y}{dt^2} - \frac{2e}{m_i r_0^2}(U + V\cos\omega t)y = 0$$

$$\frac{d^2z}{dt^2} = 0$$

The solution of above equations for the stable trajectories of charged particles inside quadrupole exist for particular values of parameters a and q defined as:

$$q = \frac{4eV}{m\omega^2 r_0^2} \qquad a = \frac{8eU}{m\omega^2 r_0^2}$$

The set of values for a and q for stable trajectories are shown in Fig. 1.14

Considering the 1st stability region, the stable trajectories of charged particles exists only for the set of a, q values as shown in Fig. 1.15. For given geometry of quadrupole and frequency of RF field the values a and q are decided by the DC potential, the RF potential and m/q of ion. The plot of a against q for given ratio of DC and RF potential is called as load line. For higher resolution, the values of DC and RF potentials are selected in such a way that the load line passes through a region near the tip of the stability zone. The stable region for both x

and *y* trajectories will allow charged particles to pass through the quadrupole and hence it will decide the mass resolution.

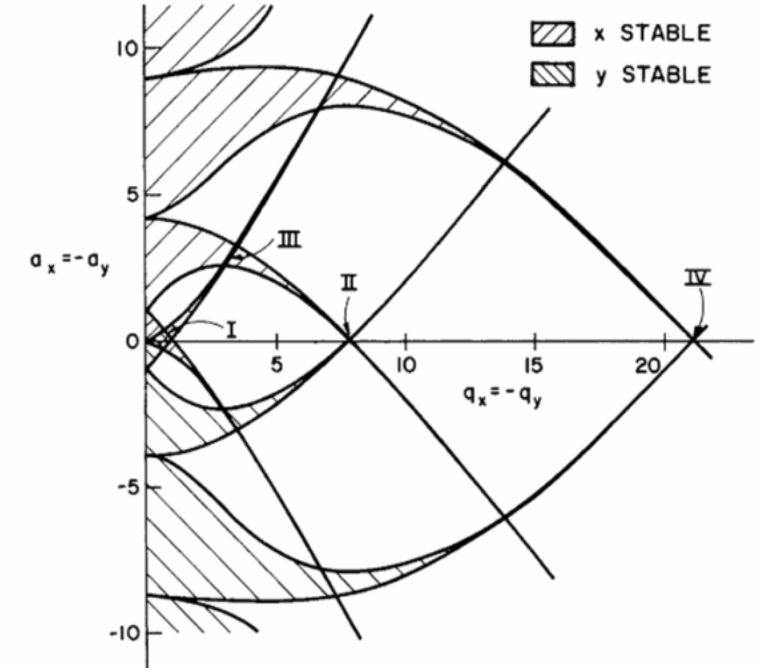

Fig. 1.14: The stability region of quadrupole

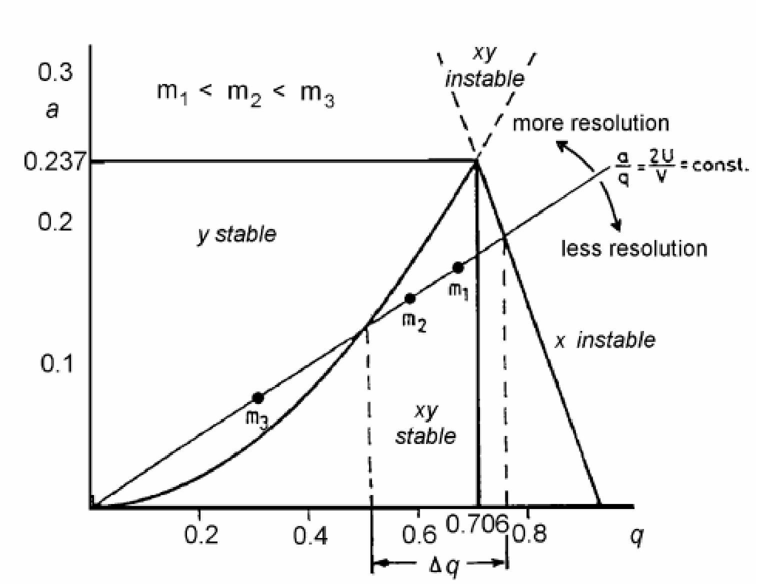

Fig. 1.15: Conditions for high resolution in 1st stability zone

The resolution is also decided by the number of oscillations undertaken by the charged particle within quadrupole field and in turn depends on time spent by charged particle in the same region. The parameters contributing to these requirements are kinetic energy of charged particle as decided by the accelerating potential (V_z) in the ion source used for generating charged particle, length of quadrupole rod (L) and frequency of RF field. The mass resolution of quadrupole with rod diameter (r_o), RF potential V_m is given by:

$$M_m / \Delta M_{min} = \frac{L^2}{r_o^2} \frac{V_m}{V_Z} \frac{1}{290}$$

The design parameters of quadrupole like radius, length of rods and the mechanical tolerances involved in their fabrication and assembly are very critical parameters affecting the mass range and resolution of the quadrupole.

1.4.3 Time of Flight (TOF) analyser

The TOF analyser [4, 13] is widely employed for the applications which require very high resolution and mass range to analyse molecules or molecular clusters of very high molecular mass. Owing to very large mass range and resolution provided by TOF, it is mostly used with MALDI and ESI ion source in biological applications. The principle of separation of ions (as per their mass to charge ratio) is based on mass dependent arrival times of ions with same kinetic energy after passing through field free drift space of given length. The arrival of respective ions is recorded by the fast response detector and is calibrated in term of their masses.

The time (t) taken by any charged particle in a field free region of length ‘L’ is given by:

$$t = L/v \tag{1.11}$$

$$v = \sqrt{(2\, e\, V / m)} \tag{1.12}$$

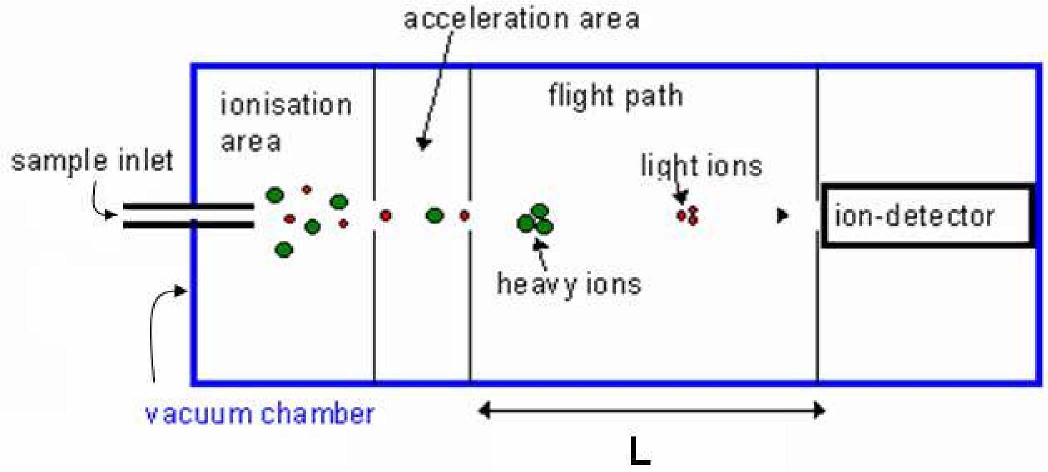

Fig. 1.16: Schematic showing the separation of ions in TOF analyser

Where v, m are the velocity and mass of charged particle; V is the accelerating potential of the charged particle

Eliminating v from equation 1.11 and 1.12 above:

$$t = L \sqrt{[m / (2 e V)]} \tag{1.13}$$

Above equation shows that the arrival time of a charged particle is directly proportional to square root of its mass. The lighter mass takes less time to travel a given distance in the TOF and hence reaches the detector earlier than the heavier masses. The difference in the arrival times of the ions with different masses is exploited by using a fast response detector that can detect ions reaching with short time intervals in between. The pre requisite for TOF measurements is a detector with very fast response on the time scale of nano seconds. This was the main hurdle in achieving good resolution in the early period of development of TOF instruments. The dependence of resolution on smaller detectable time intervals is further explained below.

Taking logarithm and then differentiating eq. 1.13 for t and m.

$$m/\Delta m = \tfrac{1}{2}\, t/\Delta t \tag{1.14}$$

i.e. mass resolution ($m/\Delta m$) is inversely proportional to Δt, the difference in the arrival time between two ions with Δm mass difference at mass m. This implies that the resolution depends on the response time of the detector. The faster is the response time of the detector, smaller will be the detectable time interval between ions of adjacent masses and hence higher resolution. At very high mass the time difference per unit mass difference decreases which puts limit on the resolution of TOF. For example the Δt per unit mass is 114 ns at mass 20 amu, 36 ns at 200 amu and 11 ns at mass 2000 amu for ions accelerated to 19.5 kV and the flight path of 2m.

The equation 1.14 also implies that resolution depends on the arrival time of given mass m which in turn depends on length *L* of flight tube and kinetic energy of the ion. For *t* to be higher requires the larger length of flight tube and lower kinetic energy. However larger *L* will increase the transmission losses along with the foot print of the instrument. The lower kinetic energy will also result into lower sensitivity and higher relative energy spread of the ions. Therefore the length and kinetic energy are optimised to certain values. In general, flight tube length of 2-5 meter and accelerating potential around 5 - 20 keV are used in a TOF instruments.

Apart from fast detector, other requirements for obtaining higher resolution in TOF are:

1. The starting time of the ions should be same. This requires the generation of ions in pulses of very short duration (less than the time resolution of the detector). The pulsed laser ionization is most suitable for TOF. In case of other ionization techniques vis. electron impact the extraction of ions is executed with very short pulses of extraction potential in the ion source. The advent of laser source with femto second pulse size makes MALDI-TOF an ideal combination for the analysis of bio molecules with very large molecular masses.
2. The ions in a given pulse should exhibit same kinetic energy i.e. smaller energy spread. The main reasons for the higher energy spread are: 1) The random thermal energy of analyte particles which is added to the kinetic energy of ions after their acceleration and hence produces energy spread. 2) Generation of ions at different locations with different electrostatic potential so that they acquire different kinetic energy during their acceleration within the ion source.

The energy spread can be circumvented by different techniques namely - supersonic jet technique, delay extraction technique and reflectron type TOF. In super sonic jet technique the gas sample is introduced under high pressure difference so that formation of supersonic jet takes place and the sample molecules get cooled to very low temperature thereby reducing the energy spread. In delayed extraction technique, the difference in thermal energies is compensated by the different potentials applied at the time of their extraction from the ion source. The ions are allowed to spread for short duration before their extraction so that ions with higher thermal energy moves towards the exit slit faster than the low energy ions. At the time of extraction the field distribution near the exit slit is such that the higher energy ions are accelerated to lower potential and vice versa thereby the energy spread is reduced. The reflectron is electrostatic mirror which is placed at one end of the TOF (Fig. 1.17). The ions penetrate against the repelling electric field in such a way that ions with higher energy travels longer distance as compared to that with lower energy. This allows the ions to reach the detector at same time irrespective of their energies and hence energy focusing takes place.

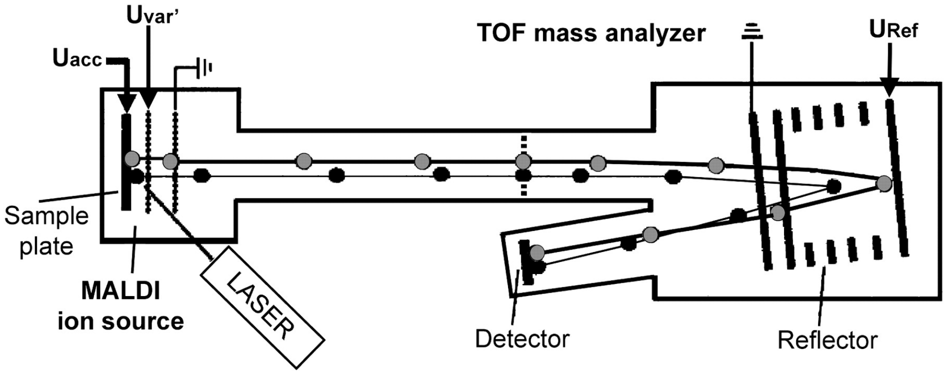

Fig.1.17: Schematic showing the Reflectron type TOF analyser

During early development period of TOF the resolution was limited to 50 – 100 mainly because of unavailability of fast detector. The development of fast response detectors could increase the resolution but the higher energy spread still limited it up to 1000. The advent of techniques for cooling of sample could increase the resolution to around 4000. Nowadays a resolution of as high as 50000 – 100000 is achievable with the help of Reflectron TOF, delayed extraction technique and lasers with smaller pulse width in the range of femto seconds.

1.4.4 Ion trap analyser

The ion traps [14] are widely used for applications related to biological and chemical sciences. These are suitable for the studies of large bio-organic molecules due to high mass resolution, mass range and sensitivity. Owing to the confinement capability of the charged particles, they are employed for the gas phase ion chemistry and elucidation of molecular structures by the use of repeated stages of mass selection known as tandem mass spectrometry or MS/MS techniques. The technique is advantageous over other competitive MS-MS techniques by the fact that different MS steps can be executed in the same set up in shorter duration of time as compared to other techniques which involve different setups for each MS stage.

There are two types of ion traps: Linear quadrupole ion trap and three dimensional quadrupole ion trap. The linear (quadrupole) ion trap (LIT) consists of quadrupole (as explained in earlier section) with electrodes of higher potential on both the ends as shown in Fig. 1.18. The RF potential at quadrupole rods and DC potential of same polarity on the end electrodes enable the trapping of ions along the axis of the quadrupole. It is capable of scanning the mass of ions, the radial and axial excitation of ions and precursor ion selection for MS/MS experiments. It is used in combination with other quadrupoles or Fourier transform ion cyclotron resonance analyser to enhance the sensitivity of the measurements related to molecular ion studies.

The quadrupole ion trap (QIT) creates a three dimensional RF quadrupole field to store ions within defined boundaries. It consists of two hyperbolic electrodes serving as end caps and a ring electrode placed in between. The end caps are electrically shorted and DC and RF potentials are applied on them with respect to the ring electrode.

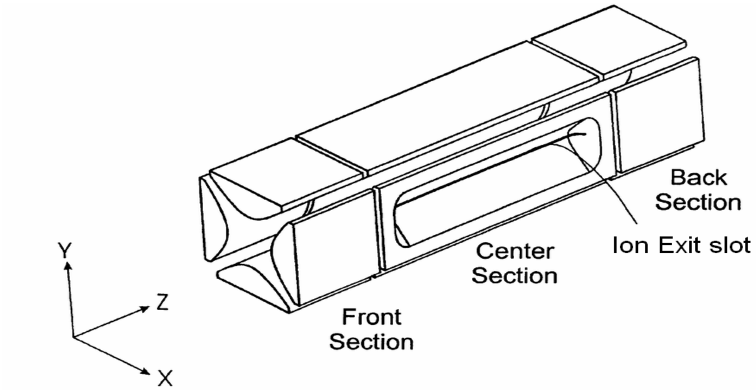

Fig. 1.18: Schematic of a linear quadrupole ion trap

The working principle of QIT is based on creating stable trajectories of ion with certain *m/q* or with in some *m/q* range by generating trapping potential region within the QIT with the help of suitable DC and RF potentials applied on the ring and the end caps. The basic theory of motion of charge particles in QIT is similar to that for RF quadrupole as explained in earlier section with a difference of using *a* and *q* parameters in radial and azimuthal co-ordinates instead of x and y co-ordinates earlier.

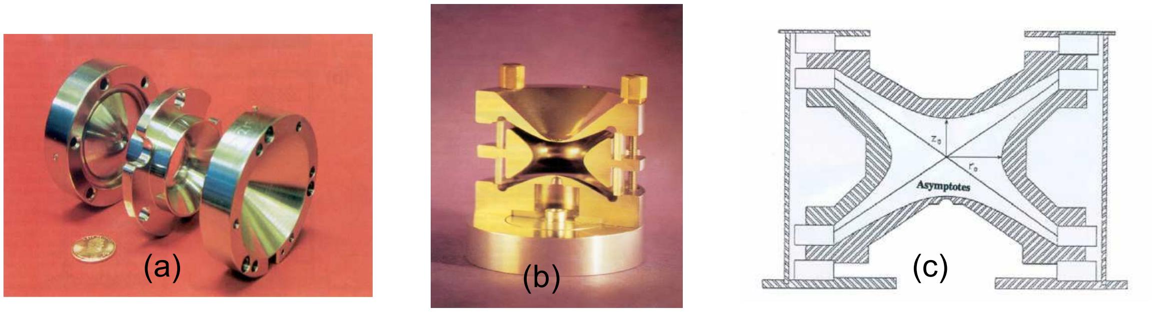

Fig. 1.19: Quadrupole ion trap. (a) Three electrodes of ion trap shown in open array. (b) ion trap cut in half along the axis of cylindrical symmetry. (c) Schematic of ion trap showing the asymptotes and dimensions r_o and z_o

The different modes of operation of QIT are: the mass selective stability mode, mass selective instability mode, resonant ejection and axial modulation. In mass selective stability mode, ions of desired mass range are trapped by setting suitable parameters followed by their ejection by applying negative pulse across the end caps. The mode is rarely used because of its slow speed and low sensitivity. In case of mass selective instability mode ions of all masses are firstly trapped. Subsequently, with the end caps grounded an RF voltage scan is applied to the ring electrode causing consecutive ejection of ions in the order of their *m*/*q* values. This mode is relatively faster than mass selective stability mode but suffers from poor efficiency because of space charge effects. The resonant ejection is the mostly used mode in QIT. It is based on ejection of ions with particular axial secular frequency by applying a supplementary RF voltage (of few milli volts) across the end electrode. The scan can be carried out in forward or reverse manner allowing for the selective storage of ion of a certain *m*/*q* value by eliminating ions below and above particular *m*/*q* value. Axial excitation can also be used to cause collision induced dissociation (CID) of the ions. The axial modulation incorporates application of modulation voltage with a fixed amplitude and frequency between the end caps during RF scan. The frequency is chosen slightly below the half of fundamental frequency. The mode is mainly employed to facilitate the efficient ejection of ions in mass selective instability mode during RF scan to circumvent the problems related to space charge effect.

In early developments QIT were used with internal ion sources whereby ionization occurs inside the region of QIT limiting its applications. However the development of techniques to interface ions generated outside has increased its versatility. In present MS systems QIT can be combined with a number of ionization techniques like electron impact, chemical ionization, atmospheric pressure ionization and electro spray ionization etc. The resolution as high as 10^6 and mass range up to 70,000 amu by QIT has been reported.

1.5 Detectors

1.5.1 Faraday collector

The Faraday detector [1-3, 24, 25] is employed for the measurement of ion beam in mass spectrometers with ion beam intensity above 10^{-14} A. It is typically used in applications related to precise isotopic ratio measurements on magnetic sector mass spectrometers. The major advantage of the detector is the precise measurement of ion current because of absence of any mass discrimination effects as present in other types of detectors like electron multiplier. However it has slow response because of the high resistance used in the amplifier which exhibit high RC (resistance-capacitance) time constant. The slow response along with its low detection limit (10^{-14}A) make this detector not suitable for application like TOF-MS, trace elemental analysis and compositional characterization of materials.

A Faraday collector consists of a main collector, a secondary electron suppressor and entry aperture at ground potential as shown in the Fig. 1.20. The components are assembled together using proper insulations in between. The combination is covered with another metallic cover at ground potential to screen the collector from any stray charged particles. The principle of detection is based on measurement of the ion current using electrometer amplifier connected to the main collector. The charged particles impinge on the surface of main collector thereby transferring the charge to the collector surface that is connected to an electrometer amplifier. The rate of charging due to impinging ions is neutralized by an equivalent electronic current passing through the high resistance (typically 10^{11} ohm) connected in the feedback loop of the electrometer amplifier. The ion current is measured in terms of voltage drop across the resistor. For the isotopic ratio measurement a plurality of Faraday collectors are used in mass spectrometer. The ion beams corresponding to the different isotopes are collected in the respective Faraday collectors and the isotopic ratio is calculated using ion currents measured for the respective isotopes.

The measurement by Faraday collectors suffers from various errors *viz*. Johnson's noise due to high resistor in amplifier, non uniform amplifier gain from one collector to another. The noise of the amplifier can be circumvented by putting the amplifiers under vacuum (~10^{-1} torr) and controlling the temperature of the amplifiers within +/- 0.1°. The amplifiers are calibrated using stable current source on daily basis prior to analysis schedule to circumvent the error due to gain variation with time. Apart from this, various methodologies have been developed to address the error related issues viz. using multi-dynamic mode of ratio measurements and virtual amplifier concept [26]. Using Faraday collectors the precision of the order of 5 ppm can be achieved for the isotopic ratio measurements of some of the elements like Sr and Nd.

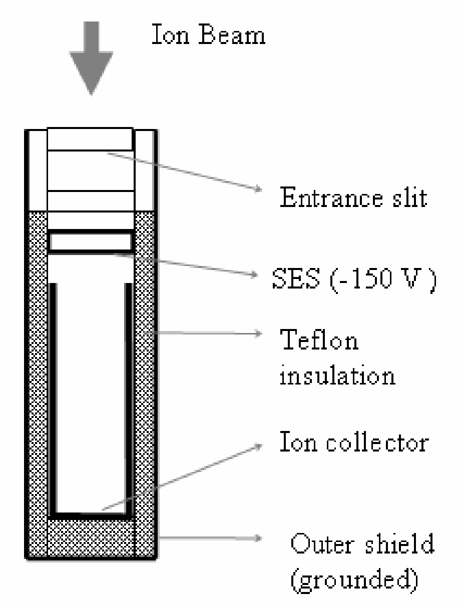

Fig. 1.20: Schematic of a Faraday collector

1.5.2 Electron Multiplier detectors

The Electron Multiplier detector [1-3, 26] is used for the measurement of very small ion currents below 10^{-14} A that are not measurable by Faraday collector. It is mainly employed for trace elemental detection or compositional analysis involving concentration of analyte in the range of ppm or below. The detection principle is based on the amplification of ion current by multiplication of secondary electrons at different stages of the multiplier so that the total electron current produced at the last stage is high enough to be measured by an electrometer amplifier. The major advantages of the detectors are their high gain, high dynamic range and fast response. The limitations of electrometer amplifier are: 1) gain variation with time and 2) gain dependence on mass of the ions under measurement. The different types of electron multiplier detectors are: Discrete dynode electron multiplier, Continuous dynode or Channeltron, Micro-channel plate (MCP) and Daly detector.

1.5.3 Discrete dynode electron multiplier detector

It consists of plurality of dynodes (Fig. 1.21) [1-3, 26] made of materials with high secondary emission coefficient *viz*. Copper-Beryllium or Aluminium. The dynodes are electrically biased in such a way that electrons generated at first dynode get accelerated and directed towards adjacent dynode down the line. The first dynode (conversion dynode) is kept at negative potential and the last dynode at ground potential for the measurement of positive ions. In case of negative ions the conversion dynode is at ground potential and the last dynode is kept at positive voltage. The incident ions under measurement are allowed to hit at the conversion dynode to generate secondary electrons with a multiplication factor of β. These electrons are accelerated to second dynode due to positive electrical bias and further generate secondary electrons with multiplication factor Γ. The process of electron multiplication continues till the last dynode where total number of secondary electrons produced is $\beta.\ \Gamma^N$ where N is the number of dynodes. This corresponds to the ratio of output current to the input current of the detector and is called as gain. Along with the dependence on design and material characteristics of the detector the gain also depends on the bias voltage, mass and energy of the ion under measurement. A discrete dynode electron multiplier can produce a gain as high as $10^7 – 10^8$ with a dark noise < 0.1 counts/sec. The main limit to the highest achievable gain is posed by non linearity due to the space charge effect and the emission of secondary ions at the dynodes (ion feedback effect) in the last stages of the detector.

There are two modes of measurements of ion currents - Analog mode and ion counting/ pulse counting mode. The analog mode is used for the ion currents generally above 10^{-16} A. It incorporates the measurement of output electron current integrated over time. In case of pulse counting mode, each ion is counted in terms of the pulses produced by the secondary electrons at the output. The detector is set at high gain and the numbers of pulses produced per unit second are recorded by the pulse counting unit. This can generate very accurate results as compared to analog mode for the ion current below 10^{-14} A. In the higher ion current region the measurement accuracy is limited due to dead time effects.

Another advantage of the detector is higher dynamic range due to the high bias current (> 100 μA) which extends the measurable range of the detector to higher ion currents. The main drawback of the detector is gain variation with time due to change in surface conditions. Another disadvantage is the mass discrimination i.e. gain variation with mass of the ion. This limits the use of this detector in mass spectrometer for precise isotopic ratio measurements. The detector must be shielded from any magnetic or electric field (in the surrounding) which can disturb the paths of secondary electrons and hence affect the gain.

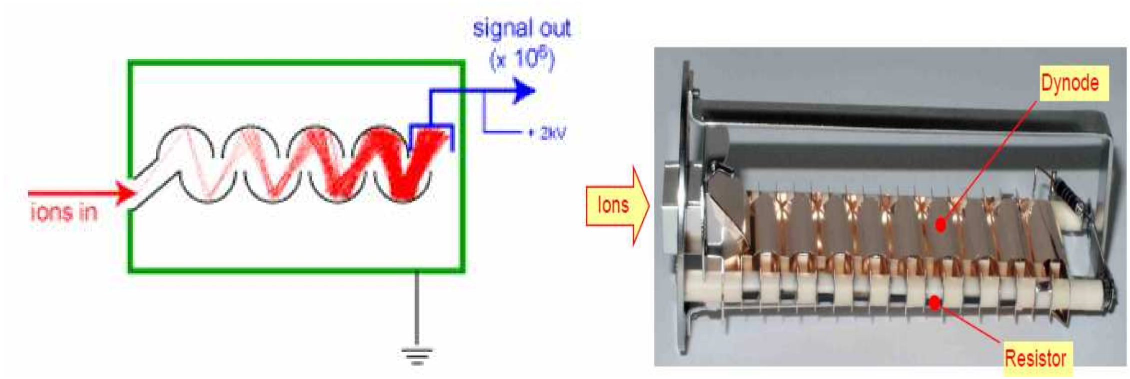

(a) (b)

Fig. 1.21: a) Schematic showing the working of discrete dynode electron multiplier b) Photograph of a discrete dynode EM

1.5.4 Continuous dynode detector/ Channel electron multiplier (CEM /Channeltron)

It is an alternative to the discrete dynode electron multiplier [27]. The main advantage is its compactness, durability and better gain stability as compared to discrete dynode type. However it exhibits lower dynamic range as compared to discrete dynode multipliers due to lower bias current.

CEM consists of tubular structure made of specially formulated lead silicate glass with inner diameter of 1 mm and outer diameter in the range of 2 – 6 mm. The electro-emissive surface of SiO_2 with thickness 200 nm is responsible for emission of secondary electrons.

Beneath this the conductive layer of lead (thickness around 2 μm) helps to electrically bias CEM and generating bias current. The input end of the tube is given conical shaping and the body is shaped in curve as shown in Fig. 1.22. During operation, the input and output ends of the detector are electrically biased with high voltage in the range up to 3 kV. The primary ion beam is allowed to fall on the input end of the detector to produce secondary electrons. An ion striking the input face of the device typically produces 2-3 secondary electrons which get accelerated towards the out put end due to positive bias. The electrons get multiplied due to further collisions within the electro-emissive surface of the detector to produce multiple electrons in the range of 10^7-10^8 (typically for a voltage of 2-3 kV applied across the multiplier). For the detection of positive ions, the input end is at negative potential and the out put end is kept at ground potential. In case of negative ions, input end is kept at ground potential and positive potential is applied on output end.

The gain of CEM depends on various factors *viz.* secondary emission coefficient of glass, the applied voltage to CEM and the length to diameter ratio of the CEM tube. The variation of gain of the CEM with applied voltage is shown in Fig. 1.23. The gain at higher voltage becomes non linear due to space charge effect. The ion feedback due to emission of secondary ions near the output end also limits the gain in the range of 10^4-10^5 in straight CEM. The curved shape helps in minimizing ion feedback and extends the gain to a range of 10^7-10^8.

Similar to discrete dynode type, it also suffers from mass discrimination effect which reduces the efficiency of the detector for higher masses causing errors in the concentration measurement of elements with different masses present in an analyte material. It can be circumvented up to some extent by introducing separate dynode at the input end of the detector. This also extends the life of the detector as the direct exposure can damage the surface of detector in case of ions of very high energy.

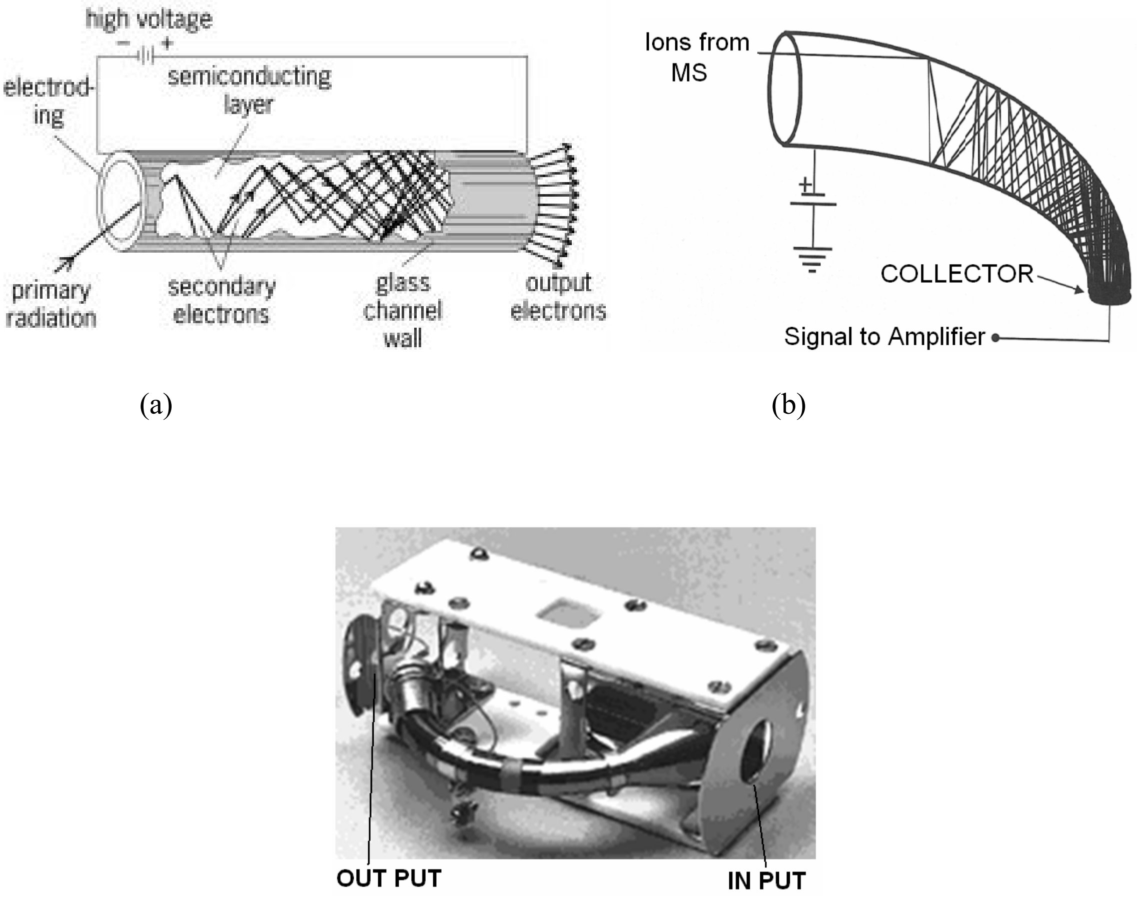

(a) (b)

(c)

Fig. 1.22: Channel electron multiplier a) Straight Channeltron b) Channeltron with curved shape c) The photograph of Channel electron multiplier

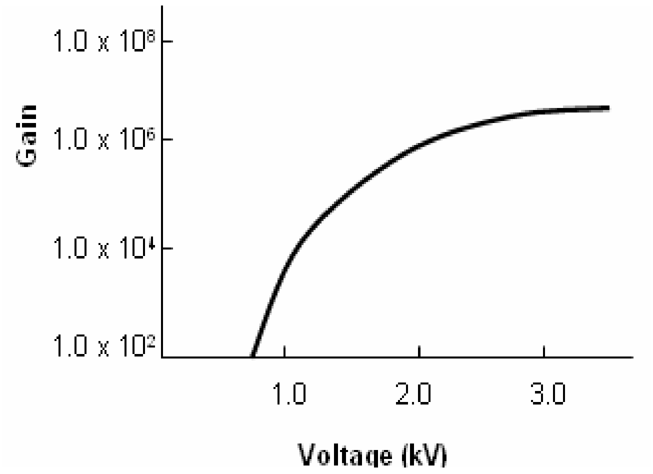

Fig. 1.23: Variation of gain with applied voltage across CEM

1.5.5 Micro-channel plate (MCP)

It is a two dimensional array of many small sized Channeltrons stacked together (Fig. 1.24) [28]. The detector is mainly employed for the measurement of ion currents in TOF-MS due to its fast response time in the range of 0.1 ns (much better than Channeltron). It can also be used for intensity profiling of the cross section of ion beams when used in combination with phosphor screen.

The detector is fabricated of glass fibers consisting of chemically dissolvable core glass and wall glass as lead silicate. The fibers are stacked together in lead glass substrate to form a boule which is sliced along a plane at an angle 8° - 15° with respect to normal to the channel axis. The core glass is removed by chemical etching leaving hollow lead silicates fibers. Subsequently, the reduction in hydrogen atmosphere converts the surface of fibers to semi conducting layer of lead. Each channel has cross section of 10 – 20 micron diameter and length around 0.5 mm. The channels are placed uniformly with separation of around 5 – 10 micron from each other. Each channel is provided with a parallel electric contact by coating of thin layer of Nichrome or Inconnel on the front and rear surfaces of MCP, which also serves as the input and output electrodes of MCP. The total resistance between the electrodes is of the order of 10^9 **Ω**. The MCP can generate electron multiplication (gain) in the range of 10^4 - 10^7 with ultra high time resolution < 0.1ns and spatial resolution around 10 μm.

Each channel in the MCP works as individual electron multiplier. The Primary ions falling on the input surface of MCP generate secondary electrons that get multiplied within each channel. The secondary electrons exiting from the output surface are collected on metallic electrode and measured using electrometer amplifier. Ion beam profiling can also be carried out using phosphor screen just beneath and parallel to the output surface of MCP. The phosphor screen is raised to positive potential around 3 kV to accelerate the secondary electrons (from MCP out put end) towards it to generate scintillation.

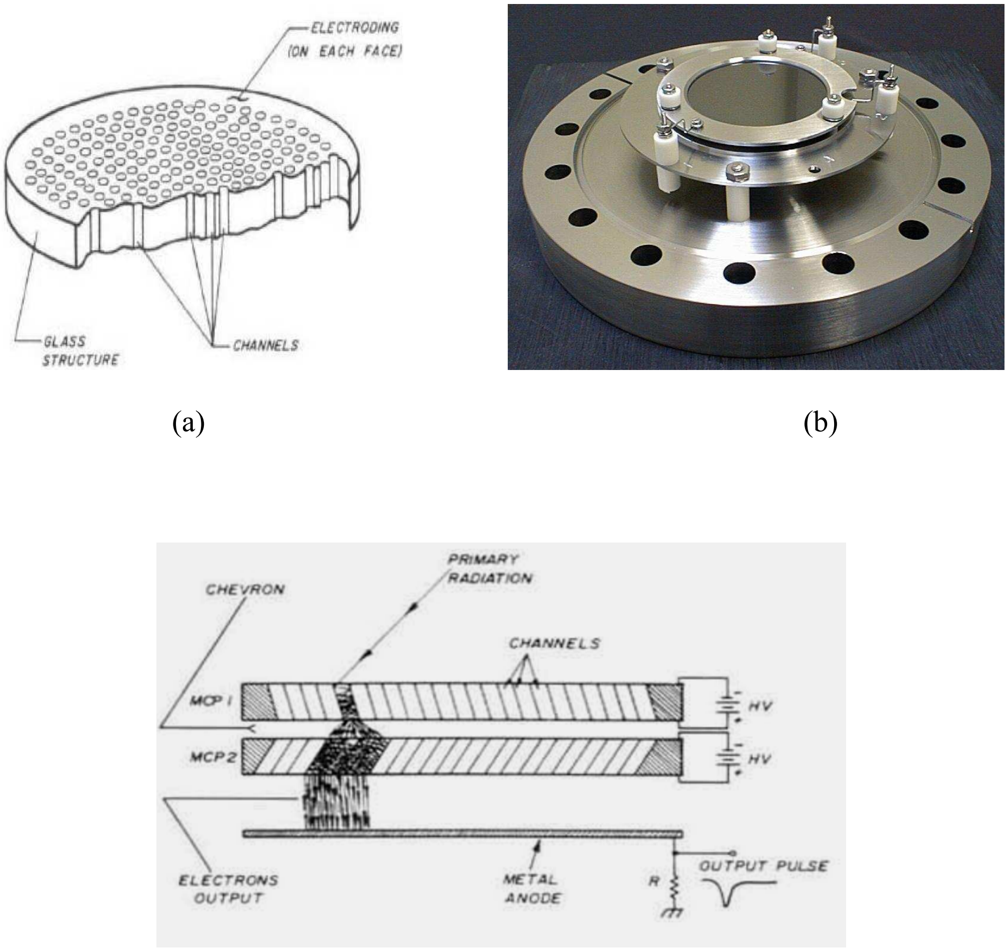

(a) (b)

(c)

Fig. 1.24: (a) Cut view of MCP (b) Photograph of MCP (c) chevron type MCP

The gain of single stage MCP is limited to 10^4-10^5 due to the ion feed back and space charge effect. This is circumvented by using two stages MCP (also called as Chevron type MCP) with configuration of channels as shown in Fig. 1.24c. The Chevron MCP is capable of generating maximum gain of more than 10^7, around two orders more than single stage MCP.

The main advantages of MCP are its higher gain and very fast response. Along with charged particles, it is also sensitive to UV radiations and X rays. The operation of MCP is not affected by the external magnetic field as in case of other detectors. However it also suffers from gain variations with time and mass discrimination and hence is not applied in precise isotopic ratio measurements. It is more delicate than other electron multiplier detectors and prone to any sudden changes in pressure and humidity of environment in which it is operated and hence has to be handled very carefully.

1.5.6 Daly detector

The Daly detector [29] is used as an alternative to other electron multiplier detectors. It has very low detection limits ranging up to 10^{-20} A. It consists of a metallic knob, a scintillator and photo multiplier tube as shown in Fig. 1.25.

The metallic knob (stainless steel make coated with Aluminium) is raised to high negative potential of 40 kV. The detection process consists of three steps of conversion. Firstly, the ion beam accelerated at V_1 potential from the mass spectrometer is further accelerated to fall on the knob to emit secondary electrons from the surface. Because of the higher momentum of the ions impinging on the conversion knob and high secondary emission coefficient of the knob material, a large number of secondary electrons are released. In the second step these electrons are accelerated to the phosphor screen at ground potential. The high energy electrons lose part of their energy in the phosphor to emit photons. In the third step, the emitted photons are introduced to photo multiplier tube (PMT) and are converted to photo electrons that get multiplied and measured in PMT. The application of high negative potential and using energetic electrons enhances the emission efficiency of the phosphor material thereby improving the detection efficiency of the detector. This detector is mainly suitable for the detection of positive ions. In case of negative ions, the polarity of knob has to be positive and the very high positive potentials are to be applied on scintillator and PMT. This generates very high electric field in the vicinity of PMT and can generate noise. Therefore the Daly detectors are typically employed for the detection of positive ions.

The major advantage of this detector with respect to other electron multiplier detectors is the absence of mass discrimination when used in pulsed counting mode. However, the requirement of very high voltage, larger size of the detector and its inability to measure negative ions make this detector less preferable over other electron multiplier detectors.

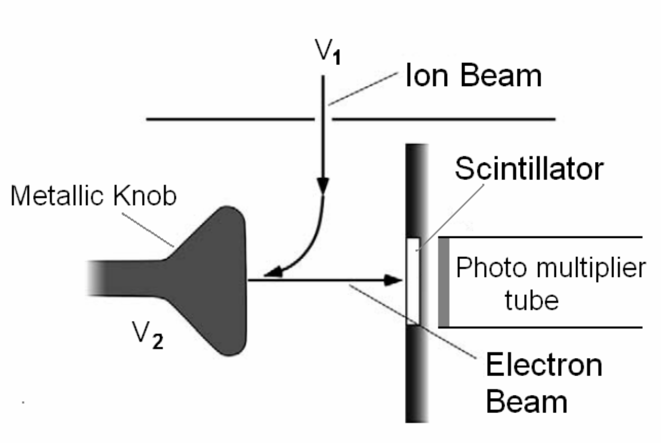

Fig. 1.25: Schematic of Daly detector

1.6 Scope of the present work

The work reported in the thesis is concerned with the development of a magnetic sector mass spectrometer i.e. thermal ionization mass spectrometer. The earlier developed magnetic sector mass spectrometers in BARC have some limitations in terms of sensitivity and precision. Studies were carried out to locate various regions of the mass spectrometer which need modification to address to the issues mentioned above. The studies include computer simulations followed by experimental studies. Based on this new designs of various subsystems were worked out and implemented for the development of the improved mass spectrometer. The improved version exhibit enhanced performance in terms of sensitivity and precision as compared to the earlier versions. Following are the highlights of the work.

- The magnetic analyser was modified by putting curved shims on entry and the exit boundaries of the magnetic analyser. This has helped in rotating the focal plane of the magnetic analyser normal to the principal axis which facilitated the removal of unwieldiness of the collector system and converted it into a compact design to accommodate large number of collectors for certain applications.
- A new compact and rugged geometry collector system was developed incorporating variable dispersion zoom optics. The wider dispersion as rendered by the new system provided the scope of using Faraday collectors with wider apertures which helped in

obtaining more flatness in the peak shapes. The new system has helped in improving the precision of TIMS from 22 ppm earlier to 8 ppm for isotopic ratio ($^{87}Sr/^{86}Sr$) measurement of Strontium.

- The experimental studies on Faraday collectors were carried out to design new Faraday collectors for TIMS. The new Faraday collector has simpler and sturdier geometry as compared with conventional design. The new features i.e. graphite coating, inclined collector surface and magnetic field (instead of electric field used earlier) for the suppression of secondary electrons has helped in improving the collection efficiency. This has helped in improving the internal precision on $^{87}Sr/^{86}Sr$ ratio measurements to around 5 ppm as compared to 9 ppm with conventional collectors.

- The ion source was redesigned for better transmission and more electrical insulation for the application of higher accelerating potential up to 10 kV as compared to 5 kV in the earlier conventional design. This has helped in improving the sensitivity to better than 1 ion for 450 atoms for Uranium. The design of filament assemblies was also modified to get stable ion beam during the operation of mass spectrometer. An additional feature includes the provisions to accommodate an electron impact ion source in place of thermal ion source to analyse gas samples also. This has enabled the isotopic ratio analysis of Oxygen isotopes $^{18}O/^{16}O$ in form of CO_2 gas which otherwise was not possible using thermal ionization source.

CHAPTER-2

THERMAL IONIZATION MASS SPECTROMETER

Introduction

Thermal Ionization Mass Spectrometry (TIMS) is widely accepted technique for precise and accurate measurements of various elements in periodic table [1-4]. Owing to its sensitivity, selectivity and precision it holds very important place in the field of nuclear technology and geochronology. In case of nuclear technology, the requirement of smallest possible amount of radio-active sample due to radiation doze is a fundamental requirement and TIMS fulfils this requirement owing to its high sensitivity. At almost every stage of nuclear technology, TIMS is used. For example – Nuclear fuel exploration that exploits the isotopic ratio measurement of Strontium, Neodymium and Lead etc. employing TIMS [4, 30-33], Fuel fabrication process involves the authentication of fuel in terms of enrichment level of particular isotope that requires TIMS, reprocessing of used fuel in nuclear reactor requires the quantitative measurements of various isotopes which employ TIMS. In addition to this the isotopic analysis of various other elements finding applications in nuclear technology is carried out using TIMS for example - Deuterium, Boron, Lithium, Gadolinium and Lead which are used in various parts of nuclear reactor like coolant, control rods and structural material etc. In geochronology, the age determination is based on the measurement of change in the isotopic composition of certain element due to the radio active decay of another element to one of its isotope. The alteration in the isotopic content has to be measured very accurately with a precision better than say 10 ppm which is possible by using TIMS only. Along with the isotopic ratio measurement the technique can also be employed for the concentration measurement of various elements in variety of matrices using isotopic dilution technique [4]. Apart from this

TIMS is also used in biological studies for example: the determination of small abundance of various elements present in biological sample of human. Nowadays, even though other techniques like multi-collector inductively coupled plasma mass spectrometry have emerged as an alternative to TIMS but still TIMS is considered indispensable because of the simpler instrumentation and better accuracy achieved with this technique. In all, TIMS is very important technique and highly useful for most of the applications owing to its high sensitivity, precision and accuracy.

Principle

The technique is based on ionization of analyte material by thermal ionization on a hot metallic surface with high work function. The analyte ions are accelerated to 5 – 10 keV and introduced to magnetic sector analyser whereby they are separated as per their mass to charge ratio. The separated ion beams are measured individually using Faraday collectors placed at focusing points of respective ion beams.

The following part of the chapter has been divided into three sections namely:

2.1 Components of TIMS

2.2 Measurement techniques

2.3 Terms used in TIMS

2.1 Components of TIMS

The main sub systems of TIMS are: Ion source, Analyzer, collector system, vacuum system and electronics. These are explained in the following.

2.1.1 Ion source

The ionization of the sample is obtained by thermal ionization process which is already explained in chapter 1. The ion source consists of filament assembly (single or multiple filaments) for ionization and various electrode plates for extraction, acceleration and collimation of the ions as shown in Fig 2.1. Generally for alkali elements single filament assembly (Fig. 1.1 in chapter-1) is used and for other elements triple or double filament assembly (Fig. 1.1 in chapter-1) is used [34]. In single filament assembly the sample is loaded on a single filament and heated under vacuum in the ion source for evaporation and ionization on the same filament. In case of triple/double filaments assembly the sample is loaded on sample filament i.e. the side filaments in case of triple filament assembly and one of the filament in double filament assembly.

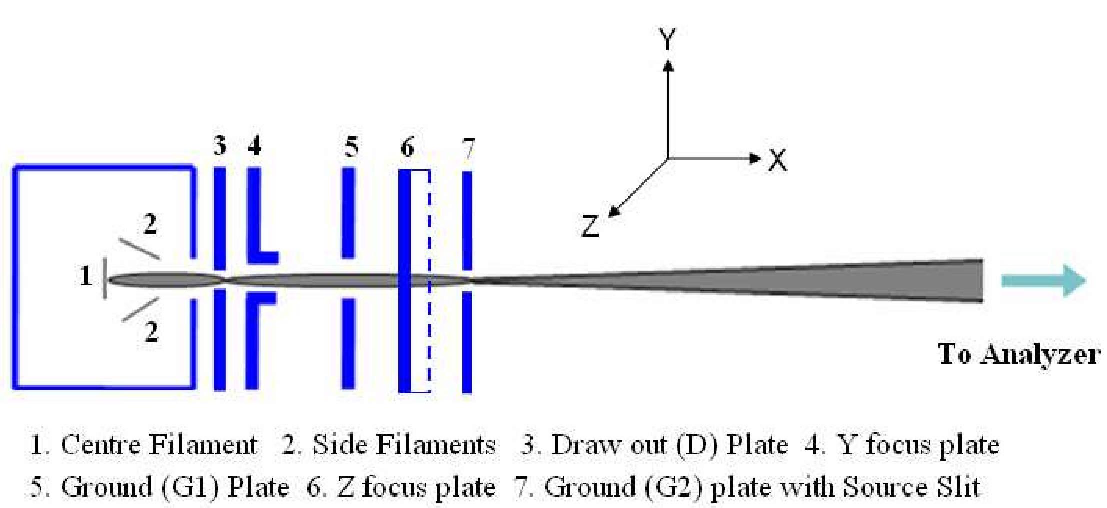

Fig. 2.1: Schematic of thermal ionization ion source

The sample filaments are heated under vacuum conditions in the ion source to evaporate the sample and the ionization filament is heated to a temperature (specific to different elements) for ionization of the vapors. The filaments and shield cup are raised to high accelerating potential in the range of 5 – 10 keV for acceleration of the ions. The ions are accelerated and focused by applying potentials on various accelerating and focus electrodes [34]. The electrodes plates *D*, *Y* are applied with potentials equal to around 90% and 75% of that on shield cup respectively. The ions produced on the filaments are extracted out of the shield cup through the exit slit by the electric field (produced due to differential voltage between shield cup and the *D* plate) penetrating inside the shield cup. As the ions exhibit very small energy within the shield cup, there is very sharp focusing between shield cup and draw out plate. Subsequently the ions are re-focused on G_2 plate by the potential on Y plates. The G_2 plate consists of a rectangular aperture (source slit) with typical dimensions 0.3 mm (width) x 8 mm (height). The ions get accelerated to maximum kinetic energy (equal to the potential applied at shield cup) after passing through the source slit and subsequently travel towards magnetic analyser in form of diverging ion beam with divergence angle defined by the baffle placed just before the magnetic analyser. The divergence angle is determined by the ratio of the width of baffle and the distance between the baffle and source slit. Typically, a divergence angle of ± 0.5° is used to control the effect of spherical aberration [19, 22, 36] which can affect the resolution of the mass spectrometer.

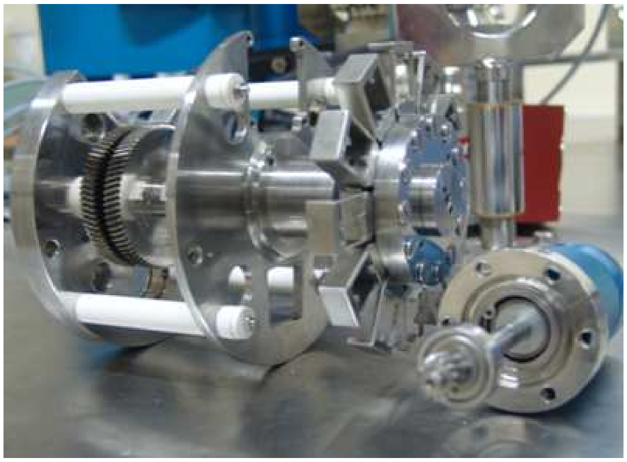

Fig. 2.2: Turret (sample changer) with 12 filament assemblies

In TIMS the sample is loaded on filaments in atmosphere and therefore it requires an arrangement whereby multiple samples can be loaded on a plurality of filament assemblies at one time so that frequent breaking of vacuum for every analysis can be avoided. This helps in increasing the throughput (number of analysis in given time) of the instrument. This arrangement is called turret (Fig. 2.2) which consists of disc with mechanical arrangement to accommodate twelve (or more) filament assemblies. The turret with the multiple filaments loaded with samples is put inside the source chamber and one of the filaments is placed in front of the extraction section (D, Y and ground electrodes) of the ion source. The turret can be rotated in-situ with the help of mechanical arrangement consisting of rotation motion feed-through connected with the turret axle through gear type arrangement. By rotating the turret, all the filaments can be placed sequentially before the extraction section of ion source and analysis of samples can be carried out.

2.1.2 Analyser – Magnetic sector

The magnetic sector is vital part of MS which determines the resolution and mass range of the MS. It is characterized by various parameters *viz.* sector angle, radius of curvature, entry/exit angle, maximum magnetic field and field homogeneity. In general 90° sector angle is used for most of the applications of TIMS. However for the special purpose instrument where very small resolution is required sector angle of 60° is also used. The basics of magnetic sector are already explained in chapter-1. In this section the directional focusing of ions and various aberrations are discussed.

2.1.2.1 Directional focusing

The magnetic field deflects the ions due to Lorentz force F as given by:

$$\boldsymbol{F = q\ (v \times B)} \tag{2.1}$$

Where q : charge on ion, v : velocity of the ion and B : magnetic field strength

The Lorentz force allows the charged particle of mass m to move along circular path with radius r as given by:

$$\boldsymbol{F = mv^2 / r} \tag{2.2}$$

From (2.1) and (2.2)

$$\boldsymbol{m\ v^2 / r = q\ (v \times B)}$$

For a charged particle moving in a plane orthogonal to the magnetic field

$$\boldsymbol{m\ v^2 / r = q\ v\ B} \tag{2.3}$$

The velocity ‘v’ of charged particle is related to accelerating potential V as-

$$\boldsymbol{\tfrac{1}{2}\ m\ v^2 = q\ V} \tag{2.4}$$

Eliminating v from equation 2.3 and 2.4

$$m / q = B^2 r^2 / (2V) \tag{2.5}$$

Above equation is also called basic mass spectrometry equation for magnetic sector. It relates the radius of curvature to mass to charge (m/q) ratio of the charged particle accelerated to given potential V and in a particular magnetic field B.

Consider diverging beam of charged particles as representing by three lines 1, 2, 3 emanating from point S and passing through the sector magnetic field AOB as shown in the Fig. 2.3. The charged particles along line 1, 2, 3 enter the magnetic field in different directions. Even though the radius of curvature is same but the region traversed (and hence the deflection) by the charged particles along these lines is different. Therefore the deflection of the charged particles reduces from line 3 to 1 and hence after leaving the magnetic field the charged particles meet at point I. This is called directional focusing.

In general, the distance I_o of image point or refocusing point from exit boundary of the magnet sector for a sector field with sector angle Φ is given by:

$$I_o = \frac{S_o\,[\cos\Phi + (\tan\varepsilon_1 \,.\, \sin\Phi)] + (r \,.\, \sin\Phi)}{(S_o/r)\,[\sin\Phi - (\tan\varepsilon_1 + \tan\varepsilon_2)\cos\Phi - (\tan\varepsilon_1 \,.\, \tan\varepsilon_2 \,.\, \sin\Phi)] - \cos\Phi - (\tan\varepsilon_2 \,.\, \sin\Phi)} \tag{2.5a}$$

Where ε_1 and ε_2 – entry and exit angle of ion beam with respect to normal to the entry and exit boundary of the sector magnet, S_o – distance of source point of the diverging ion beam from entrance boundary of the sector magnet, r – radius of curvature of charged particle in magnetic field (all parameters shown in Fig. 2.3)

Taking square root, log and then differentiating B and r (for constant m, q and V) of equation 2.5, we get.

$$\Delta r / r = - \Delta B / B \tag{2.6}$$

Above equation indicates that any variation in B also introduces variations in r. Since the location of focusing point and the deflection angle of ion (after passing through the magnetic region) depends on *r*, its variation will affect the focusing of charged particles.

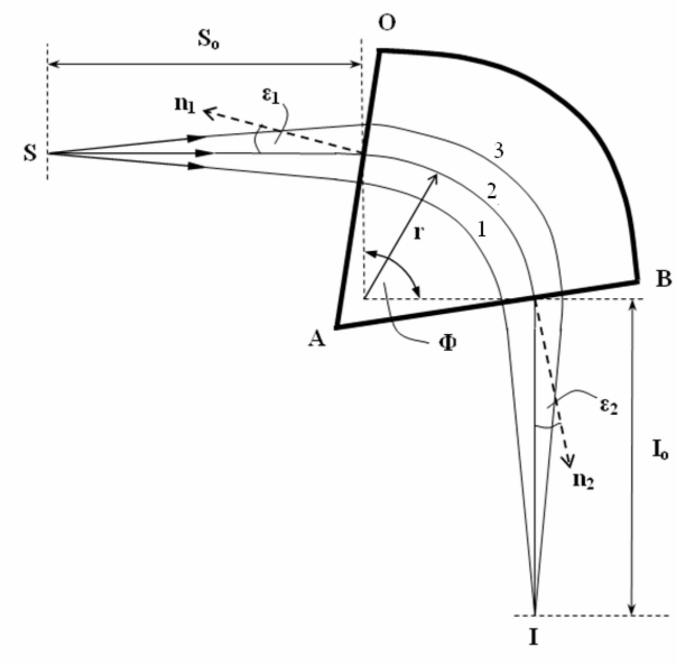

Fig. 2.3: Directional focusing of charged particles in magnetic sector

In general, TIMS uses an electromagnet to generate required magnetic field by passing DC electric current through the coil. The variations in magnetic field can be temporal and spatial. The temporal variation is because of the instabilities in the current power supply and the spatial variation is because of the field distribution between the pole gaps of electromagnet. To control the temporal variation, highly stable current power supply with stability better than 5 ppm is used. The spatial distribution in the directions i.e. median plane (plane orthogonal to magnetic field) and vertical plane (along the magnetic field) affects the focusing of ions. The homogeneity in median plane is controlled by using poles with good surface finish (a few microns) and maintaining highly precise parallelism between the poles (better than 10 microns). Typical value for the field homogeneity in median plane is better than 500 ppm within good field region which is illustrated in the Fig 2.4. The in-homogeneity in vertical direction can introduce curvature along the height of the image at the re-focusing point for ion beam having rectangular cross section. This limits the vertical dimension of the rectangular aperture (source slit) in the ion source.

2.1.2.2 Fringe field region

It is well known that the magnetic field is not confined to the region within poles and extends exponentially up to large distances outside the physical boundaries of the magnetic sector [37, 38]. Typically the magnetic field with significant strength (> 1% of the field with in main region) is extended up to a distance equal to around 8 – 10 pole gaps. The fringe field has significant effect on the focusing of ions and has to be accounted while considering focusing of ions. As the magnetic sector is defined as region with uniform magnetic field, the fringe field extends the boundaries of magnetic sector beyond the physical boundaries of the poles of the electromagnet by 1 – 2 pole gaps. While designing the magnet, the physical dimensions of the poles are calculated in such a way that the effective boundaries should match with the ideal boundaries of the required geometry of the magnetic sector.

The fringe field exhibits very important role to play in stigmatic geometry by introducing vertical focusing of the ions. Since the entry and exit angles are non-zero in case of stigmatic geometry, a component of magnetic field along the median plane is generated so that ions on both sides of the median plane are deflected towards it due the Lorentz force. For a given geometry of the magnetic sector there exists particular combination of entry and exit angles of the ion beam for which the re-focusing points in horizontal and vertical planes match with each other. This condition is called stigmatic focusing. Typically for magnetic sector with *90°* deflection angle the stigmatic condition exists for angles *26.5°* on entry and exit boundary of the magnetic sector in case of symmetric configuration of ion source and collector system. There exist other non symmetric configurations also for which stigmatic conditions can exist. The stigmatic focusing helps in increasing the transmission of magnetic sector thereby contributing to the sensitivity of MS. The other advantage of stigmatic geometry is increased dispersion (by a factor of two for *90°* magnetic sector) which makes provisions for increasing the width of various apertures and hence increases the transmission and sensitivity of the system as a whole.

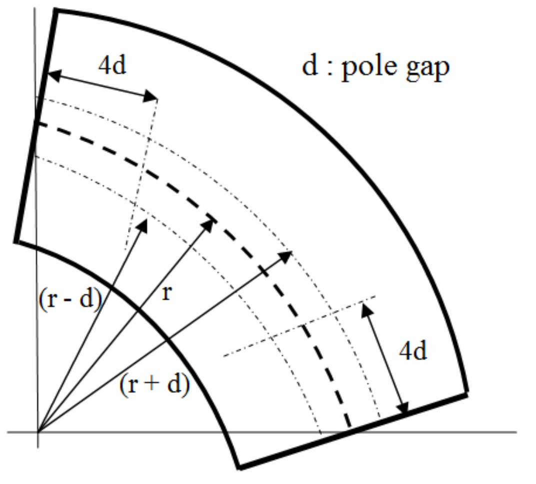

Fig. 2.4: Good field region inside the magnetic sector

2.1.3 Detector system

TIMS consists of plurality of Faraday collectors depending upon the requirement. The collector system also employs electron multiplier for the measurement of very small ion currents corresponding to isotopes with very small abundance. For the isotopic ratio measurement, the magnetic field is adjusted to a value so that ions corresponding to required isotopes are collected within respective collectors connected to electrometer amplifiers individually. The ion beam intensities corresponding to respective isotope abundance are measured individually using given collector and amplifier combination and subsequently the isotopic ratio can be measured by computing ratios of the respective signals [1-3]. The Faraday collector and the electron multiplier detector are already explained in chapter – 1.

2.1.4 Vacuum System

Vacuum is fundamental requirement of TIMS [39-41]. The vacuum allows the ions generated within the ion source are to be transported to the collector system which otherwise lose kinetic energy due to collisions with the background gas particles. In general the mean free path of the background gas particles should be more than the path length of ions travelling from ion source to collector. A high vacuum ensures the minimization of the collisional losses within the instrument thereby increase the sensitivity and abundance sensitivity of MS.

The vacuum system of TIMS consists of a turbo-molecular pump, two sputter ion pumps, a rotary pump and a diaphragm pump (oil free pump). Various vacuum gauges vis. cold cathode gauge, Penning gauge and Pirani gauge are used for monitoring the vacuum level in different parts of the instrument.

The ion source chamber is pumped by a turbo molecular pump (TMP) with a pumping capacity of 500 L/s. This is backed by a rotary pump with capacity of 200 L/min. The amplifier chamber is pumped by a separate dry pump with a pumping speed 30 L/min. The collector side has one TMP with pumping speed 200 L/s and one ion pump (35 L/s) is mounted just before the analyser tube. The collector and the source side are separated by an electro-pneumatically controlled gate valve. A vacuum level of 1.5 x 10^{-7} torr is maintained in source chamber (turret) and 2 x 10^{-8} torr in the collector system.

2.2 Measurement techniques

The isotopic ratio data is measured in set of multiple measurements. The result of particular analysis is represented by the average value of the set with relative standard deviation over the data as the range of uncertainty. The isotopic ratio measurement suffers from various systematic and non systematic errors in TIMS [42-44]. The systematic errors involve non uniformity of the amplifier gains, noise of the amplifier, non uniform collection efficiency of collectors, instabilities of various power supplies etc. The non systemic error involves mass discrimination due to fractionation during evaporation of different isotopes. There are different methodologies of isotopic ratio measurements which are specific to types of elements. These are based on circumventing various errors and to overcome the limitations posed by the instrument *viz.* limited dispersion etc. Following are various measurement techniques employed for the measurement of isotopic ratio and concentration measurement.

1. Single collector peak jumping method
2. Multi-collector ratio measurement
3. Multi-collector peak jumping or multi dynamic mode
4. The virtual amplifier method
5. Isotopic dilution method

Above methods are explained in the following.

2.2.1 Single collector peak jumping method

During the initial development of isotope ratio spectrometry, single collector peak jumping mode was used for the measurement of isotopic ratio. It involves the measurement of ion beams corresponding to respective isotopes on single collector sequentially by setting the magnetic field accordingly. Since same set of collector and electrometer amplifier is used, the error due to amplifier bias and collection efficiency is eliminated. But it suffers from error due to variation of ion beam intensity with time. The error can be circumvented as long as the variation in ion beam intensity is monotonic. For example: in case of isotopic ratio of two isotopes say A and B, the signals corresponding to A and B are measured sequentially with certain time delay in between as shown in Fig. 2.5. For ion beam intensity varying with very slow rate, the variation is almost linear with time. In this case the time average of signal A for two successive measurements corresponds to the value expected when signal of B is measured between these two steps. Hence the ratio of time averaged signal A to that with signal B is the time corrected ratio. In case of fast varying signals with time, the signal corresponding to A and B are recorded in multiple steps and by curve fitting the values of signal corresponding to A and B are calculated at different time steps. However any random fluctuation (variation in both sides) can not be corrected by this method that limits the precision of measurement. Nowadays, the method is not employed in routine isotopic ratio measurements and is used only for the measurements where the small relative mass difference ($\Delta m/m$) between the adjacent isotopes doesn't allow them to be collected simultaneously on the adjacent collectors due to limited dispersion of magnetic sector.

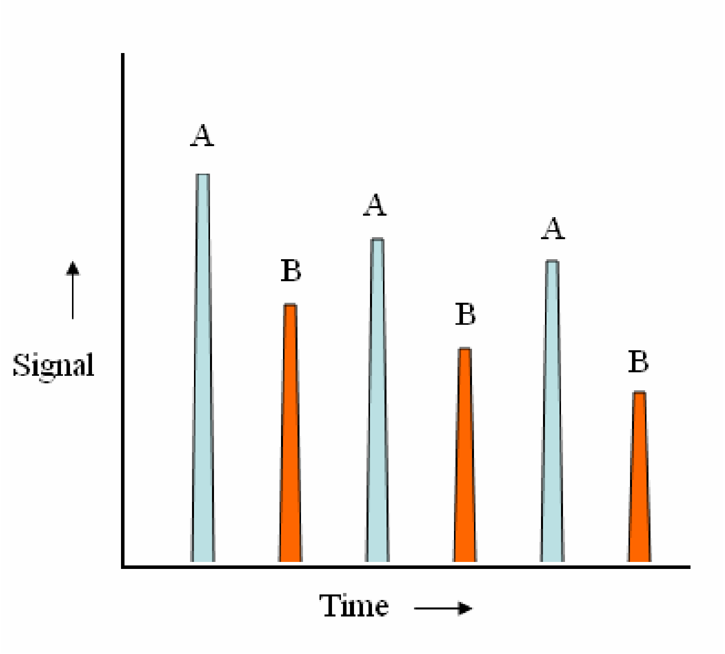

Fig. 2.5: Single collector peak jumping

2.2.2 Multi collector ratio measurement

It involves the measurement of ion currents corresponding to different isotopes on different collectors [45- 46] simultaneously. The ratio of the signals on different collectors corresponds to the isotopic ratio of the respective isotopes. To improve S/N ratio, signals corresponding to each isotope are integrated over a period of time usually 10 seconds. Each integrated measurement is called a cycle of measurement. Analysis consists of 20 to 30 cycles and the average of computed ratios gives the measured value with RSD which reflects the internal precision of the analysis. The simultaneous measurement of isotopes eliminates any error due to any variation of the ion beam intensity of isotopes. However since the ion beams are measured on different collectors connected to respective amplifiers, the measurements suffer from error due to different gain factors of amplifiers and different collection efficiency of the collectors. The error due to amplifier bias is eliminated by calibrating the amplifiers using standard and highly stable current source with stability of 5 ppm. A fixed value of current is passed through all the amplifiers sequentially and the corresponding signals are recorded. These signals are used to calculate the gain factor of each amplifier (relative to reference amplifier) during isotopic ratio calculation on set of amplifiers. However as the amplifiers are calibrated independently using standard current source with certain uncertainly say 5 ppm the ratio of the amplifier signal will produce an error given as $\surd\ (5^2 + 5^2) = \sim 7$ ppm. This puts a lower limit of 7 ppm to the minimum possible uncertainty in ratio measurement due to amplifier gain variations. However the measurement precision in this mode is mainly limited to higher values due to mass discrimination effects.

2.2.3 Multi-collector peak jumping or multi dynamic mode

This mode [1] is used for the correction of errors due to mass fractionation effect by internal normalization. It also circumvents the other errors due to non uniform amplifier gains of the detector system. It involves the measurement of isotopic ratio for set of isotope on given set of collectors sequentially. For example consider three isotopes as A, B, C of any element with same relative mass difference. The isotope A and B are taken as stable isotopes with known ratio (R_{1t}). The isotopic ratio of B to C (R_{2t}) is required to be measured. The collectors involved are C_1 and C_2 as shown in Fig 2.6. In first step magnetic field is set for isotope A and B to be collected on collectors C_1 and C_2 respectively. The signals are measured and after some time delay the magnetic field is set to another value for isotopes B and C to be on collectors C_1 and C_2 respectively. The true isotopic ratio (R_{2t}) for B and C isotopes can be calculated using measured ratios R_{1m} (A/B) and R_{2m} (B/C) as follows.

$$\boldsymbol{R_{1m} = R_{1t}\,(c_1/c_2) * (b_1/b_2) * F_{AB}} \tag{2.7}$$

$$\boldsymbol{R_{2m} = R_{2t}\,(c_1/c_2) * (b_1/b_2) * F_{BC}} \tag{2.8}$$

Where F_{AB} and F_{AB} are the mass bias factors for isotope A (with respect to isotope B) and for isotope B (with respect to isotope C) respectively.

Dividing eq. 2.7 by 2.8:

$$\boldsymbol{R_{1m} / R_{2m} = R_{1t} / R_{2t}\ (F_{AB} / F_{BC})} \tag{2.9}$$

As relative mass difference of A to B and that of B to C is same then $F_{AB} = F_{BC}$

So that eq. 2.9 can be written as:

$$\boldsymbol{R_{2t} = (R_{1t} / R_{1m})\, R_{2m}} \tag{2.10}$$

Hence true ratio of isotopes B to C can be calculated using measured ratio R_{1m}, R_{2m} and the true ratio R_{1t}. The errors due to bias factors (*b*), collection efficiency (*c*) and mass discrimination (*F*) are eliminated using this methodology.

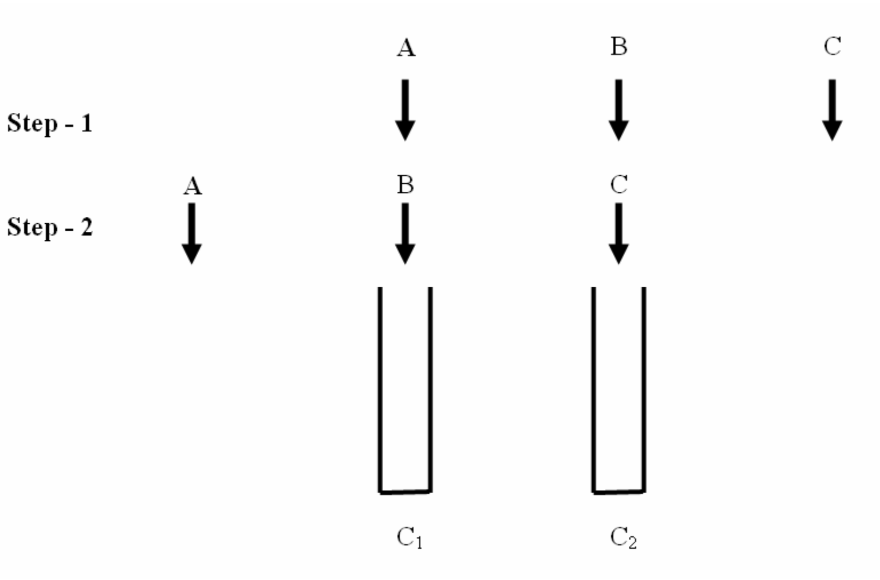

Fig. 2.6: Scheme for multi-dynamic mode of ratio measurement

Some of the applications of this methodology are in geochronology for the isotopic ratio measurement of Sr and Nd. The isotopic ratio ^{87}Sr/^{86}Sr for Sr is measured and internally normalized using stable ratio of ^{86}Sr and ^{88}Sr isotopes in multi-dynamic mode. Similarly in case of Nd the isotopic ratios ^{143}Nd/^{144}Nd and ^{145}Nd/^{144}Nd are internally normalized using isotopic ratio of stable isotopes ^{146}Nd and ^{144}Nd.

2.2.4 Virtual amplifier method

The Virtual amplifier concept [26] is used to circumvent the uncertainty due to gain calibration of the amplifiers in static multi-collector mode of ratio measurements whereby the amplifiers are calibrated using highly stable current source with stability (not better than) 5 ppm. Due to the uncertainty of 5 ppm associated with each amplifier individually, the ratio measured using given set of collectors and amplifiers will be given by $\sqrt{(5^2 + 5^2)} = 7$ ppm which limits the precision to 7 ppm. To break this barrier, virtual amplifier concept is used where every amplifier is connected to each collector using grid of high insulation switches (relays) as shown in Fig. 2.7. During measurement, a set of amplifiers are connected to given set of collectors and after one block of measurements the amplifiers are interchanged among the collectors. To understand the concept, consider the measurement using two collectors say (C_1 and C_2) and amplifiers (A_1 and A_2). The measurement is carried out in two blocks. In first block collectors C_1 and C_2 are connected to amplifiers A_1 and A_2 respectively and in second block they are interchanged i.e. C_1 is connected to A_2 and C_2 is connected to A_1. The ratios R_1 and R_2 in two blocks are given as:

$$R_t = R_1 + a_{12} \tag{2.11}$$

$$R_t = R_2 - a_{21} \tag{2.12}$$

Where R_1 and R_2 are the gain corrected measured ratios in block 1 and 2. The deviations in the ratio (a_{12} and a_{21}) from true value will be in opposite directions from one block to other block due to interchanged amplifiers. However the run average of both the blocks will eliminate the uncertainty to a great extent and the average value will be much closer to the true value and hence the barrier of 7 ppm precision (due to uncertainty of gains) is broken. In the same way the isotopic ratios can be corrected for number of isotopes more than two. The main limitation of this arrangement is that resistance of the relay (switch) in open state should be much higher (10^{13} ohm) than amplifier resistance (10^{11} ohm) and should exhibit very small temperature coefficient.

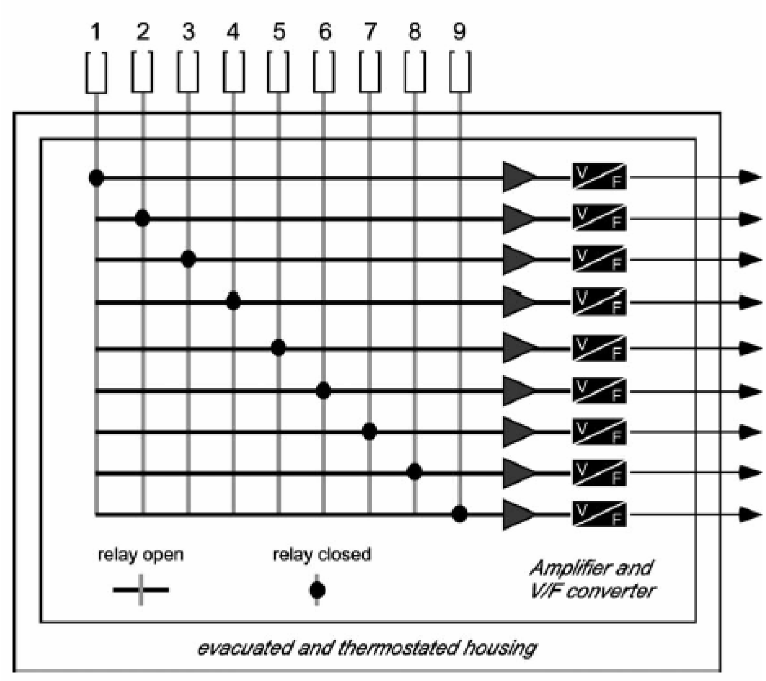

Fig. 2.7: The virtual amplifier method

2.2.5 Isotopic dilution method

This is highly accurate and precise technique for the concentration measurement of any element in some matrix [4]. The accuracy of other techniques vis. X-ray fluorescence, atomic absorption spectroscopy and inductively coupled plasma mass spectrometry is affected mainly because of matrix effects. The instruments using above techniques are calibrated for the signal intensities of analytes corresponding to their concentrations using standards but any changes in the composition of matrix of sample (with respect to standard) may affect the signal intensity of the analyte ions thereby affecting the accuracy of the measurement. One of the ways to overcome this problem is to purify the sample before analysis by separating out the impurities. But the purification process is itself very tedious and secondly there are chances of alteration of the concentration of the element of interest which is not tolerable at least when the analyte concentration is very small. However the isotopic dilution technique is independent of any matrix effect because it employs the measurements of isotopic ratios rather than signal intensities. The isotopic ratio measurement is carried out using mass spectrometers like TIMS, MC-ICPMS, GDMS and GCMS etc. Since the isotopic ratio does not depend on the composition of the matrix of the analyte, the concentration measurement exhibits high accuracy as compared to other techniques.

The technique is based on change of isotopic ratio of analyte element after addition of known quantity of the standard of same element. The change in isotopic ratio of analyte is dependent on parameters *viz*. the concentration of sample and standard, the isotopic ratio of sample before mixing of standard and the isotopic ratio of standard. To measure the sample concentration particular isotopes (say I_1 and I_2) of sample and standard are selected and their ratios are measured in sample and standard before mixing. Mostly the isotopes most abundant in the sample and standard are considered. Subsequently, the known quantity of the standard is mixed with the sample and the isotopic ratio of the mixture is again measured for the same isotopes. The concentration (C_{s1}) of isotope (I_1) in the sample can be expressed in terms of parameters *viz*. the isotopic ratio (R_{s21}) of the sample (before mixing), the isotopic ratio (R_{st21}) of standard, the isotopic ratio (R_{m21}) of the mixture and the concentration (C_{st1}) of the isotope (I_1) in standard as given below:

$$C_{s1} = C_{st1}\,(R_{m21} - R_{st21}) / (R_{s21} - R_{m21}) \tag{2.19}$$

Where R_{s21}, R_{st21} and R_{m21} represent the isotopic ratios in sample, standard and the mixture respectively for isotopes I_2 to I_1.

Using above equation 2.19 one can calculate the concentration of given isotope in sample using terms on right side which are either known or can be measured using TIMS. The total concentration (C_s) of the element with isotopes (I_1 and I_2) can be calculated following equation:

$$C_s = C_{s1}\,(1 + R_{s21}) \tag{2.20}$$

The technique can also be used for combination of sample and standard comprising exclusive isotopes i.e. isotope present in sample is absent in standard. In this case the isotopic ratio of the exclusive isotopes (say I_1 in sample and I_2 in standard) in the mixture of sample and standard is straightway proportional to the ratio of their concentration for equal volumes of sample and standard. The concentration of the sample isotope (C_{s1}) can be expressed in terms of isotopic ratio (R_{m12}) in the mixture and the known concentration of the standard isotope (C_{st2}) as follows:

$$C_{s1} = C_{st2} (R_{m12}) \qquad (2.21)$$

Where R_{m12} represents isotopic ratio for isotope I_1 to I_2.

The total concentration of the element can be calculated from equation 2.20.

For example, the concentration measurement of Uranium can be carried out by mixing known quantity of U-233 spike with the given Uranium sample. The isotopic ratio $^{238}U/^{233}U$ can be used to calculate the concentration of respective isotopes and subsequently the total concentration can be measured using equation 2.20.

The technique exhibit very high sensitivity for most of the elements and can produce very small detection limits. In case of IDMS employing TIMS, the applicability is limited to the elements with ionization potential less than 8 eV. However for most of the elements in nuclear and geochronological applications, the technique is highly useful. The detection limit depends upon the sensitivity of the mass spectrometer for a given element and also dependent on the volatility and the ionisability of the analyte element. It is also determined by the isotopic enrichment of the tracer and the smallest possible quantity of the tracer that can be used for the particular isotopic ratio measurement. The detection limit in this case is given as the minimum concentration of the analyte sample which when added with the smallest amount of tracer will bring about a measurable change (say 5%) in the isotopic ratio of the selected isotopes of the tracer. Typically for Rubidium and Uranium the detection limits extends up to 0.1 ppb and 0.1 ppm respectively.

2.3 Terms used in TIMS

2.3.1 Resolution

It is the capability of MS to resolve adjacent peaks on a detector [1, 2]. For TIMS it is defined as the ratio of average mass (m) and the mass difference (Δm) for two just resolvable peaks on the detector. As per 10% valley definition, the adjacent peaks are considered resolvable if the valley between two peaks is 10% of the average peak intensity of the peaks as shown in the Fig. 2.8. The resolution is dependent on the radius of analyser magnet (r), collector slit width (W_c) and ion beam width (W_b) by following equation.

$$\frac{m}{\Delta m} = \frac{k \cdot r}{(W_c + W_b)} \tag{2.13}$$

Where k is constant which depends on the geometry of the magnetic sector. The values of k are *1* and *2* for normal and stigmatic geometries respectively.

Typically for magnetic sector (with stigmatic geometry) radius of 300 mm, collector slit width as 1mm and ion beam width of 0.5 mm the resolution as per above equitation will be 400. For given magnetic sector and collector the resolution depends on beam width at the collector. In case of ion source and detector placed symmetrically about the analyser magnet, the magnification (ratio of beam width at refocusing point to source slit width) is unity that implies the beam width at refocusing point to be equal to source slit width. The ideal beam width should be equal to the width of source slit i.e. 0.3 mm in general. However due to various errors vis. spherical aberration, energy spread, instabilities in power supplies and non uniformity in magnetic field the effective beam width at the refocusing point of the magnetic sector generally lies between 0.5 – 0.7 mm.

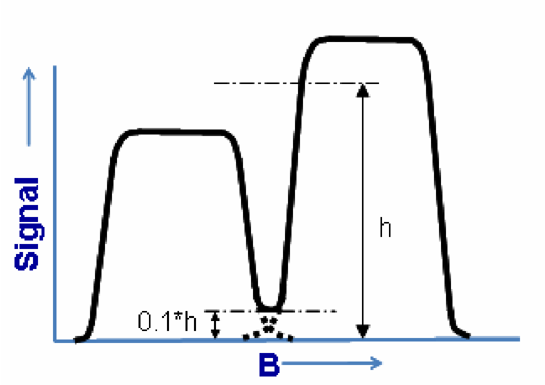

Fig. 2.8: The resolution as per 10 % valley definition

The resolution on a magnetic sector instrument can be measured with the help of peak shape on the collector. The peak corresponding to a given mass can be obtained on a collector by increasing the magnetic field in fine steps and recording the signal as the ion beam moves across the detector. The peak shape for a well focused ion beam i.e. the beam width less than the detector width is flat topped peak as shown in Fig. 2.8. The peak shape is characterised by the base width and the width of the flat region (also called as peak flatness). The dimensions of the peak (in terms of magnetic field) are related to the width of ion beam at collector (W_b) and collector slit width (W_c) by following relation (for 90° sector magnet with stigmatic geometry).

$$\boldsymbol{w = 4r \,.\, \Delta B \,/\, B} \qquad (2.14)$$

Where $w = (W_c + W_b)$ for base width and $(W_c - W_b)$ for flat top width, r – radius of magnetic sector, $\Delta B / B$ – relative change in the magnetic field for movement of ion beam

Hence, for a given radius of the magnetic sector the value of w can be expressed in terms of $\Delta B/B$ which is generally expressed in ppm (parts per million). Typically for a beam width of 0.6mm, collector slit width of 1 mm, width of flat portion of peak is 0.4 mm which can also be expressed as 666 ppm and the base width (i.e. $W_c + W_b$) is given by 1333 ppm.

The resolution can be measured by determining beam width from the peak shape by using following equation.

$$W_b = \frac{W_1 - W_2}{W_1 + W_2} \qquad (2.15)$$

Where W_1 and W_2 are the dimensions of base and top region of the peak as shown in the Fig. 2.9.

Alternatively, the resolution can also be measured using two adjacent peaks on a given collector (as shown in the Fig. 2.10) by following equation.

$$\textbf{Resolution} = \frac{d}{b}\,\frac{M}{\Delta M} \qquad (2.16)$$

Where d and b are shown in the Fig. 2.10, M and ΔM are the average mass and mass difference corresponding to the peaks.

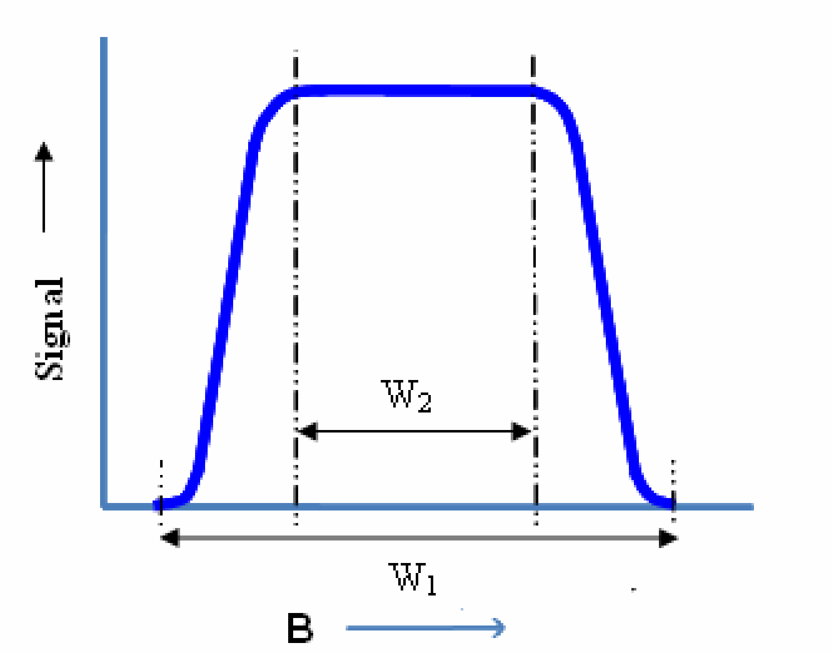

Fig. 2.9: Typical peak shape across a collector in TIMS

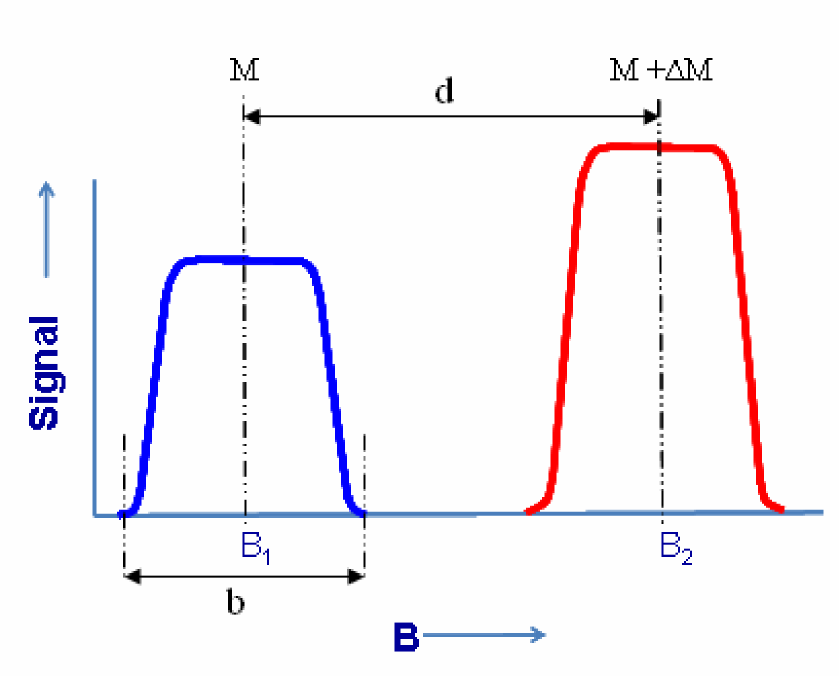

Fig. 2.10: Measurement of resolution using two adjacent peaks

2.3.2 Sensitivity

It is the ability of a mass spectrometer to respond to the given amount of analyte sample used for the measurement [1-2]. For TIMS, sensitivity is very important parameter as it decides the quantity of the sample to be used for isotopic ratio measurement and in case of radio- active analyte material it becomes very important parameter in view of radiation hazard for large quantity of the analyte. The sensitivity for TIMS is represented in terms of number of atoms of analyte element used for one ion measured at the detector. The analyte atoms are lost at various stages of measurements *viz*. vaporization, ionization, transmission from the ion source, transmission through the flight path in instrument etc. The sensitivity depends upon various factors like work function of the filament used for ionization, ionization potential (IP) of the analyte element, vapor pressure of the analyte, transmission of the ion source and gain of the amplifier used for the measurement of ions.

For multiple filament assembly the alignment and distance between the sample and ionization filament is very important and can affect sensitivity to a great extent. The maximum number of atoms evaporating from the sample filaments should approach the ionization filament. This requires that the distance between the filaments should be as low as possible. However due to practical difficulty of loading the sample for very close filaments, the distance between the filaments is optimized. According to Saha Langmuir's equation in chapter-1, the work function of the filament should be as high as possible. At the same time, the filament should withstand high temperature that is required for the ionization of many elements with high IP. Therefore, typically Rhenium filament is used because of its high work function (5.2 eV) and melting point (~3180° C). In case of elements with low ionization potential *viz*. alkali metals and alkaline earth metals very high sensitivity is obtained even at lower temperature because of their low ionization potential.

Sensitivity of TIMS is element specific. To measure the sensitivity, a precisely known quantity of the reference (standard) sample is loaded on the sample filament. The sample is heated at operating temperature and the signal is recorded on the collector continuously till the whole sample is consumed. The integration of the signal over acquisition time provides the amount of charge collected by the collector that can be converted to the number of ions collected. The number of atoms of the sample element can be calculated from the known quantity and the atomic mass of the element. The ratio of number of ions collected and the number of atoms deposited on the sample filament gives the sensitivity of the TIMS. Typically for Uranium the sensitivity obtained is 500 – 600 atoms for one ion.

2.3.3 Precision and accuracy

Precision is the capability of a mass spectrometer to repeat a given result with a number of trials [1, 2]. It is obtained by taking a number of measurements for a given sample and measuring the relative standard deviation (RSD) over the data. A lower value for the RSD signifies higher precision of the measurement. In case of TIMS the precision is measured both internally and externally. The internal precision is given by the RSD of the isotopic ratio data measured for single loading of the sample. It accounts for the variation of data due to random/statistical errors like noise in the electrometer amplifiers, the instabilities in power supplies such as HV and statistical variation in ion currents. The external precision is calculated by relative standard variation over the average values obtained from the data collected for same sample on different filament assemblies. It represents the variation in data due to systematic errors like mass discrimination and mechanical misalignments etc. Any mechanical misalignment reduces the sensitivity of the instrument which leads to higher operating temperature for a given analysis. The higher temperature increases the mass fractionation (during evaporation of the sample) and hence deteriorates the precision. The result for a given measurement of isotopic ratio is represented by average ratio of the data with external precision as the uncertainty range. The probability of getting the true measurement within given uncertainty range is 68.3% for single sigma (σ), 95.5% for two sigma (2σ) and 99.7% for three sigma (3σ) where sigma represents the RSD over the data.

2.3.4 Abundance sensitivity

It is the capability of the MS to detect a minor ion isotope in the vicinity of a major isotope [1, 2, 47-50]. It is defined as the ratio of signal corresponding to the scattered ions of a major isotope at unit mass away and the signal corresponding to the major isotope. The abundance sensitivity is considered an important parameter for the applications where very small isotopic ratios are to be measured e.g. ^{230}Th/ ^{232}Th, ^{9}Be/^{10}Be, ^{235}U/^{238}U etc. for which the minor isotopes are in the range of few tens to hundreds of ppm with respect to major isotopes. The measurement of abundance sensitivity can be carried out for a major isotope that doesn't have any adjacent isotope peak at unit mass away. The abundance sensitivity is measured by the ratio of signal (I_s) for the scatter ions (at location of mass M-1) of mass M to the signal (I) for mass M as shown in Fig. 2.11. The abundance sensitivity is mainly dependent on the vacuum level of MS. The analyte ions while passing through the MS lose their energy due to collision with the background gas particles and undergo more deflection by the magnetic field. This leads to collection of scattered ions of given mass on collectors meant for lower masses. These scattered ions interfere with the ion signals at lower masses during measurement of isotopic ratio thereby affecting the accuracy of the measurement. Since the interference is in range of few ppm the measurement is not affected as long as the abundance of minor isotope is considerable with respect to the major isotope on high mass side. However for very small abundance of minor isotope, the measurement can be affected to a great extent which leads to the requirement of high abundance sensitivity. At lower vacuum levels there are more scattering losses and hence abundance sensitivity is poor. In general for a vacuum level in the range of 10^{-8} torr, abundance sensitivity lies in the range of 10 – 50 ppm. It can be further improved to within 10 ppm by improving the vacuum level. However, due to scattering losses of ions at various apertures in the MS, it is limited to a range of 1- 5 ppm. For the further improvements different types of energy filters are used for example: retarding potential lens (RPL), retarding potential quadrupole (RPQ) and wide angle retarding potential (WARP) etc.

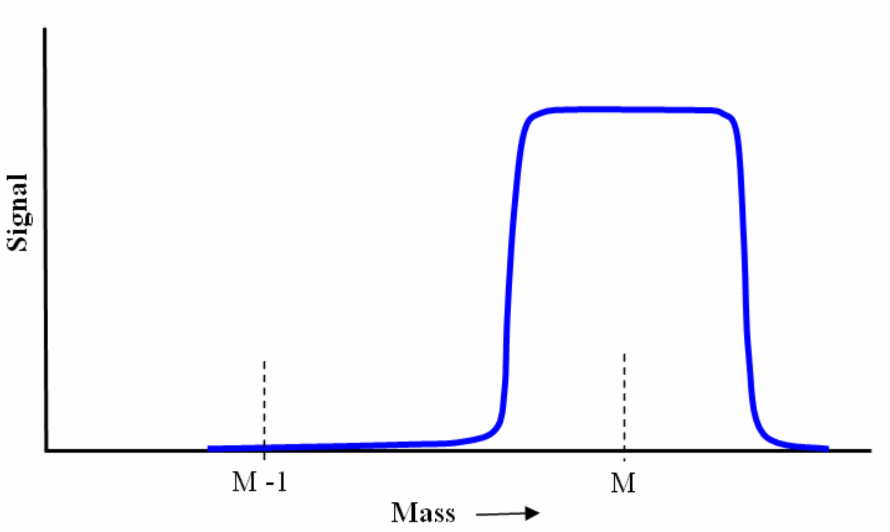

Fig. 2.11: Measurement of abundance sensitivity

2.3.5 Mass discrimination

This is one of the main sources of error in the determination of isotopic ratio in TIMS [1, 2, 44]. The mass discrimination is generated due to mass and time dependent evaporation of sample from the hot surface of the filament. The evaporation rate is inversely proportional to mass that leads to evaporation of lower mass at a rate faster than that of higher mass. This leads to isotopic ratio (for lower to higher mass) to be higher than the true value in the initial period of measurement. However, the faster rate of evaporation leads to higher rate of depletion of lower mass from the sample on the filament and hence its rate of evaporation starts reducing with time at a rate faster than that of higher mass thereby reducing the isotopic ratio for lower to higher mass as shown in Fig. 2.12. In general, the trend of isotopic ratio (low mass / high mass) follows a pattern as: at the beginning of an analysis the observed ratio is more than the true ratio and reduces continuously with time to approach it. It keeps on reducing and after long time becomes lower than the true value. The rate of reduction of isotopic ratio depends on various parameters that include sample size, chemical composition and purity, sample loading procedures on the filament, the material of ionization and evaporation filaments, filament temperatures and the rate of sample heating.

The deviation of the measured ratio from the true value may be expressed by following equation:

$$\boldsymbol{K = R_{tr} / R_{meas}} \qquad (2.17)$$

Where K: mass fractionation factor, R_{tr} : true ratio, R_{meas} : measured ratio

To correct for the fractionation factor, the K value for standard of particular elements with different ratios are measured on the TIMS. The quantities of the sample, loading procedure, filament material, data acquisition time etc are precisely controlled during K factor measurement. For the unknown sample also same procedure of ratio measurement is followed and the K value corresponding to the standard with nearest ratio is applied to get the true ratio. This process is also called external normalisation and is applied for the samples not having any set of stable isotopes for internal normalisation.

There are various models to explain the variation of ratio with time. One of the models [51] for single filament ion source, explains the dependence of the observed ratio (R_m) on the fraction of sample (Q) remaining on the filament. It is assumed that the sample molecule (AB) can evaporate as neutral molecule (AB^o) or ion (AB^+), neutral atom (A^o, B^o) or atomic vapor (A^+, B^+). The model shows that the observed isotopic ratio equals the true ratio after ~ 63% of the sample is vaporized. The other model [52] for triple filament ion source shows that sample evaporates mostly in form of molecular species from the sample filament. The molecules can undergo change in their composition during ionization on the other filament i.e. they can dissociate first before ionization to atomic ion or ionize to molecular ions followed by the dissociation to atomic ions. This model explains the anomalous behavior of the fractionation pattern which can not be explained by models adopted for single filament ion source. Typically for Uranium deposited on the filament as nitrate salt and converted to U_3O_8 [53] the variation of isotopic ratio exhibits anomalous behavior which can be due to evaporation of U_3O_8 in form of UO_2 and U_3O_8 simultaneously. Owing to their drastically different molecular masses they obey different evaporation profiles. Depending upon the chemical form of the sample the predominant species (UO_2 or U_3O_8) decides the overall evaporation profile and hence the isotopic ratio profile of the sample.

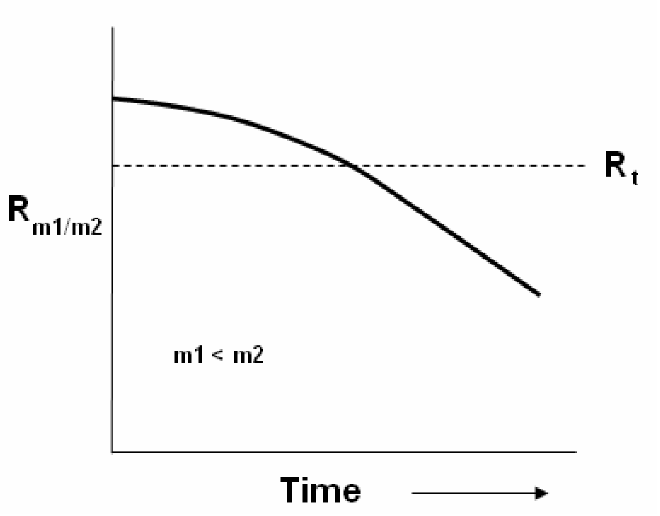

Fig. 2.12: Variation of measured ratio ($R_{m1/m2}$) with time due to isotopic fractionation

Corrections for the fractionation can be applied mathematically in form of four laws [1, 54]:

1. Linear law
2. Power law
3. Exponential law
4. Rayleigh law

Above laws are used to calculate K factor (K_1) for isotopic ratio for masses say m_1 and m_3 when the K factor (K_2) for isotopic ratio for masses m_2 and m_3 is known. These can be expressed in one general formula:

$$K_1 = b\,(K_2)^a + c \tag{2.18}$$

where the subscript m and t stands for measured and true ratios. The constants a, b and c have values for different laws as follows:

Linear law: $a = 1$, $b = (m_2 - m_3)\,(m_1 - m_3)$, $c = 1\text{-}b$

Power law: $a = (m_2\text{-}m_3) / (m_1\text{-}m_3)$, $b = 1$, $c = 0$

Exponential law: $a = \ln(m_2/m_3) / \ln(m_1/m_3)$, $b = 1$, $c = 0$

Rayleigh law: $a = [1-(m_3/m_2)^{1/2}] / [1-(m_3/m_1)^{1/2}]$, $b = (m_3/m_2)^{1/2} / (m_3/m_1)^{1/2}$, $c = 0$

Alternately following expressions can also be used for correcting the mass fractionation:

Linear law: $K_1 = 1 + \Delta m \times F$

Power law: $K_1 = (1 + F)^{\Delta m}$

Exponential law: $K_1 = \exp(\Delta m \times F)$

Where Δm_1 : mass difference between the isotopes m_1 and m_3 and F : fractionation factor per unit mass difference. The Factor F can be calculated from the known K factor (K_2 ; for masses m_2 and m_3) using $F = (1-K_2)/ \Delta m_2$;where Δm_2 is the mass difference between masses m_2 and m_3.

The error due to mass fractionation effect can be circumvented by internal and external normalization. The internal normalization is employed for the elements with more than two isotopes and at least two isotopes to be stable with known (standard) ratios. The same can be present naturally in the sample or can be added externally into the sample. For example Sr and Nd has natural stable isotopes but in case of Uranium the U-233 and U-236 spikes with precisely known quantities are added externally in the sample. The ratio of stable isotopes is also measured along with the ratio of required isotopes and its variation with respect to standard ratio is monitored with time which is used to correct for the error in ratio of required isotopes. The internal normalization can be carried out in multi-dynamic mode and static multi-collector. As the standard and the analyte isotopes occur within same sample all the parameters from sample loading to data acquisition are same for both. Hence they follow similar profile for the ratio variation leading to efficient elimination of errors that result into very high precision for the isotopic ratio measurement. For example a precision of better than 10 ppm is obtained for the isotopic ratio analysis of Sr and Nd using internal normalization.

The external normalization is applied to the elements which do not exhibit any pair of stable isotopes. In this case the mass discrimination is circumvented using standard of same element. The isotopic ratio measurement is carried out for the given isotopes in standard and *K* factor is measured which is defined as the ratio of measured isotopic ratio to the certified isotopic ratio of standard. Various parameters *viz.* the quantities of the sample, loading procedure, filament material, analysis procedures and data acquisition time etc. are precisely controlled during *K* factor measurement. The *K* factor is applied to the measured isotopic ratio of sample to correct it for the fractionation provided sample also follows same profile of ratio variation as that of standard which is ensured by maintaining similar parameters (from sample loading to data acquisition) as with the standard. However the external normalization can not eliminate the error due to fractionation completely and so the precision is poorer than that obtained with internal normalization.

2.4 Summary

TIMS is a useful mass spectrometric technique to assay of inorganic material in terms of isotopic ratio of its constituent elements. Owing to its high sensitivity and precision it is irreplaceable technique for the isotopic analysis of long lived nuclear material. It is also employed for concentration measurement of an element in some matrix using isotopic dilution technique. Different sub-systems of TIMS *viz*. ion source, analyzer and collector systems along with various measurement techniques for isotopic ratio and concentration measurement were explained. The main limitation of the technique (in terms of precision) is mass discrimination due to mass dependent evaporation of the analyte molecules. Various methods to circumvent mass discrimination were also explained.

Chapter-3

Ion Source design

Introduction

Ion source is a fundamental part of TIMS and is one of the main components deciding the sensitivity and precision. The sensitivity is considered very important characteristic of TIMS particularly for nuclear field where smaller quantity needs to be handled because of radiation hazards. Moreover smaller quantity also makes it possible to sustain higher vacuum conditions in the source and enables the application of higher acceleration potential which in turn enhances the precision of the given analysis. Efforts have been made in our laboratory in recent past to improve the overall performance of TIMS in general and sensitivity and precision in particular [55 -57]. In one of the earlier developments [57], ion source design was modified to make it suitable for operation at 10 kV accelerating potential instead of 5 kV used earlier. But due to occasional electrical breakdown at higher potentials the operational potential was restricted to 6 kV in routine usage with sensitivity limited to around 1 ion for 600 atoms of Uranium. Considering further scope of improvements in the ion source for increasing sensitivity of TIMS various studies were undertaken as part of the thesis. The studies incorporated the modification of different parts of ion source namely the electrostatic lens and the filament assembly. In addition, the development of an electron impact ion source that may be attached to the collimator system of TIMS ion source was carried out. This was required by Heavy water plant, Manuguru for the isotopic ratio analysis of Oxygen in the form of CO_2 gas sample. The design of electrostatic lens was optimized for higher transmission using computer simulation followed by experimental validation. The design of filament assembly was modified to make it sturdier and optimizing it to enhance the ionization efficiency. The improved designs were compared with the earlier used conventional design and found to be better in terms of sensitivity and precision. The experimental data collected was found to be in good agreement with that obtained from the computer simulations. The chapter explains the methodology adopted for the studies and the evaluation of the modified ion source. As all the above studies are independent to each other, these are explained in separate sections in the following. Section 3.1 explains the studies on design of the electrostatic lens, section 3.2 explains the studies on filament assembly and section 3.3 explains the studies on electron impact ion source.

3.1 Studies on modification of electrostatic lens

3.1.1 Theory and design aspects

The electrostatic lens of TIMS is an immersion lens which extracts ions from the ionization region and accelerates them towards magnetic sector analyzer for the separation and subsequently to collectors for the measurement. During acceleration, the ions pass through various apertures in the lens and finally undergo focusing on an aperture called as source slit. The electrostatic lens (Schematic given in Figs 2.1 of chapter-2) consists of various electrodes known as Shield plate, Draw out electrode (*D* electrode), the *Y* focus electrode (*Y* electrode), Ground electrodes (G_1 and G_2 electrodes) and *Z* focus electrode (*Z* electrode). The *Y* electrode is further split into two parts known as Y_l and Y_r electrodes which are used to adjust direction of ion beam in XY plane. Similarly the *Z* electrode is also divided in two parts namely Z_u and Z_d which control the ion beam direction in XZ plane. The schematic representation of the ion source is shown in Fig. 2.1 of chapter 2 where ion beam direction is taken along X axis and the cut view in XY plane is shown. The ions are generated on centre filament of filament assembly which is enclosed in shield cup made of stainless steel with an aperture of size 1-2 mm wide and 8 mm high in front of the filament. The filaments and shield cup are raised to an accelerating potential followed by reducing potentials on *D* and *Y* plates. The ions are extracted out of the shield cup by the electric filed penetrating through the exit aperture of the shied cup due to the potential difference between *D* and Shield. As the ions exhibit very small kinetic energy in shield cup, they undergo very sharp focusing at the exit aperture called as the first focusing point as shown in Fig 2.1 of chapter 2. After the first focusing point the diverging ion beam is further converged due to the field distribution between *D*, *Y* and first ground plate (G_1) and re-focuses on source slit at G_2 electrode.

An electrostatic lens is characterized by its properties namely focal length and magnification which depends on the geometry and voltages applied on various electrodes. The properties of electrostatic lens with different number of elements are discussed in various references [58-65]. The designing parameters of an electrostatic lens incorporate dimensions of various electrodes, apertures and the gaps between the electrodes. The focusing of ion beam takes place due to the curvature of equipotential lines in the region with non uniform potential between the electrodes or at an aperture separating two regions with different potentials. The focusing of an ion beam through an electrostatic lens with three electrodes is depicted in Fig. 3.1. The focal lengths f_1 and f_2 are related to the voltages V_1 and V_3 applied on first and third electrode by following relation.

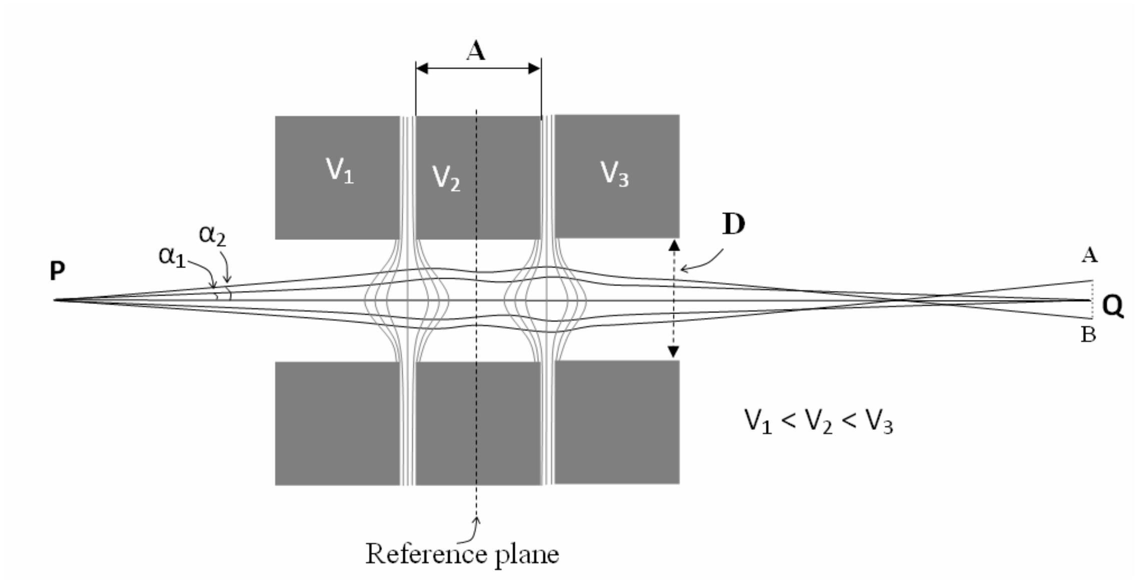

Fig. 3.1: Schematic showing the focusing of ion beam by three element electrostatic lens

$$f_1 / f_2 = (V_3 / V_1)^{1/2} \tag{3.1}$$

The distance *p, q* (of points P and *Q* with respect to reference plane respectively) and magnification *M* of the image are related to focal length *f* by following relations [64].

$$M = - f_1 / (p - F_1) = - (q - F_2) / f_2 \tag{3.2}$$

In case of TIMS, the object location (position of filament), the image location (source slit), the size of object (filament width) and the image (source slit) are fixed. The design criterion followed is to extract the ions from their generation point (filament) and focus them on source slit i.e. the geometry of various electrodes is to be optimized for a magnification of 0.3 (ions generated on filament with width 1 mm along y axis are to be focused on source slit with width 0.3 mm along y axis) for given object and image locations of the lens. The gaps between the electrodes are also to be optimized for sufficient electrical insulations between them so that higher accelerating potential can be applied on the ion source. The transmission of the electrostatic lens is mainly affected by the spherical aberration which causes focusing of the ion with higher divergence angle at a smaller image distance as compared to ions with smaller divergence angle as shown in Fig. 3.1. The figure shows the focusing of ions with angle α_2 at a location closer to reference plane than the focusing point *Q* of the ions with lower divergence angle α_1. The sharper focusing of ions with α_2 divergence angle generates extra width of the image as shown by the line 'AB' at point *Q*. This causes lower transmission of the ions source. Another type of aberration i.e. chromatic aberration is negligible in case of TIMS because of very small energy spread (< 1 eV). Therefore only spherical aberration is considered for the design optimization.

The increase in the image width (ΔI) due to spherical aberration is related to the divergence angle of the ion (α) by following relation [62].

$$\Delta I = C_s M \alpha^3 \tag{3.3}$$

Where C_s – coefficient of spherical aberration, M – magnification

According to equation 3.3 the spherical aberration is more for higher divergence angle. Therefore, the design of the ion source needs to be optimized in such a way that the ions follow a path close to the ion optical axis (X axis) of electrostatic lens. In reference [65] the coefficient of spherical aberration C_s has been studied for electrostatic lens in terms of their variation with respect to voltages on various electrodes and for different values of *A/D* ratios where *A* and *D* are the length and diameter of the electrode as shown in Fig. 3.1. It is shown that spherical aberration is lower for a lens with higher *A/D* ratio for a given magnification. This is because of the confinement of ions closer to axis by the electrodes with larger length. The application of higher accelerating potential also circumvents the aberration because the ions spend less time in the aberrated region. Taking this into consideration the design of conventional ion source was modified with following changes- 1) Using larger *A/D* ratio for the electrode to reduce the spherical aberration 2) Inserting additional electrode (elements) in the electrostatic lens to increase the electrical insulation of the ion source so that higher accelerating potential can be applied. The higher accelerating potential along with reduction of spherical aberration also reduces the divergence of the ion beam according to Liouvelle's theorem [36] and hence increases the transmission of the ion source.

In view of the above, the modifications of the conventional design (design-1; Fig. 3.2 a) was carried out in two steps. In first step the design-1 was converted to design-2 by modifying the geometry of *Y* electrode by increasing the aperture width (*d* in Fig. 3.2a) from 2 mm (in design -1) to 5 mm (in design -2) and the electrode length (*L* in Fig. 3.2a) from 1.5 mm (in design-1) to 5 mm (in design-2) by shaping it like L type plate as shown in Fig. 3.2b. In the second step, the design-2 was further modified to design -3 by inserting another electrode called as Y_{aux} (with same dimensions of *d* and *L* as for Y electrode) between *Y* and G_1 electrodes as shown in Fig. 3.2 c. Above designs were studied for their transmissions using computer simulations and the details are given in the following sections.

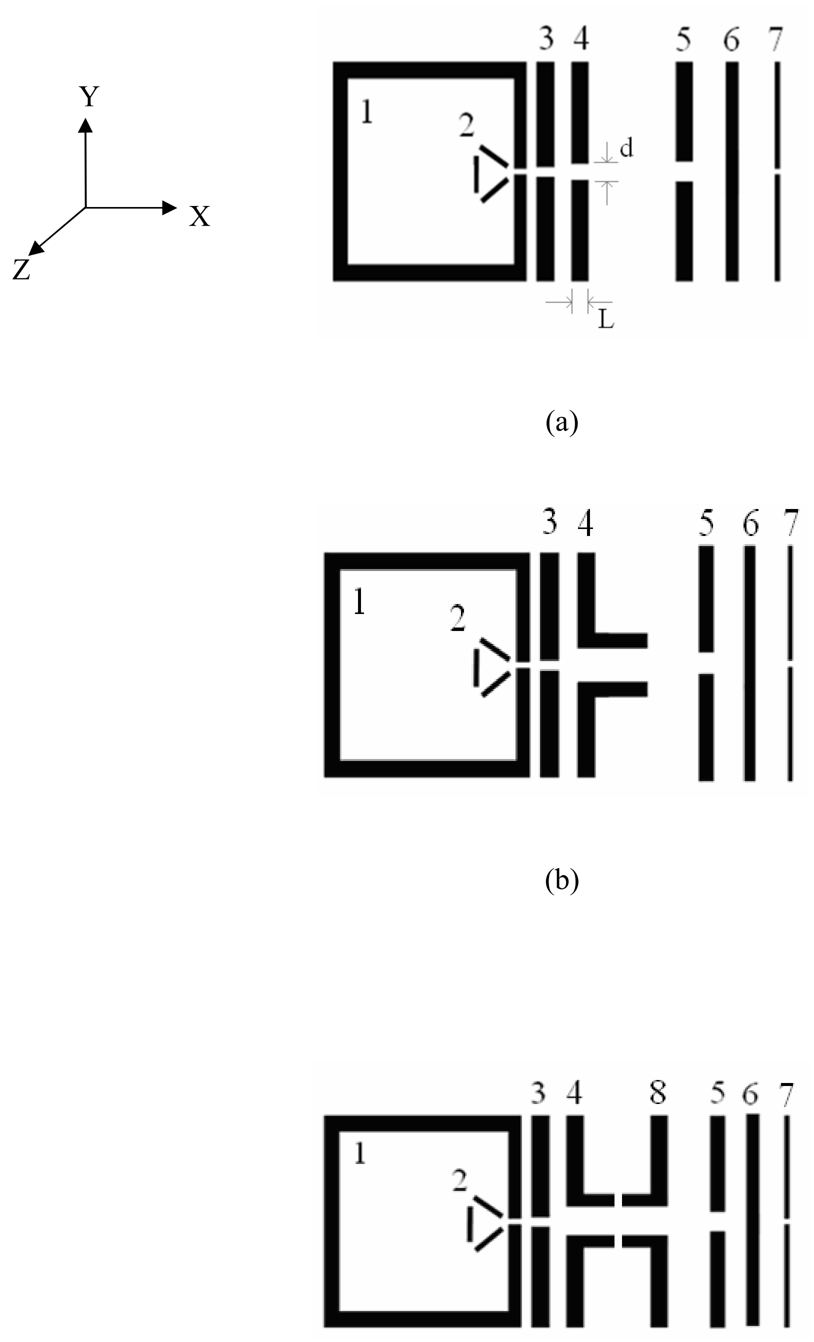

(a)

(b)

(c)

1) Shield 2) Filaments 3) D plate 4) Y plate 5) G_1 plate 6) Z plate 7) G_2 plate

8) Y_{aux} plate

Fig. 3.2: Schematic of the ion source designs; a) Design -1, b) modified design-2, c) modified design-3

3.1.2 Computer simulations

The simulations were carried out using software Simion 7.0 [66]. The geometries of different designs were generated in separate potential arrays. An electrode with slit dimensions as 1 mm (*x* axis) x 6 mm (*y* axis) x 7 mm (*z* axis) was also generated at a distance of 400 mm from the source slit to collect the ions as shown in Fig. 3.3. For each design, ions were generated from the middle region of the centre filament with range of different parameters as - Δy: 1mm, Δz: 4 mm, divergence angle (XY plane): $\pm$ 25° and divergence angle (XZ plane): $\pm$ 10°. The voltages on various electrodes were optimized to focus the ions on the source slit and obtaining maximum number of ions on the ion collector as shown in Fig. 3.3.

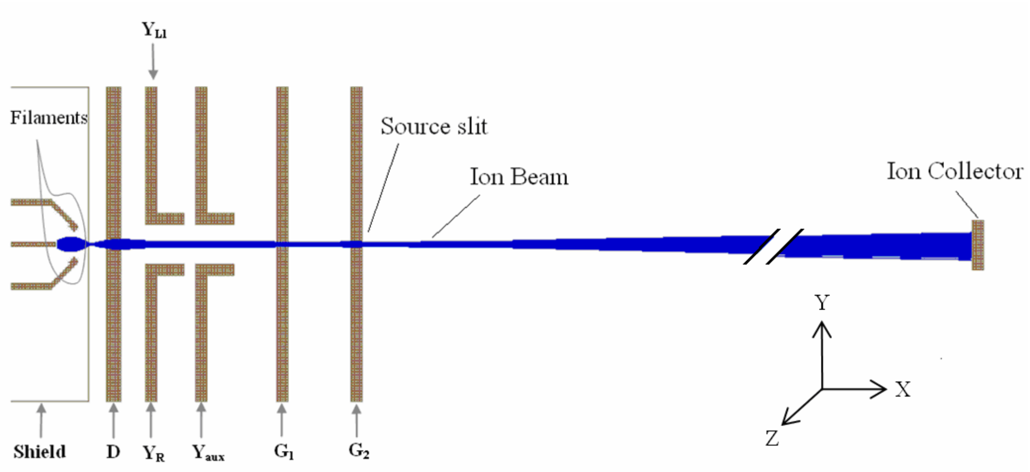

Fig. 3.3: Simulation of design -3; ion beam in blue is shown transmitting through various electrodes

The transmission was determined by calculating the ratio of number of ions collected on the ion collector to the number of ions generated on the filament. The transmission for all the designs were measured for different acceleration potentials ranging from 3 kV to 6 kV. The transmission profile of ions with increasing acceleration potential is shown in Fig. 3.4a. It shows that the transmission for all the design increases with the acceleration potential as expected theoretically. The transmission profile for design-3 was found to exhibit more slope as compared with other designs. The transmission for design-3 was also found to be more as compared to other designs in whole range (3 kV to 6 kV) of accelerating potential. The comparison of design 1 and 2 shows that in the lower potential range design 1 exhibit more transmission but in the higher potential region (more than 5 kV) the design 2 shows better transmission as compared to design-1. The comparison study of all the three designs shows that design-3 exhibit highest transmission which is more by a factor of about 2 than that for other designs at an accelerating potential of 6 kV.

3.1.3 Experimental

Based on the simulation study, the ion sources with all three designs were assembled and installed sequentially in the turret chamber of the TIMS. Ions of ^{187}Re^{+} generated from the central filament of the given filament assembly were used for the experimental study. Since the Re^{+} ions are produced from the filament itself, the ion current remains stable for very long period. However the ion currents obtained from any real analyte sample deposited on the filament do not remain stable with time. Therefore measurement of Re^{+} ion currents is advantageous than using real sample for the comparison study of the ion source designs. It ensures the stability of input ion current so that transmission through the ion source can be investigated by studying its dependence only on the design parameters. The same input ion currents of Re^{+} for all the designs were also ensured by using same filament and with same amount of filament current. Considering the constancy of input ion current, the transmissions of different ion source designs were compared simply by comparison of the ion currents of ^{187}Re^{+} on Faraday cup in each case.

For a given design, the magnetic field of the sector magnet was set to obtain ^{187}Re^{+} signal on the Faraday collector followed by signal optimization by adjusting voltages on various electrodes of the ion source. The focusing of the ion beam in the collector was ensured by taking magnetic scan of the ion beam across the collector. Subsequently peak centering was done by setting the magnetic field corresponding to the middle point on the flat top region of peak. The signal for $^{187}Re^+$ was measured with integration time of 5 seconds. The average of ten such measurements was taken to represent the data. Same procedure was adopted for other designs also. The data was collected for accelerating potential from 3 kV to 6 kV in steps of 1 kV for each design and plotted in Fig. 3.4 b.

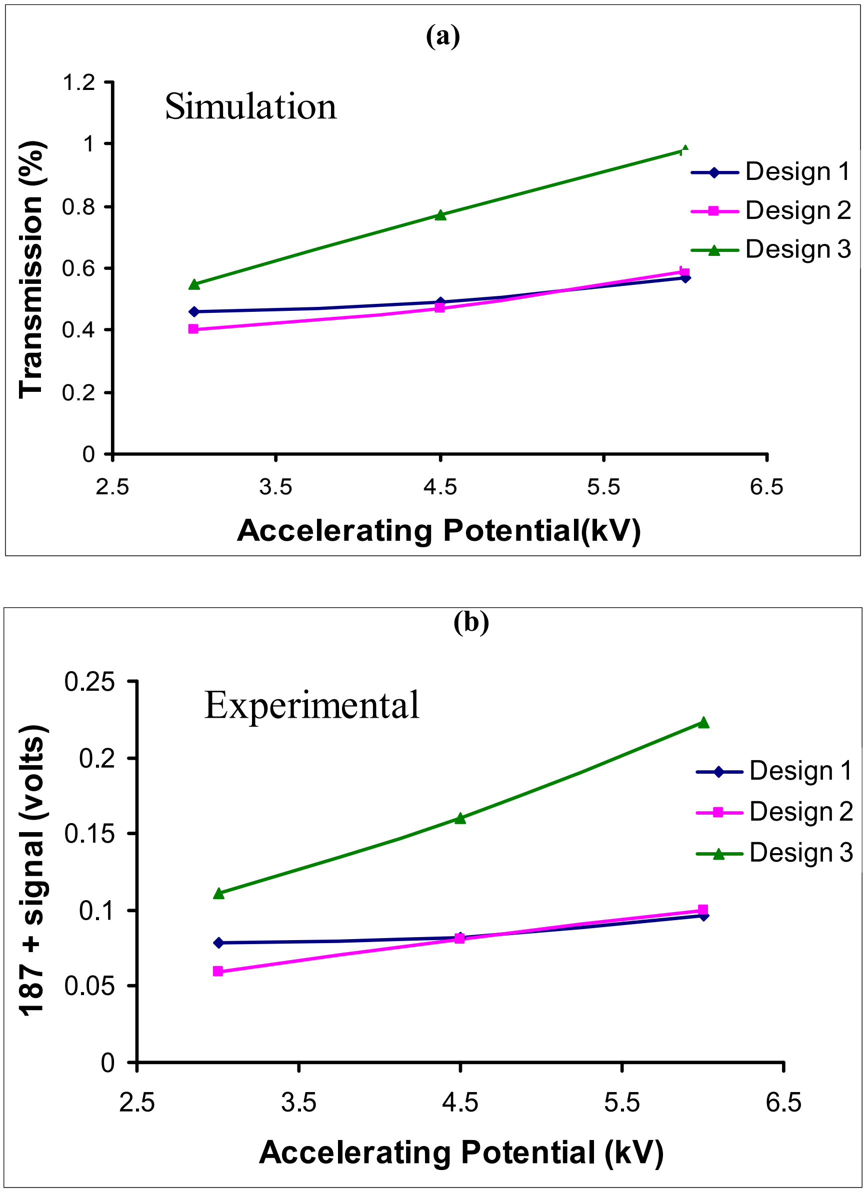

Fig. 3.4: Graphical representation of the variation of transmission with accelerating potential in a) simulation and b) experimental

The evaluation of the ion source was carried out by isotopic ratio measurement of Uranium standard (ISU-09). Same sample was loaded on 12 filament assemblies of the turret system and isotopic ratio ($^{235}U/^{238}U$) was measured for each assembly. The data is presented in table 3.1.

Table 3.1: The isotopic ratio ($^{235}U/^{238}U$) data for Uranium standard (ISU-09)

S. No.	Ratio (235/238)	RSD (%)
1	0.011024	0.04
2	0.011000	0.05
3	0.011034	0.03
4	0.011022	0.04
5	0.011027	0.04
6	0.011015	0.04
7	0.011026	0.03
8	0.011024	0.07
9	0.011021	0.05
10	0.011014	0.03
11	0.011024	0.04
12	0.011025	0.06
Average Ratio	**0.011021**	
Precision	**.077%**	

3.1.4 Results and discussion

The variation of ion current intensity of $^{187}Re^{+}$ with accelerating potential for all the designs (Fig. 3.4 b) shows that the transmission of ion source increases with accelerating potential for all the designs as expected theoretically. The slope of transmission profile is shown to be increasing from design-1 to design-3. This shows that at higher accelerating potentials the spherical aberrations are better taken care from design -1 to design-3 due to higher A/D ratio in design-2 and an additional electrode Y_{aux} in design-3. Comparison between design 1 and 2 shows that design 1 exhibit more transmission at potentials lower than 4.5 kV but due to higher slope of transmission profile for design-2, the transmission for design-2 becomes more than design-1 after accelerating potential above 4.5 kV. The transmission of design-3 was found to be highest among all the designs for whole range of accelerating potential. The transmission of design- 3 was found to be higher by a factor of two as compared to other designs at an accelerating potential of 6 kV.

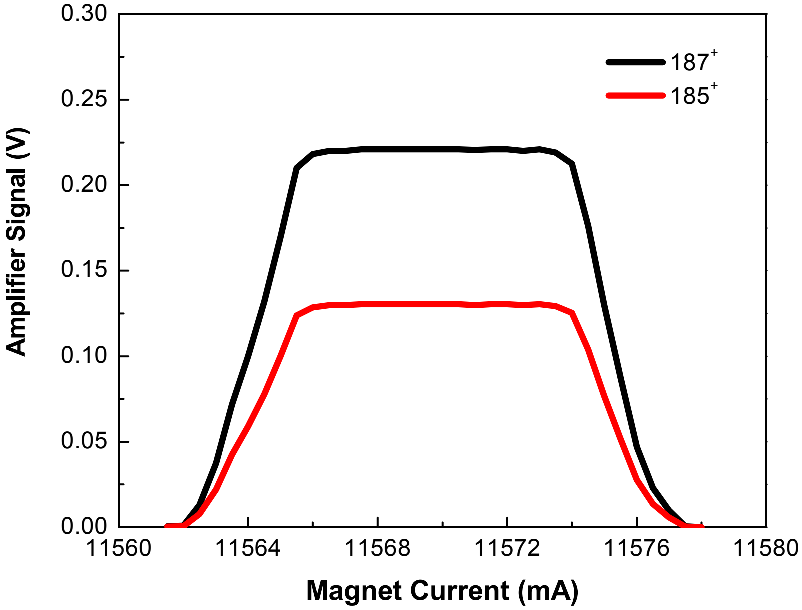

Fig. 3.5: Typical peak shape for rhenium isotopes

The results obtained are in agreement with the computer simulations. Moreover, the incorporation of additional Y_{aux} plates between Y plates and ground plates provides gradual reduction in the voltage from Y to ground plate and hence better electrical insulation. The peak shapes for Re ion beam obtained with design 3 as shown in Fig. 3.5 reveals that ions are well focused on the faraday collector. Similar peak shapes were obtained with other two designs also. The comparison study has been carried out only up to an acceleration potential of 6 kV but the trends obtained show that the transmission will further increase at even higher potentials.

The data presented in table 3.1 shows a precision of .077% for ISU-09 Uranium standard. This shows that the ion source is suitable for the routine isotopic ratio measurements on TIMS.

3.1.5 Conclusion

The design of ion source was studied by computer simulations followed by experimental validation on the thermal ionization mass spectrometer. The experimental results obtained were found to be in good agreement with the computer simulation. Based on this study, an ion source with modified design was developed and installed on the TIMS. The modified ion source enabled increasing the sensitivity of the TIMS by a factor of around 2. The modified design also exhibit better electrical insulation as compared with the conventional design and hence can work at higher acceleration potential which can further enhance the sensitivity of TIMS. The TIMS with the modified ion source was tested with different Uranium standards and precision of 0.077% was obtained.

3.2 Studies on design modification of filament assembly

3.2.1 Introduction

The filament assembly is employed in TIMS for loading and ionization [1 -3] of the analyte in a TIMS as explained in chapter -1 and 2. It plays vital role in effecting the sensitivity of TIMS. The TIMS developed by BARC typically uses triple filament assembly [43, 57] whereby the side filaments are used for sample loading and the centre filament is used for ionization of the sample. The filaments are arranged in a configuration (as shown in Fig. 3.6) so that the sample vapors from side filaments are directed towards the centre filament. The conventional filament assembly consisted of stainless steel (SS) pins sealed on SS base plate using glass to metal (GM) sealing. However during operations at high temperature for the isotopic analysis of the sample, the GM seals get softened resulting into the misaligning of the centre and side filaments. This causes reduction (and sometimes disappearance) of the analyte signals on collectors resulting into difficulties in the analysis. This also causes occasional failure in getting results for some of the filament assemblies thereby affecting the throughput of the instrument. To overcome this problem a modified filament assembly with ceramic (fired alumina) was developed. It was evaluated on TIMS and found to be much better than conventional filament assembly in terms of signal stability and durability and hence helped to improve the performance of the TIMS.

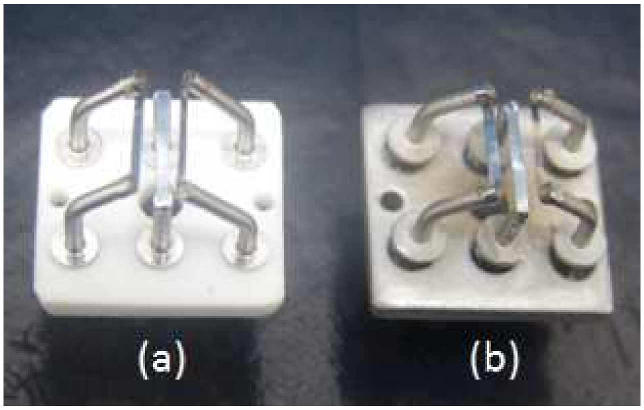

Fig. 3.6: Photograph of Filament assemblies: (a) new modified filament assembly with ceramic base (b) old type filament assembly with metallic base and glass to metal sealing

3.2.2 Design aspects

The new triple filament assembly consists of ceramic base and six stainless steel (SS) pins attached to the base as shown in the Fig. 3.7. The dimensional details of the assembly are given in Fig. 3.8. For the initial design optimization machinable ceramic was used for the fabrication of base of the filament assembly. The holes were drilled at six positions as shown in the drawing in Fig 3.8. The SS pins were fabricated with threading at one end and an orthogonal circular disc in between the pin to lock the pin from one side of the ceramic plate as shown in Fig 3.7. Six such pins are attached with the ceramic base by inserting the pins into respective holes from one side of the base plate and tightening the SS nuts from other side as shown in the Fig 3.7 and Fig. 3.8. The pins for the side filaments are bent with appropriate bending angles so that maximum quantity of analyte vapours approach the centre filament to provide maximum sensitivity. The fabrication of the SS pins and ceramic plate was carried out with very fine tolerances of ± 10 micron. This assures very precise placement and orientation of ribbons which plays vital role in achieving good precision of the isotopic ratio measurement on the instrument.

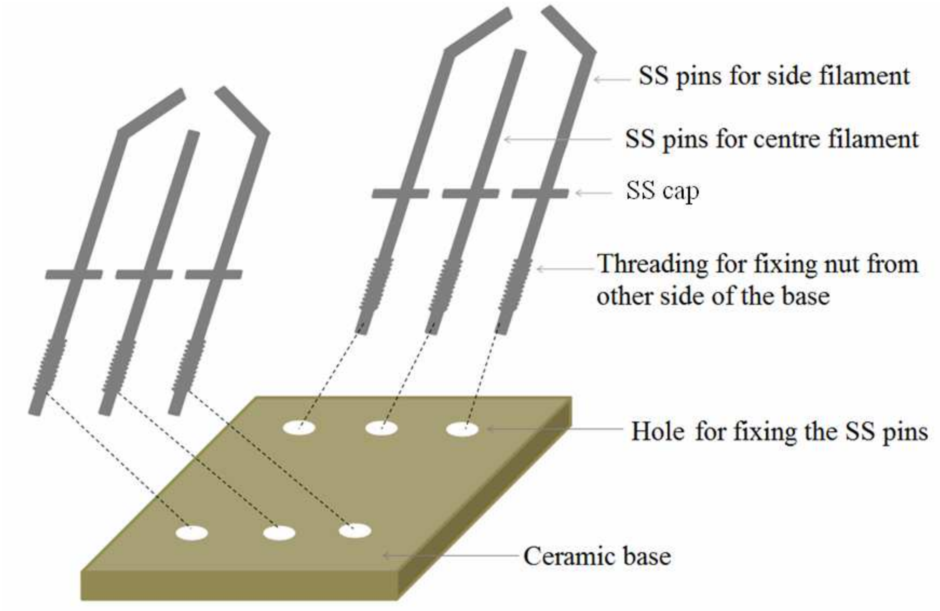

Fig. 3.7: Schematic of the filament assembly in dismantled form

3.2.3 Experimental

Rhenium filaments of size 1mm x 0.025mm were spot welded on the upper end of the pins in suitable configuration. 1-2 microgram of natural Uranium standard was used for the evaluation of filament assemblies for ratio measurements. Ten such filament assemblies were loaded with the same standard and the isotopic ratio data of $^{235}U/^{238}U$ was collected. The data was compared with that collected earlier with old type filament assemblies as shown in table 3.2.

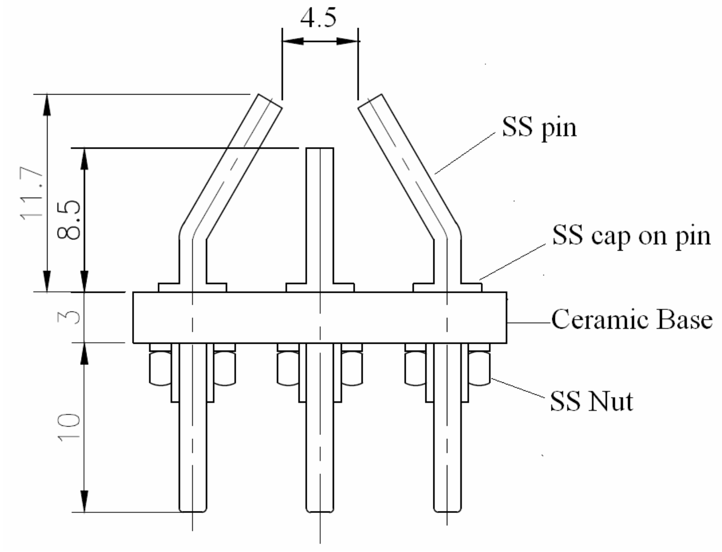

(a)

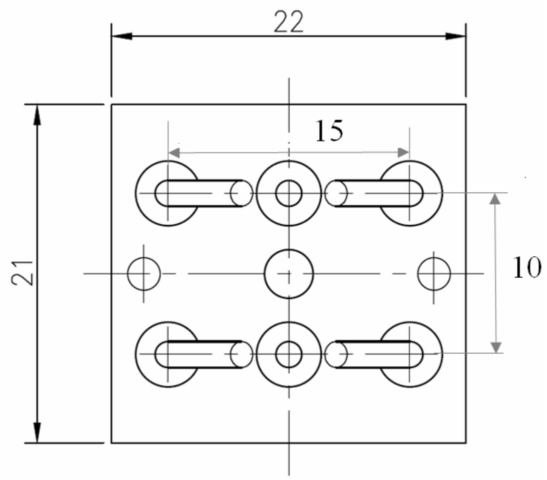

(b)

Fig. 3.8: Dimensional drawing of new Filament assembly (a) Elevation view (b) Plan view

Peak shapes of both isotopes of Uranium (^{235}U and ^{238}U) simultaneously were taken by magnetic scan as shown in Fig. 3.9. Frequent trials with a few filament assemblies were carried for ratio analysis of various samples to check the durability of the assemblies. It may be noted that peak width of ^{235}U is smaller than that of ^{238}U. This is because the size of aperture (in variable dispersion zoom optics; refer chapter -5) before the Faraday collector for ^{235}U was 2.0 mm instead of 3.0 mm for the collector used for ^{238}U. This was done to optimize the positions of Faraday collectors for use with variable dispersion zoom optics. Further the centre of peaks is not in same position in Fig. 3.9 which can be done by further adjustment of the electric fields of zoom optics. However as a large flat region of both peaks is overlapping, this was not carried out.

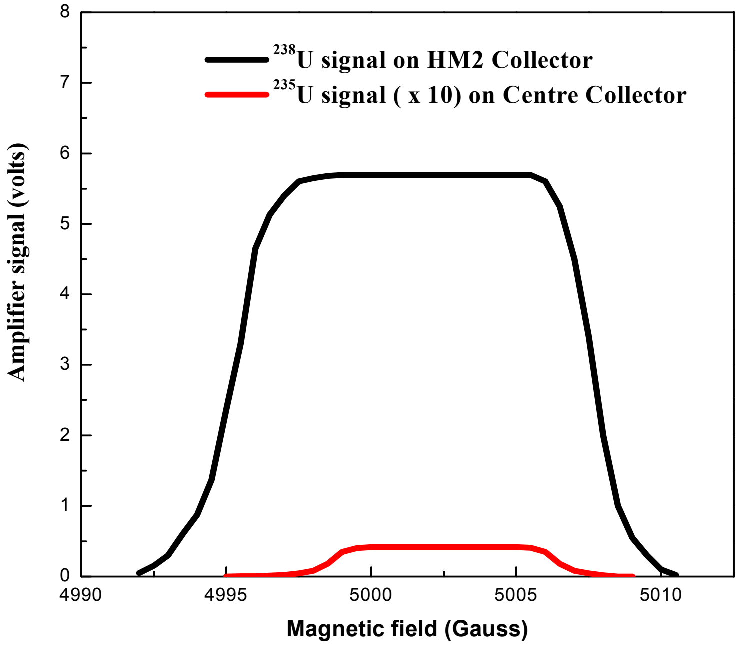

Fig. 3.9: Peak shape for Natural U standard; scale for U-235 signal is normalized by a factor 10 with respect to U-238 signal

3.2.4 Results and Discussion

The comparison of isotopic ratio data in table 3.2 collected using new assembly with that collected using old type assemblies clearly points out that new assemblies are more reliable. In case of old type assemblies results could be generated in 6 out of 10 trials made due to distortion problems with these assemblies. However owing to the sturdiness of new assemblies, results could be generated in all the trials. Moreover, the external precision using new assemblies also improved to 0.09% from 0.18% with old type assemblies. The peak shapes for Uranium isotopes (Fig. 3.9) reveal the stability and proper focusing of the ion beams on respective collectors.

Table 3.2: Comparison of conventional and new filament assembly using isotopic ratio data for Natural Uranium standard

S. No.	**Ratio ($^{235}U/^{238}U$)**	
	With new filament assembly	**With old type filament assembly**
1.	0.007342 (4)	no result
2.	0.007334 (6)	0.007300(3)
3.	0.007332 (6)	no result
4.	0.007345 (4)	no result
5.	0.007340 (4)	0.007320 (3)
6.	0.007348 (6)	0.007292 (3)
7.	0.007343 (5)	0.007299 (4)
8.	0.007331 (5)	0.007281 (4)
9.	0.007348 (9)	0.007306 (5)
10	0.007332 (4)	no result
Average	**0.007339**	**0.007300**
RSD (%)	**0.09**	**0.18**

One of the problems that might be suspected with ceramic base assembly is that due to the insulating nature of the ceramic assembly there may be charging problem. But this possibility is ruled out because of the good precision and stable flat top peaks obtained. The assemblies were tested frequently for the routine operations without any problem. After frequent operations also it was found that the assemblies were intact which certifies high durability of these assemblies as compared with the old types, which have to be discarded after very few usages.

3.2.5 Conclusion

The filament assemblies with ceramic base were developed successfully. Testing results show that the new assemblies are much better than the old type assemblies in terms of performance and durability. The sturdier design has helped in obtaining stable signal during analysis which enabled improvements in precision as compared with the old type assembly. It also helped in increasing the throughput of the system in terms of number of sample analysed within given time. The longer life of new assembly has also helped in reducing the down- time of the instrument.

3.3 Studies on development of electron impact ion source

3.3.1 Introduction

TIMS is employed for the isotopic analysis of analyte in solid form as explained in chapter-2. However for the analysis of the gaseous samples an electron impact ion source is required as explained in chapter -1. To meet a specific requirement for the isotopic ratio analysis of Oxygen in form of CO_2 by Heavy Water Plant, Manuguru, an electron impact ion source was developed [1, 2]. It was tested for its feasibility to be used on the collimator part of the ion source of TIMS. An exclusive design for this ion source was worked out whereby it can be easily attached to the collimator part of the TIMS in place of the turret that is used in routine in thermal ionization (TI) mode. Using this arrangement it was possible to use TIMS instrument for gaseous samples (in EI mode) also. This development has resulted in widening the application of the TIMS. This section explains the design details and the experimental studies carried out for the performance evaluation of the EI ion source using natural CO_2 standard.

3.3.2 Design Aspects

The basic design of EI ion source is the conventional Nier type [1, 2] with some modifications to facilitate its proper attachment to the collimator part of TIMS. The EI source consists of stainless steel base plate on which all the electrodes *viz.* case, repeller, trap and electron focus (made of SS304) are assembled at their respective locations as shown in Fig.3.10 and 3.11. The gas sample is introduced through an SS304 sample box having two SS tubes each of 0.5 mm inner diameter attached to the base plate as shown in Fig. 3.11. The ion source can be attached to the top plate (i.e *D* plate) of collimator ion optics using screws through four SS spacers welded on the base plate. The SS spacers ensure proper alignment of the ion source with collimator ion optics. EDM/wire cutting fabrication techniques were employed to ensure tight tolerances of all the components.

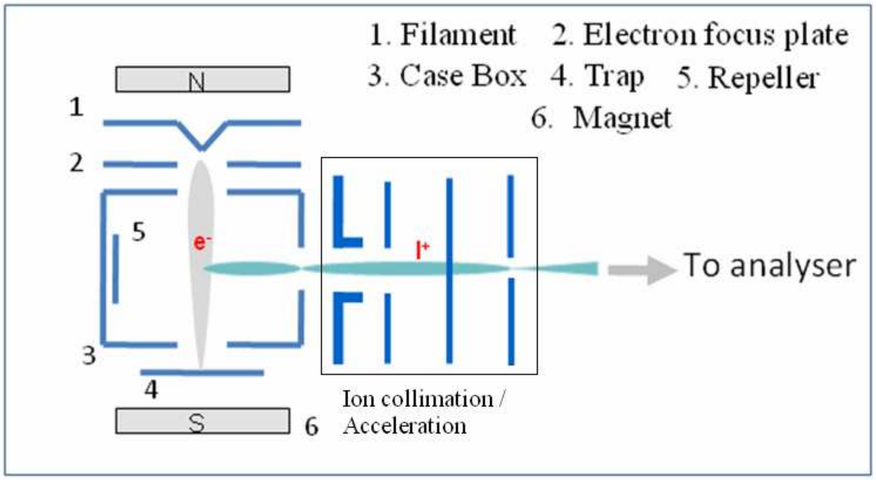

Fig. 3.10 Schematic of the electron impact (EI) ion source

3.3.3 Experimental

The ion source was mounted on the collimator ion optics of TIMS and tested with natural standard CO_2. The sensitivity was measured by introducing known quantities of CO_2 and measuring the amplifier signal corresponding to the major isotopes of Oxygen i.e. $^{12}C^{16}O^{16}O^+$ ion beam at mass 44 amu. The ion beams for masses 44 amu and 46 amu (corresponding to the ^{16}O and ^{18}O respectively) were aligned with the respective collectors and peak shapes were recorded by varying the magnetic field of the analyzer. Several trials of isotopic ratio measurements of $C^{18}O^{16}O^+/C^{16}O_2^+$ (ions at mass 46 amu and 44 amu respectively) were conducted in 'ABBA' [1] mode of ratio measurement. The 'ABBA' mode is the methodology adopted usually for isotopic ratio measurement of gaseous samples whereby ratio for sample and standard is measured in sequential runs. This takes care of various systematic errors due to factors *viz.* fractionation, memory effect, amplifier biases etc. present in the instrument. The precision of any measurement is calculated using variation in 'α ' which is defined as ratio of measured isotopic ratios of sample and standard. For same standard used in all the runs of ABBA, the value of α should be unity. The variation over unity is defined as the precision of the measurement.

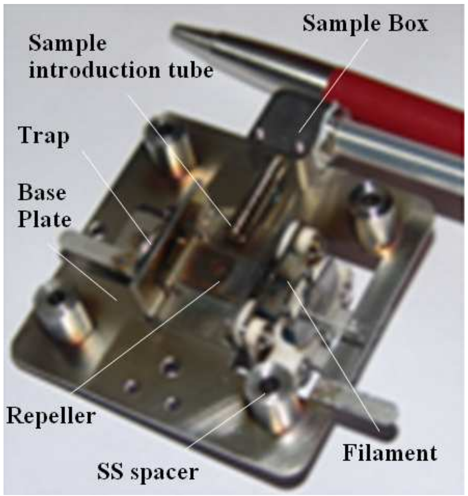

Fig. 3.11 Photograph of the EI ion source

3.3.4 Results and Discussion

The signal for 44^+ ion beam was measured to be around 4 volts across the amplifier resistance of 1×10^{11} ohms for a partial pressure of 1×10^{-7} torr for CO_2 in the ion source at 1 mA electron emission current. This corresponds to the sensitivity of 4×10^{-4} A/torr. The isotopic ratio data for CO_2 and the 'α' value is given in table 3.3. The external precision obtained for α was better than 0.05%. Good flat top peaks with flatness of ~1000 ppm of mass were obtained for CO_2^+ ions as shown in Fig. 3.12. The ion beam width measured using above peaks was found to be around 0.7 mm on all the collectors.

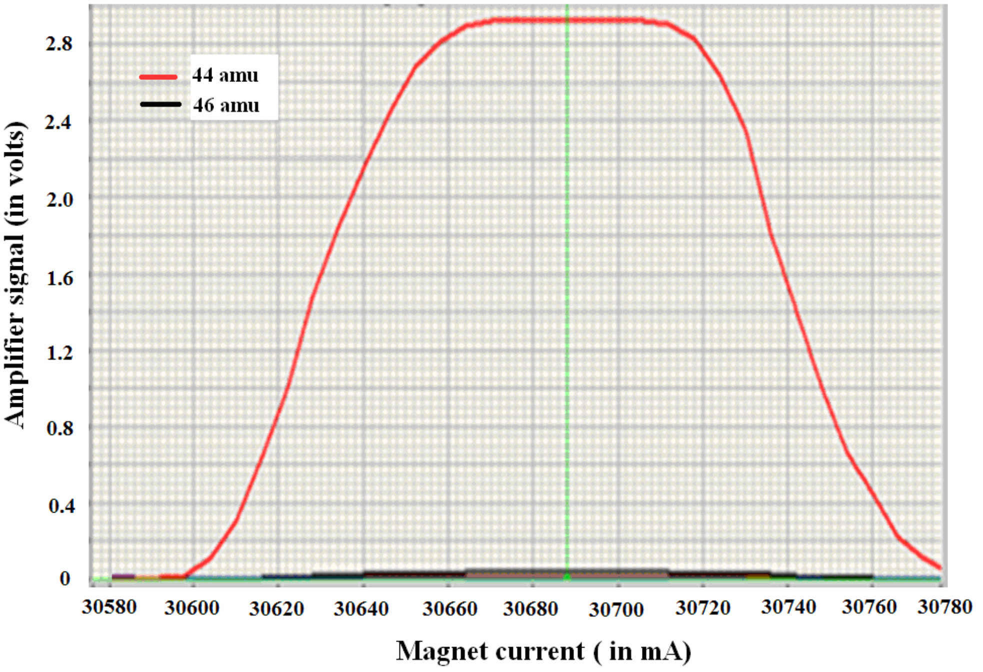

Fig. 3.12 Peak shape for Oxygen isotopes ^{16}O and ^{18}O corresponding to CO_2 ions at masses 44 amu and 46 amu respectively.

Table 3.3: Isotopic ratio data for $^{18}O/^{16}O$ using natural CO_2 standard

S.No.	Ratio ($46^+/44^+$)	RISD (%)	α [A+A')/(B+B')]
1	0.004299	0.08	1.00002
2	0.004305	0.07	1.00085
3	0.004294	0.07	1.00076
4	0.004286	0.08	1.00075
5	0.004285	0.08	1.00006
6	0.004279	0.07	0.99944
Average	0.004292	0.08	1.0003
RSD (%)			0.05

3.3.5 Conclusion

The electron impact ion source was successfully tested and evaluated on TIMS. The sensitivity (4 x 10^{-4} A/torr) and precision (0.05%) obtained were sufficient for routine measurements of Oxygen isotopic ratios. This has helped in increasing the versatility of TIMS and enhanced its usability for the isotopic ratio analysis of gaseous analyte along with the routine analysis of solid samples. This has also helped in avoiding the need of separate instrument exclusive for the analysis of gaseous samples.

Chapter-4

Magnet design

Introduction

The magnetic sector analyser is a vital part of TIMS which separates the ions as per their mass to charge ratio. The resolution and mass range of the TIMS is mainly decided by magnetic sector analyzer. The basic theory of magnetic sector has already been explained in chapter-2 whereby the dependence of focusing of ions on various geometric parameters of magnetic sector was explained. Conventionally the exit and entry boundaries of magnetic sector are straight which leads to inclining the focal plane of ion beams (with different m/q) with respect to principal beam axis. This can generate various complications particularly when there is requirement of large number of collectors. A TIMS (TIMS-B) [67] was developed for geo-chronological applications based on an earlier design of system (TIMS-A) with specifications given in Table 4.1. The TIMS-B consisted of seven faraday cups for carrying out isotopic ratio measurements on elements ranging from Sr to Pu while the earlier system (TIMS-A) had only three collectors. Ion optical parameters of the mass spectrometer decide the exact locations and separations of these collectors and multi-isotope analysis demands the adjustment of these detectors across the focal plane that normally makes an inclination of 25° to the principal beam axis. This necessarily makes the collector system very bulky and unwieldy, particularly, if large number of collectors is required. Therefore, studies were conducted to rotate the focal plane along a line normal to principle axis.

One of the ways to simplify the collector positioning and movement mechanism is to redesign the magnet so as to rotate the focal plane of the image along a line normal to the principal beam axis. Various other methods have also been used to rotate the focal plane. For example, in ref. [21] two quadrupoles: an electrostatic quadrupole at the detector side and a magnetic one at the source side of the sector magnet have been used. In reference [68], magnet (exit) pole face with curvature has been suggested for this purpose and it has been shown that exit curvature may be used to make focal plane normal to principal beam axis. Further, existing theory [19, 20] has been used for calculation of optimum exit curvature. However, the theory does not fully account for fringe fields and an experimental optimization of exit curvature is desirable. For experimental optimization, attachment of a shim at exit boundary is more convenient (compared to fabrication of magnet with curvature of pole faces) as many shims of different curvature may be easily fabricated and evaluated. In this study, we have used theory [19, 20] to determine optimum exit curvature that has been further optimized experimentally by attaching shims of different curvature. Since, theory does not adequately take fringe fields into account; optimum curvature has also been determined by computer simulation. Computer simulations also have advantage of being able to consider different field in the shim region which may occur due to small insulation gap between shim and the magnet boundary. Theoretical calculations showed optimum exit shim curvature of 177 mm while computer simulations taking fringe field into account, showed an optimum curvature of 160 mm. Variation of magnetic field in the shim region was experimentally measured and field was found to be lower by 200 Gauss. Simulations using this field variation showed optimum shim curvature of 140 mm. Experiments carried out with shims of different curvature showed good agreement with simulation data with an optimum curvature of 130 mm.

A concave curvature at exit boundary has the drawback of increasing the spherical aberration. This may be reduced by using a shim at entrance boundary with convex curvature. Optimum curvature at entrance boundary has been determined theoretically and experimental results with shims at both entrance and exit boundaries have been presented.

Table 4.1: **Salient Features of the Instrument (TIMS-A)**

Ion source	:	Thermal ionization with triple filament assembly
Analyzer	:	Sector Magnet with 300 mm Radius, 90° deflection
Collector system	:	Three faraday collectors
Resolution	:	450
Sensitivity	:	1 ion per 600 atoms of Uranium (~ 10 pA of ^{235}U for 1 μg of Natural U sample)
External Precision	:	0.1% for natural U
Ion Energy	:	Up to 10 keV

4.1 **Theory**

The image distances (from magnet edge) for ion beams of different masses, depend on ion optical parameters of the analyzer *viz*., radius of ion beam trajectory, angle of deflection and entry and exit angles [20, 69]. Typically, in a magnetic sector mass spectrometer, ions of different masses focus at different distances from magnet resulting in focal plane not being normal to beam axis as shown in Fig. 4.1. In the following, we theoretically determine if a concave curvature (as seen from outside) of magnet at exit boundary helps in rotating the focal plane normal to beam axis (shown as 'desired plane' in Fig. 4.1).

First we consider focusing of ions of a particular mass in magnetic analyzer with straight boundaries as schematically shown in Fig. 4.2. Trajectory of ions with different velocities and angles (α) to central beam is given by [20]:

$$Y= r\,\{M_1\alpha + M_2\,\beta + M_{11}\alpha^2 + M_{12}\,\alpha\,\beta + M_{22}\beta^2\} + X\,\{N_1\,\alpha + N_2\,\beta + N_{11}\,\alpha^2 + N_{12}\,\alpha\,\beta + N_{22}\,\beta^2\} \quad (4.1)$$

Where r is radius of curvature of principal trajectory of ions, Y is the displacement with respect to principal axis after deflection, β is the relative variation in velocity of the ion beam with respect to mean velocity ($\beta = \Delta v/v_0$ where v_0 is average velocity of ions and Δv is variation from v_0), X is the position along principal axis with respect to the exit edge of the magnet. Different coefficients M and N depend on the shape and dimensions of the magnetic sector analyzer. These parameters have been derived for homogeneous magnetic field for any curvature of boundaries [20, 70, 71] and the values as given by Hintenberger and König [20] have been used here.

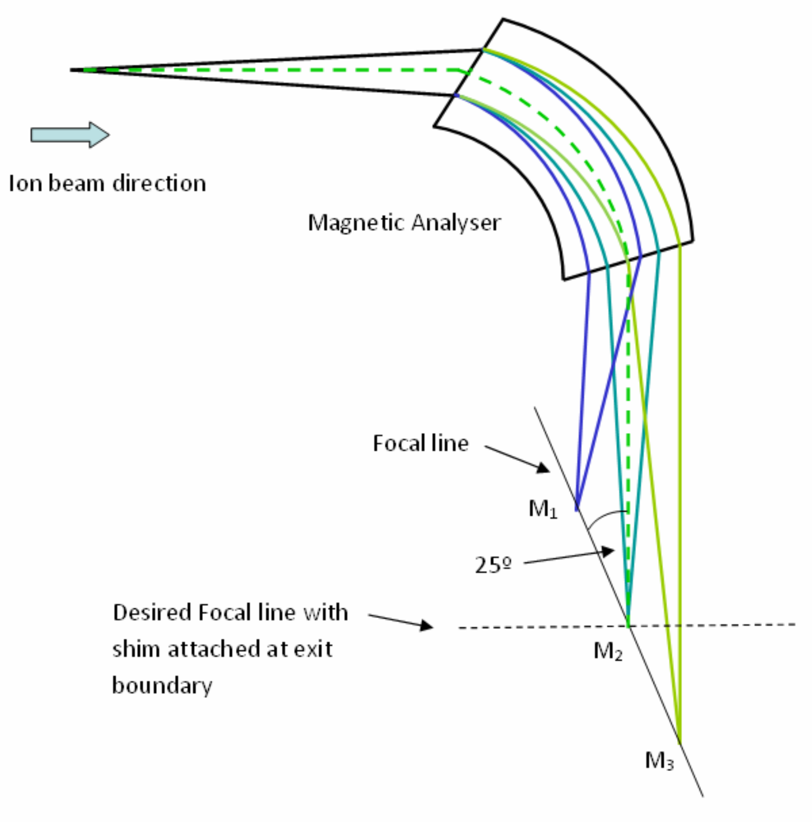

Fig. 4.1: Schematic diagram showing the inclined focal line for typical magnetic analyzer using ions of three different masses (*M3>M2>M1*). A desirable focal line for convenient placement of collectors is also shown.

Considering only the first order terms of α (first order focusing) and $\beta = 0$ in equation (4.1), image distance (S_i) from the exit boundary of the magnet (using values of parameters given in Ref. 5) is given by:

$$S_i = [S_o[\cos\Phi + t_1 \sin\Phi)] + (r \sin\Phi)] / [(S_o / r)[\sin\Phi - (t_1 + t_2) \cos\Phi - (t_1 t_2 \sin\Phi)] - \cos\Phi - (t_2 \sin\Phi)] \qquad (4.2)$$

Where, S_0 is the object distance, Φ is the bending angle of the magnet, $t_1 = \tan\epsilon_1$ and $t_2 = \tan\epsilon_2$, ϵ_1 and ϵ_2 are entry and exit angles of the principal ion beam trajectory with respect to normal at entry and exit boundary of the magnet respectively.

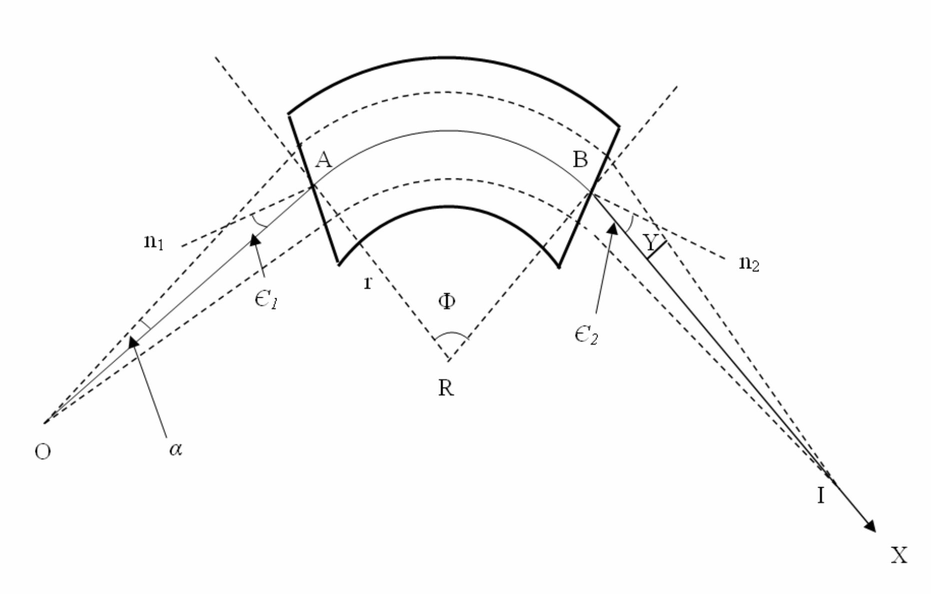

Fig. 4.2: Schematic showing the focusing of ion beam by magnetic sector

For finding focal plane orientation we need to determine focusing distance of ions with different masses. If r_0, ϵ_{20} and Φ_0 are the radius of curvature, exit angle and deflection angle for central mass (M_0), we may write radius of curvature (r), exit angle (ϵ_2) and deflection angle (Φ) for arbitrary mass (M) by [23]:

$$\Phi = \Phi_0 + d\Phi = \Phi_0 + (M_0 / M)^{1/2} [1 - (M / M_0)^{1/2} + (1 - (M / M_o)^{1/2} \cos((M_0 / M)^{1/2} - 1)) \; t_2]$$

$$r = r_0 (M / M_0)^{1/2}$$

$$\epsilon_2 = \epsilon_{20} - d\Phi$$

The spherical aberration (Y_s) for first order focusing as derived from equation 4.1 is given by [20]:

$$Y_s = (M_{1\,1} - (M_1 / N_1) N_{11}) \, r \, \alpha^2 \tag{4.3}$$

In some of the earlier studies, possibility of rotation of image plane by variation of geometric parameters of the magnetic analyzer has been discussed [72-76]. In present study we have added a shim at exit of magnet to rotate the focal plane and another shim at entrance of the magnet to minimize aberrations. Effect of shim on focal plane and aberration has been determined in the following.

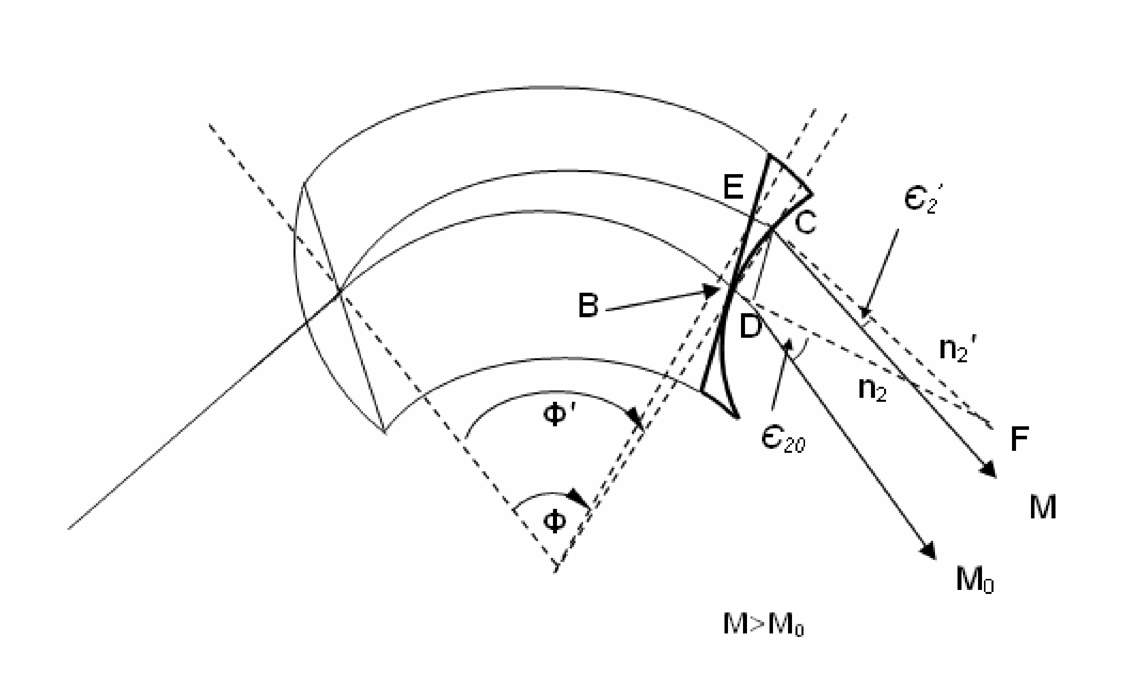

Fig. 4.3: Schematic diagrams showing central ion beam trajectories for ions of different masses with exit shims attached.

4.1.1 **Effect of exit boundary curvature on image plane**

The curvature on the exit boundary provides an extra magnetic region on both sides of the central mass and hence the exit and bending angles for masses other than the central beam are altered as schematically shown in Fig. 4.3 (for $M>M_0$). It is seen that exit angle (angle of ion trajectory with respect to normal to boundary at exit point) reduces for $M>M_0$ which in turn results in shifting of the focal point towards the magnet. On the other hand for $M<M_{0,}$ the focal points shifts away from the magnet. This results in rotating the focal line counter clockwise as desired to make it normal to ion trajectory (see Fig. 4.1). The addition of shim also increases

the deflection angle slightly (angle Φ' in Fig. 4.3). But the effect of slight alteration of deflection angle is negligible as compared to that of exit angle.

On attachment of a shim with curvature R_{c2} (= FB in Fig. 4.3) and approximation $dr \ll R_{c2}$, the modified exit angle (ϵ_2') and deflection angle (Φ') for different masses are given by:

$$\Phi' = \Phi + EC/r = \Phi + [R_{c2} - (R_{c2}^2 - dr^2)^{1/2}]/r \tag{4.4}$$

$$\epsilon_2' = \epsilon_2 - \sin^{-1}(dr/R_{c2}) + d\Phi \tag{4.5}$$

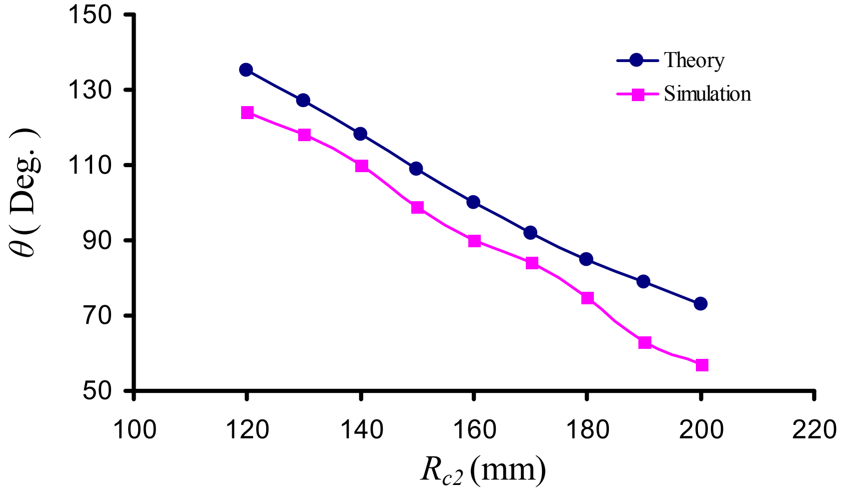

Fig. 4.4: Theoretical and simulation results on the variation of Focal line angle (θ) with radius of curvature (R_{c2}) of exit side shim.

These modified parameters have been used in equation 4.2 and the resulting image distances have been calculated for different ion masses and shims of different radii. For given shim curvature, focal line inclination was determined using image distances for different ion masses. The results obtained (for $\epsilon_1 = 26.56°$ and $S_0 = 600$ mm used in our system) are shown in Fig. 4.4. Here θ denotes angle between focal line and principal beam axis. It is seen that the inclination of focal line is 90° to the principal beam axis for exit shim curvature of 177 mm.

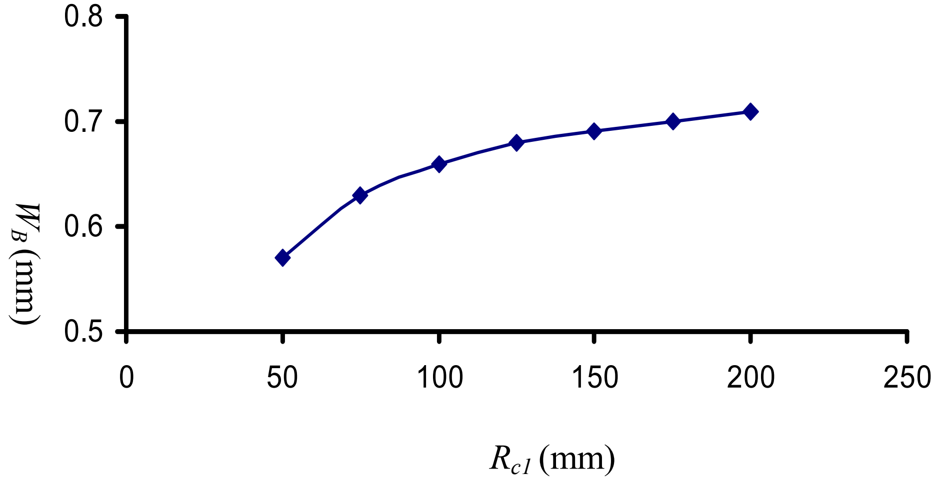

Fig. 4.5: Effect of entrance shim curvature (R_{c1}) on beam width (W_B) at focal point

4.1.2 **Effect of shim on Entry boundary of Magnet**

The Exit boundary with concave curvature (as seen from outside) with suitable radius rotates the focal plane at desired angle as explained above. However, it has the drawback of increasing the spherical aberration thereby reducing the resolving power of the magnet. The aberration due to any curvature on entry and exit side can be calculated using equation 4.3. As per the equation the spherical aberrations can generally be reduced by using suitable magnet curvatures on entry and exit boundaries of the magnet. Since in our case concave type of curvature is used on exit side, the additional aberration due to this can be circumvented by using a shim with convex curvature of suitable radius on the entry side. Using modified parameters from equation 4.4 and 4.5 in equation 4.3, the beam width at the focal point has been calculated. Fig. 4.5 shows the dependence of beam width (W_B) at focal point on entry shim curvature (R_{c1}) for fixed exit shim curvature of 177 mm. It is seen that small value of R_{c1} is desirable for suppressing the aberration and hence improving the resolution. However, we have restricted R_{c1} to 100 mm as further lowering of the radius of curvature at entry will make the location of the magnet very critical. This is because the entry angle depends on beam entry location for a curved boundary. Calculations showed that entry shim radius has no effect on the orientation of focal plane and only helps in reducing aberration**.** The results of calculations using 100 mm convex shim at entry and 177 mm concave shim at exit are shown in Table 4.2. It is observed that distance of focusing from magnet edge (S_i) for masses 210 amu to 270 amu has variation of ± 5mm (and a mean distance of 595 mm) which is negligible and hence the focal line can be considered as normal to beam axis.

Table 4.2: Calculation of Image Distance for R_{c1} = 100mm, R_{c2}= 177 mm and $\epsilon_1 = 26.56^{\circ}$

M (amu)	**ϵ_2'(°)**	**Φ' (°)**	**S_i(mm)**
210	37.1	95.0	592.6
220	32.7	92.9	597.2
230	28.5	90.9	599.5
235	26.6	90.0	599.9
240	24.6	89.1	599.8
250	21.0	87.4	598.2
260	17.4	85.8	594.8
270	14.1	84.3	590.2

4.2 **Computer simulation**

Computer simulation studies using software package SIMION 7.0 [66] have been carried out to determine effect of exit shim curvature on focal plane. The exit curvature of the magnet was varied in the range of 100 mm to 200 mm with a step size of 10 mm and movement of ion groups was analyzed with a central mass of 235 amu and mass-band of +/-35 amu. The slope of the line joining focal points for all the masses was determined using the position co-ordinates of the extreme ends of this line. The calculated slope has been plotted against the radius of curvature in Fig. 4.4. From the graph it is clear that the focal line is almost normal to principal axis for a curvature radius of 160 mm. Difference in optimum radius of curvature of 160 mm by computer simulation and 177 mm by theoretical calculations is mainly attributed to better accounting of fringe field by simulation package.

4.3 **Experimental**

Experiments were carried out by attaching metallic shims made of mild steel (shown in Fig. 4.6) with different radii in the range from 100 mm to 200 mm in steps of 10 mm at the exit boundary of the magnet. These shims were fabricated in house with one side as flat and other with required curvature. The flat side of the shim was attached to magnet boundaries (which are also flat) using non magnetic adhesive in such a way that there is minimum air gap. The pole gap uniformity between the lower and upper parts (north and south poles) of shims was ensured by using 304 Stainless Steel (non magnetic) spacers (tolerance better than 10 micron) with height equal to that of pole gap of magnet.

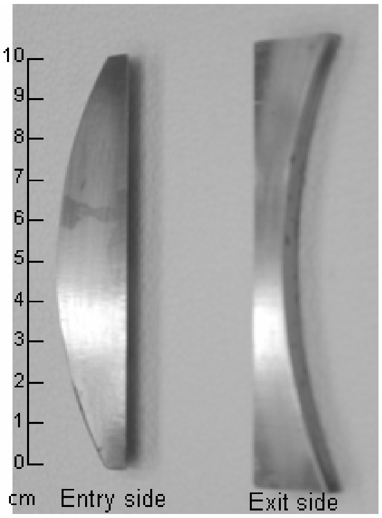

Fig. 4.6: Photograph of shims used on entry and exit side of the sector magnet

Peak shapes of Re-187 ion beam were recorded for each curvature on a single movable collector at various locations across the line normal to the ion beam axis (by changing the magnetic field). Base widths of these peaks were measured at 10% of the maximum peak height in terms of magnet current (72 mA in Fig 4.7). Lower base width indicates smaller beam width at the focal point. The base width is expected to be independent of location if the beam focuses on this line. Taking the mean position on the beam axis as zero, the peak shapes were recorded from -13 mm (low mass side) to +13 mm (high mass side). To suppress the additional aberration, a convex curvature of 100 mm radius was attached to the entry boundary of the magnet. Effect of shim at entry boundary was also studied by recording peak shapes with and without entry shim for optimum exit shim.

4.4 **Results and Discussion**

Peak shapes determined on different positions of line normal to principal beam axis (with entrance shim radius of 100 mm) showed minimum variation for exit shim radius of 130 mm. Shape of peak obtained at center position for optimum exit shim is shown in Fig. 4.7 for rhenium ions. In this case, the variation of base width at different points (± 13 mm) on normal line was found to be 72-78 mA. We may add that the beam width at collector location was 0.70 mm without any shim, it increased to ~0.86 mm on use of exit shim of 130 mm diameter and then reduced to 0.74 mm on use of both entry and exit shims.

Having found optimum entry and exit shims, seven collectors with positions suitable for analysis of Nd were installed on a line normal to principal beam axis. Results obtained for simultaneous collection of Nd isotopes are shown in Fig. 4.8. Uniformity of peak shapes on all collectors confirms the rotation of focal plane along the line normal to the central ion beam. The differences of optimum shim radius of curvature between theoretical calculations, simulations and experimental results may be due to the fringe field distribution of the magnetic field and slightly different magnetic field in the shim region that may arise due to small gap between magnet and shim as well as shim material being different from main magnet material. The theoretical calculations are based on sharp cutoff approximation i.e. field is constant up to a virtual field boundary located at a distance of approximately 1 to 2 pole gaps from pole edges.

However, in real conditions the field is extended to considerable distances from the pole boundaries. The effect of extended fringe field has been studied by Enge and others [77, 78] whereby it is stated that it alters the entry and exit angles and hence the focusing condition of the ion beams. The fringe field is better accounted for in computer simulations resulting in better agreement with experimental data. The agreement of simulation to experimental data is further improved when difference in magnetic field in shim region compared to that in main magnet is taken into account. For this purpose, the actual magnetic field profile was measured using hall probe. From the profile it was found that the field in the shim region is less by around 200 gauss compared to that expected for ideal field profile (for a central magnetic field of 5000 gauss). To see the dependence of different magnetic fields in shim region on the focal plane rotation angle, simulations have been carried out for a field of 5000 gauss in the main magnet region and different fields in the shim region. The results are shown in Fig. 4.9. It shows that there is a variation of around 20° in the focal plane angle for a field difference of 200 gauss in the shim region. The variation of 20° corresponds to 20 mm in R_{c2} as per Fig. 4.4 which means that the optimum radius will be 140 mm (instead earlier simulation value of 160 mm) in a good agreement with experimental value of 130 mm. A small difference of 10 mm could be due to different fringe field distribution in simulation and in practical case (which is difficult to verify experimentally) and also due to small unavoidable gap between main magnet and the shim.

It is recommended in US patent [68] that curvatures on the pole boundaries should ideally be introduced by removing the material for convex curvature on entry so that the deflection angle of the magnet is not altered. However, in present study shim has been added to existing magnet as it facilitates the experimental optimization of shim curvature as discussed in the introduction. The quality of the peak shapes shown in Fig. 4.8 indicates that there is no adverse effect due to this procedure.

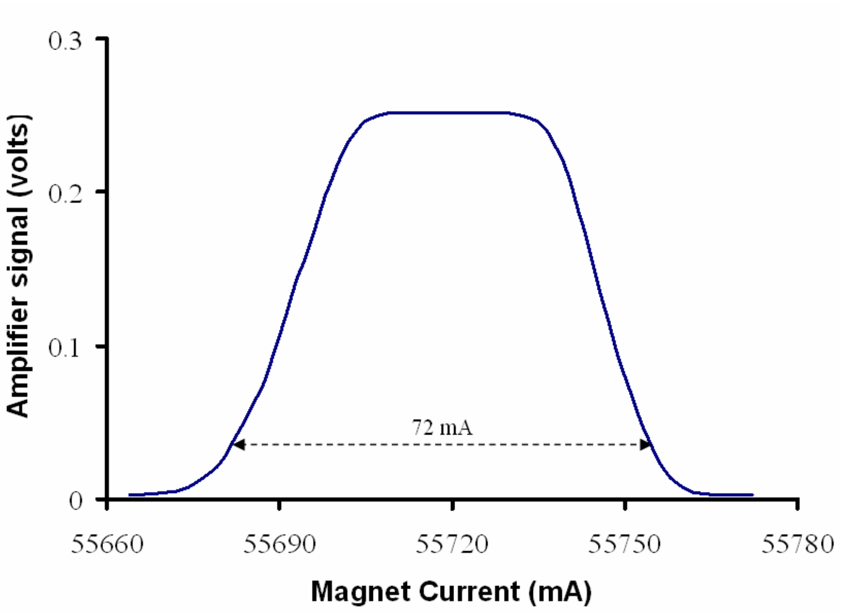

Fig. 4.7: Peak shape for rhenium ion beam on single collector located at centre of the line normal to principal beam axis; R_{c1}= 100 mm, R_{c2} = 130 mm.

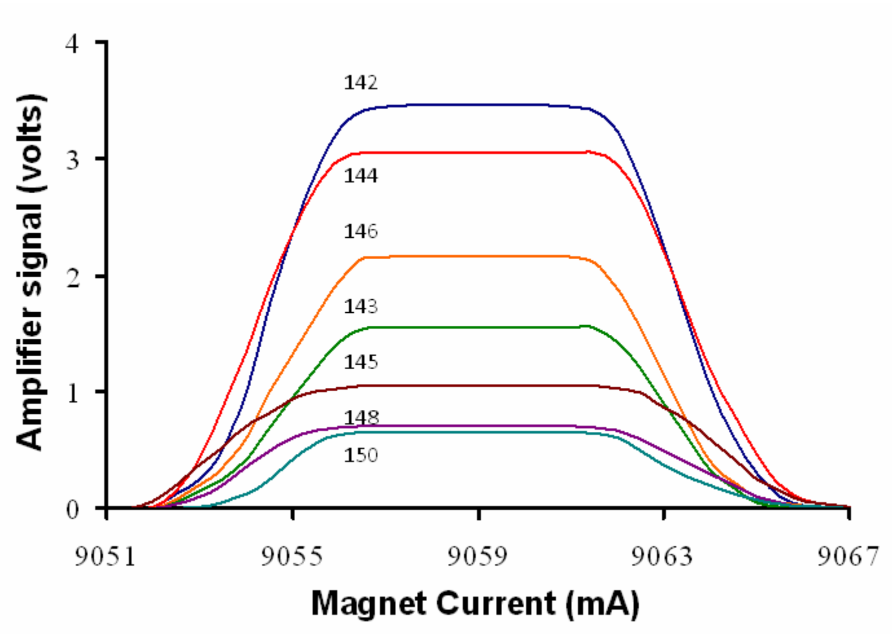

Fig. 4.8: Peak shapes for seven isotopes of Nd collected simultaneously on seven collectors placed on a line normal to principal beam axis with R_{c1} = 100 mm and R_{c2} = 130 mm; all the different peak heights are as per the abundance of different Nd isotopes.

Table 4.3: Isotopic ratio data for Sr Standard Sample

Sample No.	**Ratio (^{87}Sr/^{86}Sr)+/- SE**
1.	0.710194 +/- 0.0000056
2.	0.710210 +/- 0.0000040
3.	0.710219 +/- 0.0000042
4.	0.710199 +/- 0.0000042
5.	0.710198 +/- 0.0000042
6.	0.710239 +/- 0.0000042
7.	0.710190 +/- 0.0000046
8.	0.710222 +/- 0.0000040
9.	0.710190 +/- 0.0000042
10.	0.710220 +/- 0.0000045
Average Ratio	0.710208
External Precision	23 ppm

Further to check any effect on performance of the instrument, isotopic ratio measurement for Strontium standard sample (SRM 0987) was carried out for ^{87}Sr/^{86}Sr ratio. The sample was deposited on the side rhenium filaments of triple filament assembly. The data was collected in 10 blocks of 10 ratios each for same assembly which provides the internal precision of the measurements. The same sample was analyzed on ten separate filament assemblies on turret for calculation of external precision and the results are presented in Table 4.3. The results are quite closer to those obtained with the conventional instruments with straight boundary magnetic analyzer.

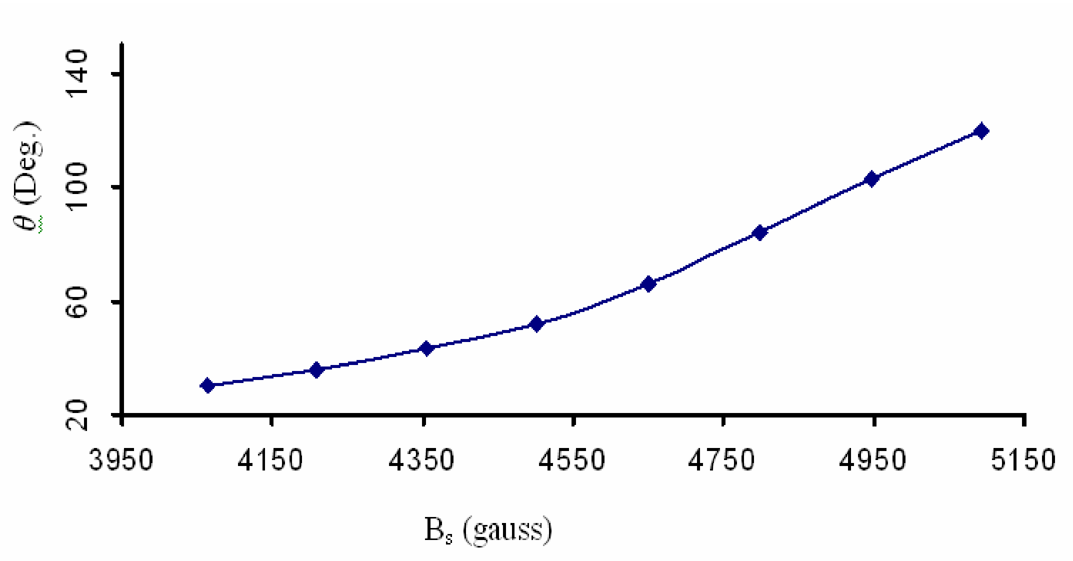

Fig. 4.9: Effect of magnetic field in shim region (B_s) on Focal line angle (θ)

4.5 Conclusion

The experimental study on rotation of focal plane has provided the optimized radii of curvature for the shims on entry and exit edge of the magnet for rotation of the focal plane along the normal to principal beam axis. The difference between the theoretical, simulated and the experimental values may be attributed to the difference in fringe field distribution and gap between shim and main magnet. This will facilitate compactness of collector chamber and easy location of the collectors in case of large number of collectors. Experiments on ^{87}Sr/^{86}Sr ratio show that the errors introduced in the system (on addition of shims to rotate focal line) are negligible and do not adversely affect the performance of the instrument.

Chapter -5

Variable dispersion zoom optics

Introduction

The TIMS employs a multi-collector system for the measurement of isotopic ratio of analyte elements. The number of collectors is decided by the number of isotopes to be measured simultaneously for the elements under study. The TIMS-B [55] already described in previous chapter-4 employs seven collectors required for the high precision isotopic ratio measurement of elements ranging from Sr to U for geo-chronological application. The other specifications of this instrument are given in Table 5.1. In TIMS, the exact locations (and separations) of the collectors depends on ion optical parameters of the system and for multi-isotope analysis, adjustability in the positions of collectors to match the dispersion of the ion beams for a given element is necessary. To achieve this, the collectors are typically mounted on mechanical feed-throughs with stepper-motor controls so that their positions may be adjusted from outside the vacuum. However, this makes the collector system very bulky and unwieldy (in case number of collectors is large). Moreover the position and angular orientation of these collectors is very critical for obtaining good peak flatness and precision of isotope ratio measurement. The complexity is further increased by the limited size (~1 mm) of the apertures (of the collectors) due to small dispersion of ions in conventional system. To overcome these limitations, a new ion optical arrangement consisting of a DC quadrupole (DCQ) followed by deflection optics and faraday collectors with fixed positions has been developed. DC quadrupole helps in small adjustment in the dispersion of ions beams (for different elements) so that they are properly aligned with the gaps (apertures) in the deflection optics while deflection optics helps in increasing dispersion and positioning of individual beams at centers of respective collectors. This facilitates the use of wider apertures for the collectors that results in improved peak flatness. This arrangement called variable dispersion zoom optics (VDZO) is depicted in Fig. 5.1. As individual collectors need not be moved for isotopic ratio analysis of different elements, this also ensures simple mechanical arrangement for the collectors.

Table 5.1: Salient Features of conventional TIMS system (TIMS-B)

Ion source	:	Thermal ionization with triple filament assembly
Analyzer	:	Stigmatic geometry sector Magnet with 300 mm Radius, 90° deflection
Collector system	:	Seven Faraday collectors
Resolution	:	400
Sensitivity	:	1 ion per 600 atoms of Uranium
Precision	:	0.1% for natural U, 23 ppm for Sr
Acceleration Voltage	:	Up to 10 kV

We may add that one of the pre-requisites to use this setup is that the path of ion beams should match with that of deflection optics (placed normal to the principal beam axis) so that the beam widths remain constant all across the deflection optics. Therefore, in the present study, TIMS-B system with curved entry and exit boundaries that enables rotation of the image plane normal to the beam axis [55] was employed. This ensures the matching of ion beam path with that of deflection optics.

Some designs of zoom optics have been reported in earlier studies and some of the commercial instruments employ variable dispersion optics. For example in Triton (Thermo

Scientific, Germany) isotope ratio mass spectrometer [26], two DCQs have been used on either side of the magnetic analyzer, to adjust the dispersion of the ion beams at the collectors.

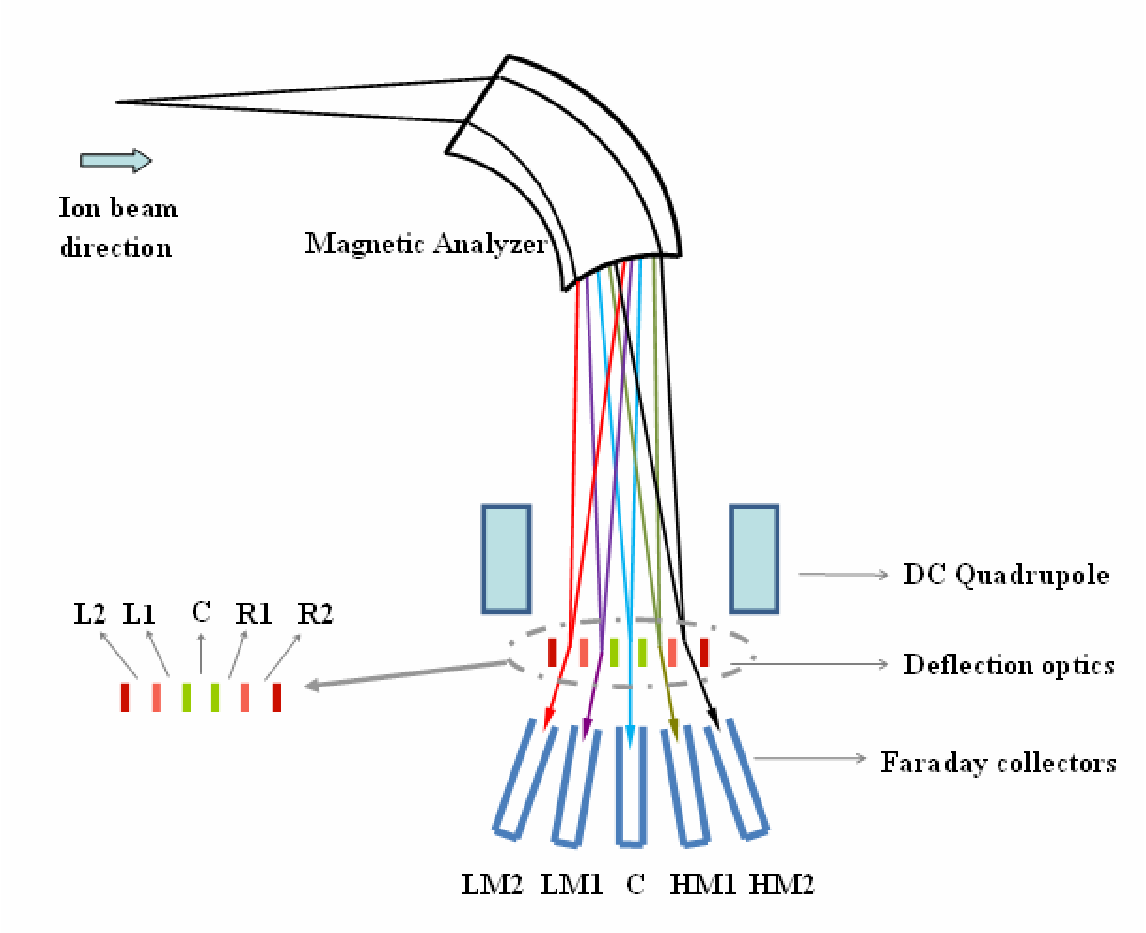

Fig. 5.1: Schematic of Variable dispersion zoom optics; five masses dispersed by magnetic analyzer adjusted for optimized dispersion by VDZO and collected by respective faraday collectors.

Quadrupole on exit side helps in adjusting the dispersion while that on the entrance side has been used to compensate, to some extent, the additional aberration introduced by the one on the exit side. But the collectors used in this setup are movable with smaller aperture sizes. In other studies [79, 80], two quadrupoles in a cross configuration followed by sextupole [79] and/or octupole [80] have been used. Sextupole rotates the focal plane of the ion beams to match with the plane of collectors and the octupole is used to correct for any curvature in the focal plane. The cross configuration of quadrupole takes care of focusing of ion beam in both horizontal and vertical planes. But this setup has been rarely used because of higher magnification leading to large aberrations in the ion beam focusing. Freedman et. al. [81] have employed two DCQs followed by an array of large number of collectors so that there is minimal need for magnification leading to lower aberrations to the ion beam focusing. But the main disadvantage of this setup is the requirement of large number of collectors which increases the mechanical complexity and adds to the difficulties in obtaining ultra high vacuum conditions mandatory for precise ratio measurements. Results of some studies made on mass spectrometers using above types of variable dispersion optics have been presented in different studies [82-86, 7]. In the present study, we use a set of electrostatic deflectors after the DCQ. The deflection optics has been designed in such a way that very small voltages are required on the quadrupoles to align the ion beams with the apertures in the deflection optics thereby introducing negligible aberrations in the ion beam focusing. Further, the deflection optics controls deviations for individual ion beams without introducing additional aberrations. In all, more efficient zooming can be carried out with this setup as compared to reported optical designs. The following sections discuss the design aspects, simulation and experimental results for this setup.

5.1 Theory and design details

5.1.1 DC Quadrupole

It consists of four parallel rods with DC potentials and electric field distribution as schematically shown in Fig. 5.2. The electrostatic potential V(x, y) at any point (x, y) on the cross section of quadrupole and electric field components are given by [12]:

$$V(x, y) = (V_0/2)\,(x^2-y^2)\,/\,R_0^2$$

$$E_x = dV(x,y)/\mathrm{d}x = (V_0/R_0^2)x$$

$$E_y = dV(x,y)/\mathrm{d}y = (V_0/R_0^2)y$$

For electric field configuration shown in the Fig. 5.2, the dispersion of the ion beams of positively charged particles (along x-axis) will decrease with better focusing along x axis and de-focusing along y axis. As a result, ion beams of rectangular cross section get their gaps reduced at the cost of elongation along the y-axis. An opposite polarity potential will increase the dispersion of the beams. By application of suitable potentials, the inter-beam distances can be optimized in such a way that the ion beams are aligned with respective apertures in the deflection optics. The defocusing of the ion beam in the vertical plane can be adequately taken care of by using larger collector slit height.

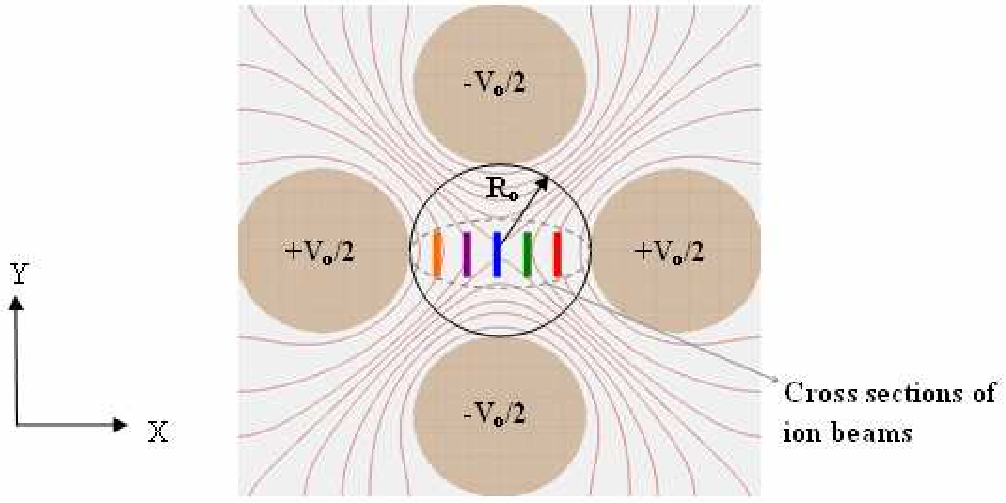

Fig. 5.2: The electrostatic potential distribution in DC quadrupole; the cross sections of the ion beams passing through quadrupole is also shown by five vertical lines.

5.1.2 Deflection Optics

It consists of six rectangular metallic strips such that gaps between the strips (apertures) provide passage to ion beams (Fig. 5.1). Both strips across central aperture (C) are at ground potential and ion beam through C is not deflected. There are two additional apertures (L1, L2 on left and R1, R2 on right) on either side of C (Fig. 5.1). Suitable potentials are applied across these apertures to increase and optimize dispersion of ion beams so that well separated (and fixed) collector cups with wider apertures may be used.

Added advantage of the deflection optics is that unwanted scattered ions (from background gases) having lower energy than the main beam are deflected to a larger extent, thereby reducing the possibility of their collection at the Faraday cups.

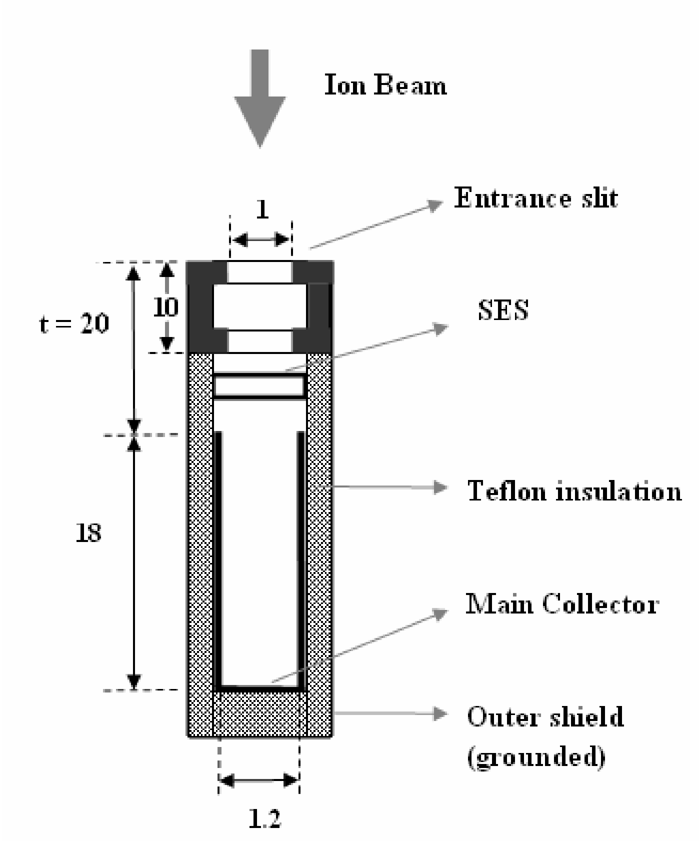

Fig. 5.3: Schematic of Faraday collector (all dimensions shown here are in mm and correspond to conventional collector)

5.1.3 Faraday cup

The collector cup consists of three parts namely the entrance slit, secondary electron suppressor (SES) and the main collector (Fig. 5.3). The entrance slit (1 mm wide, x 15 mm high x 10 mm deep), SES and the main collector (1.2 mm wide x 16 mm high x 18 mm deep) used in the convention collectors were modified with wider entry aperture (3 mm wide x 15 mm high x 10 mm deep), a secondary electron suppressor and a main collector (3 mm wide x 16 mm high x 26 mm deep). The whole assembly is insulated by Teflon sheet (0.1 mm thick) from the outer grounded body. The acceptance angle of the main collector has been reduced by means of increased distance ‘t’ (refer Fig. 5.3) between the main collector and the entrance aperture from 20 mm in conventional to 25 mm in VDZO. This may help in reducing the possibility of collection of scattered ions by the main collector which increases because of wider aperture. Five collectors have been used for the isotopic ratio measurement of elements in the range of strontium to uranium as shown in the Fig. 5.1. The collectors are placed with spacing of 5 mm. All the collectors are mounted on a stainless steel plate with a single screw for each collector. A fine manual adjustment of the orientation angle of each collector is possible to align them with the ion beam.

5.2 Computer simulation

The simulation study was carried out using SIMION 7.0 software [66]. Geometry of DCQ, deflection optics and faraday cups were created in a single potential array which was coupled with another potential array consisting of magnet geometry with 30 cm radius and 90º deflection angle. For simulating the ion paths through the above optics, ion groups with energy 7 keV and masses corresponding to isotopes of different elements *viz*. Sr, Nd, and U etc., were taken with one element at a time.

These ions were generated with a divergence of ±0.5º at a source point (slit) of 0.3 mm width placed at 60 cm from the entry point of the magnet potential array under stigmatic geometry conditions. After dispersion by the magnet, ions were allowed to pass through VDZO. The potentials on DCQ and deflection optics were optimized to align the ion beams with the apertures in the deflection optics and the faraday cups respectively. A comparison study was conducted for a variety of design features of each component and the final design was worked out for maximum transmission of the ion beams.

In the final set up quadrupole rods with 16 mm diameter and 30 mm length were used with 35 mm radius of inscribed circle (R_0 in Fig. 5.2). The dimensions of the deflection optics have been optimized so that there is minimal requirement of the DCQ potentials (and hence smaller aberrations in the ion beam focusing) for analysis of required elements. Optimized width of apertures L2, L1, C, R1 and R2 were found to be 4, 3, 2, 3 and 4 mm respectively. The thickness of plates on both sides of aperture C was taken as 1.5 mm and for all other plates it was 0.5 mm. Using these dimensions, center to center distance between each of adjacent apertures is 4 mm. The faraday cups were located around 25 mm down stream of the deflection optics. Their exact locations and the orientation angles were fixed as per the simulated flight paths of the ion beams through the deflection optics.

Table 5.2: Optimized values of potentials on VDZO for collecting various ion beams on faraday cups

Element	**Potentials on Deflection optics (L2 / L1 / C / R1 / R2) and DCQ in volts**	
	Simulations	**Experimental**
Sr	1000 / 0 / 0 / 0/ 1000 ; 140	1030 / 0 / 0 / 0 / 1100; 120
Nd	1100 / 100/ 0 / 100 / 1100 ; 30	1200 / 150 / 0 / 70 / 1150; 20
U	1000 / 0 / 0 / 0/ 1000 ; 40	1030 / 0 / 0 / 0 / 0 / 1100; 20

Required potentials for DCQ were simulated for different elements. For example, in the case of Sr, the ion beams corresponding to masses 86, 87 and 88 have dispersion of nearly 6.9 mm which needs to be expanded by ~16% for matching with L2, C and R2 respectively. Required DCQ potentials were calculated to be ± 140 volts. Similarly, for Nd, the five isotopes, 142, 143, 144, 145 and 146 can be taken through apertures L2, L1, C, R1 and R2. In this case the dispersion (4.2 mm for unit mass) almost matches with the aperture centerline positions and hence very small DCQ potentials of ± 30 volts were calculated. For uranium, the isotopes 235 and 238 have dispersion of 7.5 mm and for analysis through apertures C & R2 (or L2 & C) calculated DCQ potentials are ± 40 volts. Potential differences across L2 (and R2) and L1 (and R1) were calculated to be 1000 V and 100 V respectively for aligning the beams with Faraday cups and these are expected to be independent of mass of the element being analyzed. Simulated optimum potentials for different elements are summarized in Table 5.2.

In addition to changing the dispersion, DCQ also affects the focusing of individual ion beams in x and y directions. The effect in y direction is adequately taken care by large height (15 mm) of the faraday cup apertures. In the x-direction, the beam width was found to increase linearly with increase in dispersion using DCQ (note that the deflection optics does not change the beam width). For example, in case of ^{88}Sr the beam width before applying voltage on DCQ is 0.86 mm which corresponds to a flat top width (in terms of magnetic field dB) of ~5.9 gauss for a magnetic field (B) of 3700 gauss on magnetic analyser. The peak flatness is calculated to be dB/B ~ 1600 ppm or dm/m ~3200 ppm for a cup width of 3 mm. After applying 140 V on DCQ, the beam width increases to 1 mm and peak flatness (dm/m) is reduced to 2600 ppm. However the reduced flatness is still much higher than that obtained in our conventional set up (~ 500 ppm) with a cup width of 1.0 mm and is better than nearly 1000 ppm reported for other commercial instruments (model Triton of Thermo Fisher and model Phoenix of IsotopX)

5.3 Experimental

The simulated design was converted into a working model for experimental validation. Experimental study was carried out in three parts. In the first part a micro-channel plate (MCP) was used (instead of faraday collectors) to capture the images of the ion beams under different conditions. The second part involves placement of final collectors and obtaining flat top peaks by optimizing deflection optics potentials. Third part consists of carrying out isotopic ratio measurements on these collectors for required elements.

For the imaging experiments, Burle make MCP with active area diameter of 40 mm, coupled with a phosphor plate was used. It was placed at the location of faraday collectors. The images of isotopes of different elements were obtained and their dispersions were studied with different set of potentials on the quadrupole and deflection optics. Subsequently, five faraday cups fixed on stainless steel plate were used for ion beam measurements. Potentials of variable dispersion optics and positions of collectors were optimized by sequentially obtaining flat peaks of $^{88}Sr^+$ ion beam on all collectors. To check the effect of VDZO on performance of the instrument, DCQ potentials were optimized and isotopic ratio measurement for strontium was carried out. The Strontium standard sample (SRM 987) was used for the measurement of isotopic ratio $^{87}Sr/^{86}Sr$ using multi-dynamic mode [1]. The sample was deposited on the side rhenium filaments of a triple filament assembly. The data was collected in 10 blocks of 10 ratios each for same assembly to estimate the internal precision which is calculated as the relative standard error over all 100 ratios. The same sample was analyzed on ten separate filament assemblies on a turret/sample magazine for external precision measurement defined as the relative standard deviation of the average ratio obtained from each assembly.

A possible deleterious effect of the increased apertures of the collectors is the deterioration of the abundance sensitivity (defined as contribution of a higher mass ion beam to the adjacent lower mass beam due to the scattered ions [1, 2]). The scattered ions (from ion beam of larger mass) have lower energy and get higher deflection resulting in interference with adjacent ion beam. This can affect the measurement of very low intensity ion beams. Usually this is measured as the contribution of ^{238}U at the location of mass 237 amu. Dispersion of ^{88}Sr at 87.5 amu mass positions is nearly same as that of ^{238}U at 237 amu position and therefore abundance sensitivity was estimated by measurements of ^{88}Sr signal and scattered ions at 87.5 amu by suitably changing magnetic field.

.

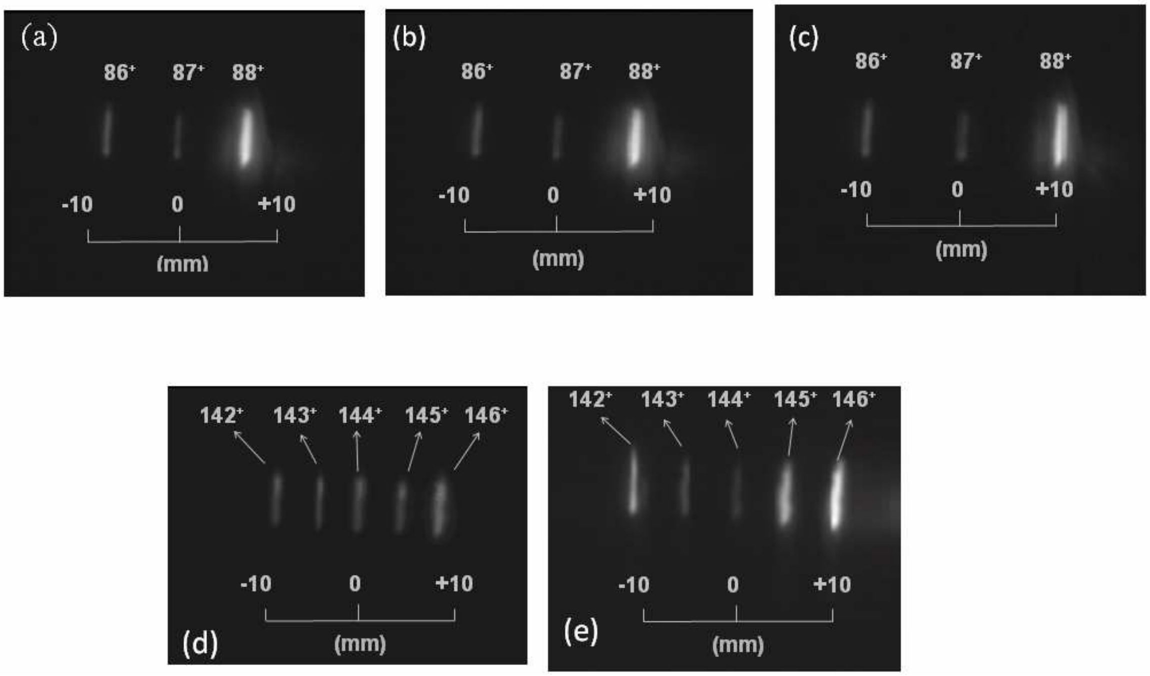

Fig. 5.4: MCP images of Sr and Nd isotopes; 4a shows Sr isotopes images without applying any voltage, 4b shows images after applying only quadrupole potentials (gaps between the ion beams increased) and 4c shows images after applying potentials on deflection optics (gaps increased further to match with the collector locations); 4d shows the images for Nd isotopes without any voltage and 4e shows after applying required voltages on DCQ and deflection optics

5.4 Results and Discussion

In the experimental studies with MCP, it was observed that the dispersions for all the elements were closely matching with the simulated values. For example the dispersions obtained for the Sr isotopes before and after the application of DCQ potentials of ±120 volts (Fig. 5.4a and 5.4b) are almost same as the simulated values of 6.9 mm and 8 mm respectively. Potentials applied on deflection optics (as given in Table 5.2) further displace these beams to locations matching with that of respective collectors as shown in Fig. 5.4c. Similarly the images obtained for Nd isotopes are shown in Figs. 5.4d and 5.4e. The images show that the ion beams pass through the respective apertures of deflections optics without obstruction and all experimental values of DCQ and deflection potentials are similar to the computer simulation results.

The peak shapes (for ^{88}Sr isotope) without DCQ potentials (but using deflection optics) were sequentially studied on all the collectors by suitably varying magnetic field. A peak flatness of ~3000 ppm of mass and a beam width of 0.8 mm was observed on each of the collectors. To collect the three isotopes of strontium (masses 86, 87 and 88) simultaneously (as required for isotopic ratio measurement) on collectors LM2, C and HM2, a potential of ± 120 volts was applied on DCQ. This increased the beam width to 1 mm and reduced peak flatness to 2500 ppm in agreement with computer simulations. Fig. 5.5 shows the simultaneous peaks of strontium isotopes on LM2, C and HM2 collectors indicating ability of VDZO to match the peaks. Similarly, the peak matching for Nd and U isotopes was also carried out for which the required optimum potentials on DCQ and deflection optics are given in Table 5.2.

The results for isotopic ratio measurement of Sr on conventional and the VDZO setup are tabulated in Table 5.3. It is seen that internal precision is nearly same in both the systems (with and without VDZO), but the external precision is much better with VDZO (8 ppm) as compared to that obtained with conventional setup (23 ppm). Accuracies for conventional and VDZO systems were found to be 50 ppm and 10 ppm respectively on comparison of average values with true value of 0.710244. Lower accuracy for conventional system arises due to a systematic error on the negative side of true value and is attributed to variation in dispersion of ion beams from one sequence to another in dynamic mode of ratio measurement. First sequence is for ratio measurement of $^{86}Sr^+/^{87}Sr^+$ and the second sequence corresponds to $^{87}Sr^+/^{88}Sr^+$ on same two collectors [1]. The relative change in dispersion from one sequence to another is around 130 ppm of mass. This relative change is expected to contribute to an inaccuracy of 25 ppm in the isotopic ratio $^{86}Sr^+/^{87}Sr^+$ for a peak flatness of 500 ppm (for conventional system). However, similar variation across the flat region of 2500 ppm (in VDZO system) reduces this inaccuracy to 5 ppm. A five fold improvement in accuracy is in agreement with experimentally measured accuracies of 50 ppm and 10 ppm in conventional and VDZO systems respectively. The improved precision and accuracy with the VDZO in comparison to conventional set up is shown graphically in Fig. 5.6 (using data of Table 5.2).

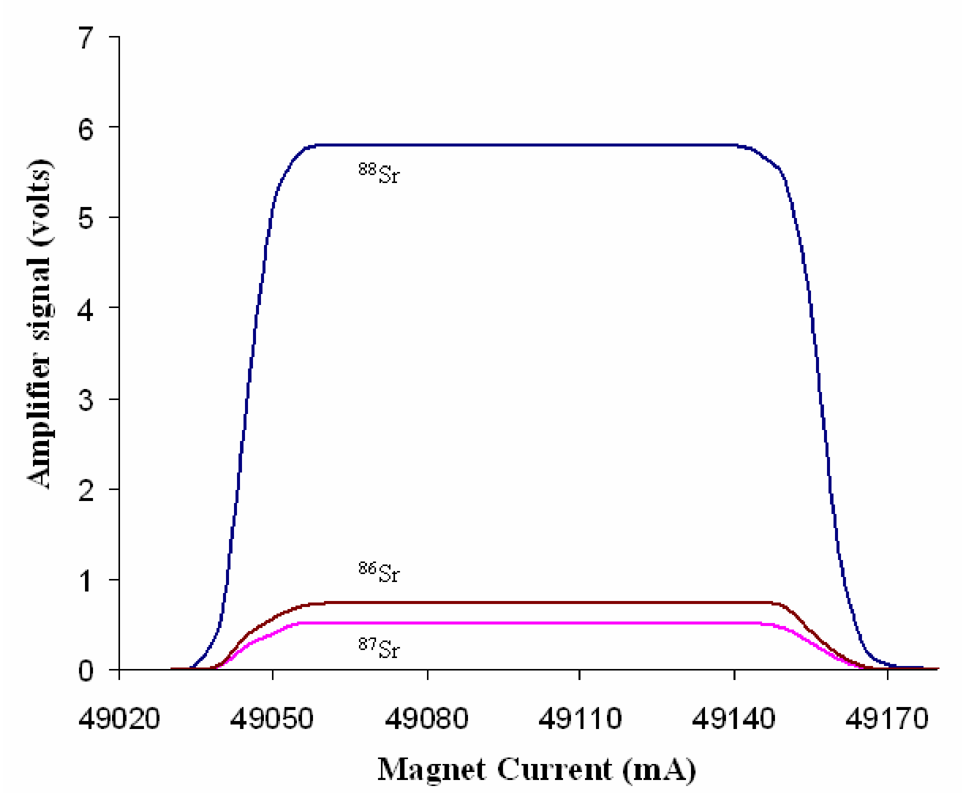

Fig. 5.5: Peak shape for Strontium isotopes (86, 87 and 88) simultaneously on three faraday collectors (LM2, C and HM2); the overlapping obtained by adjusting parameters of VDZO

The increased flatness (~3000 ppm) may enable the use of a wider source slit (presently 0.3 mm) to achieve higher sensitivity or lower sample quantity for the same signal strength. This may also enable heating the filament at lower temperature which can reduce the fractionation related problems and background gas load inside the ion source chamber leading to reduced scattering effects and hence improved abundance sensitivity.

Table 5.3: Comparison of zoom optics with conventional collector setup for isotopic ratio measurement of standard Sr sample (SRM 987). Average 87/86 ratio with relative standard error (internal precision; in parentheses)[#] has been given for each sample

Sample Number	**Ratio (^{87}Sr/^{86}Sr)**	
	On conventional setup without zoom optics	**On setup with zoom optics**
1.	0.710194 (6)	0.710246 (4)
2.	0.710210 (4)	0.710241 (8)
3.	0.710219 (4)	0.710239 (6)
4.	0.710199 (4)	0.710230 (7)
5.	0.710198 (4)	0.710242 (7)
6.	0.710239 (4)	0.710231 (8)
7.	0.710190 (5)	0.710234 (5)
8.	0.710222 (4)	0.710241 (8)
9.	0.710190 (4)	0.710230 (6)
10.	0.710220 (5)	0.710233 (5)
Average Ratio	**0.710208**	**0.710237**
RSD (external precision)	**23 ppm**	**8 ppm**

(# the value in parenthesis is the variation in last significant digit of the data)

For abundance sensitivity measurement, the ion beam intensities for ^{88}Sr$^+$ (I) and scattered ions (I_s) at mass location 87.5 amu were measured to be 8 volts and 0.25 m-volt respectively on the centre collector C (Noise of the amplifier is ~50 µV and therefore voltage of 0.25 mV may be easily measured). This corresponds to an abundance sensitivity (given by I/I_s) of ~30 ppm which is similar to that of conventional set up having collectors with 1 mm slit width.

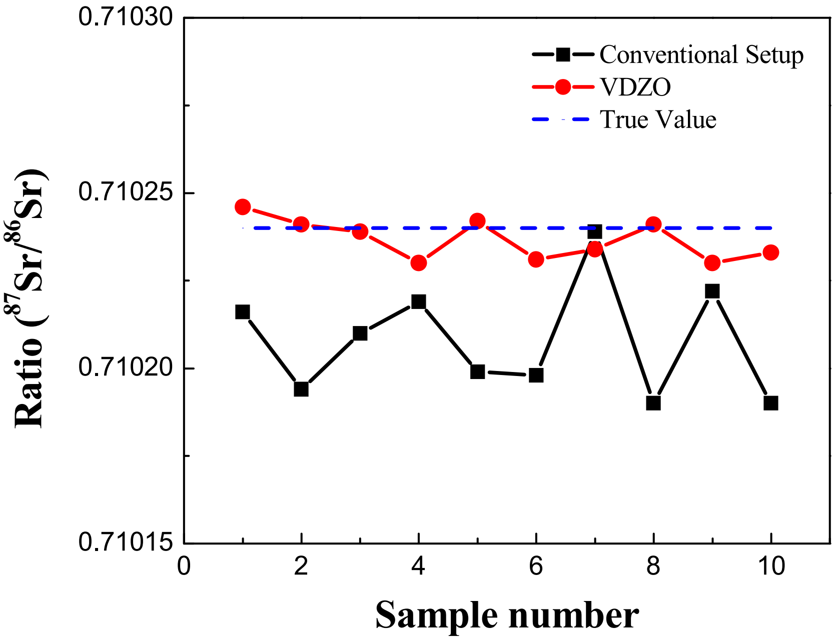

Fig. 5.6: Comparison between conventional setup and zoom optics for isotopic ratio data of Strontium standard (SRM 987)

In conventional setup, the multi-collector ratio measurement for higher masses is limited to a mass range where the dispersion of the corresponding masses is equal to the minimum adjustable distances of the adjacent collectors. In our conventional system [55], even though mass resolution is 400 (i.e. masses till 400 amu can be separated on single collector per unit mass difference), the multi-collection ratio measurement is limited to 250 amu (for unit mass difference) corresponding to the minimum adjustable distance of 2.4 mm between adjacent collectors. In case of VDZO, since the dispersion can be adjusted, it offers higher mass range for multi-collector ratio measurement. To verify this, Boron isotope ratio measurements were carried out using Cesium Borate sample (masses of 308 amu and 309 amu for ^{10}B and ^{11}B). Cesium Borate is used for precise isotopic ratio measurements due to lower fractionation effects [39, 87, 88]. For reasons cited above, the conventional set up can not be used in this case. However, using VDZO, it was demonstrated that the simultaneous measurement of these peaks was possible on adjacent collectors as shown by the well matched peaks of 308 and 309 masses on LM1 and C in Fig. 5.7. In this case the dispersion of 1.9 mm (for 308 & 309 amu) is increased to 5 mm, with an increase in the beam width to around 1.6 mm corresponding to a peak flatness of 1900 ppm of mass. The peak flatness is still much higher than 500 ppm usually obtained on our conventional set up. The isotopic ratio measurement for boron gave a precision of 0.05% that is close to best reported values confirming that VDZO facilitates higher mass range for multi-collector ratio measurement.

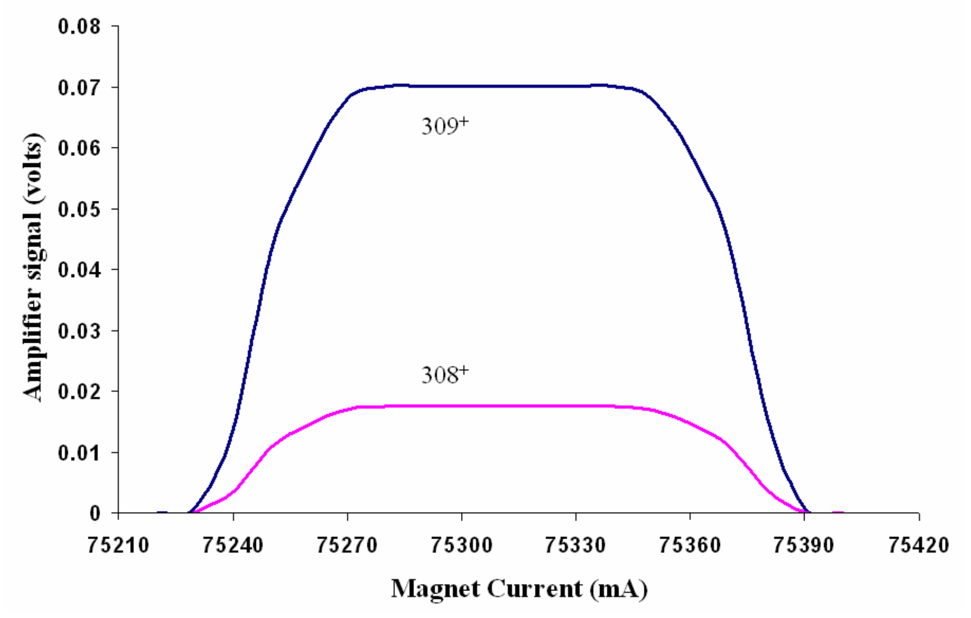

Fig. 5.7: Peak shape for Cesium Borate molecular ions (308 and 309 amu) corresponding to boron isotopes ^{10}B and ^{11}B.

5.5 Conclusion

A new Faraday collector system (with five cups) for thermal ionization mass spectrometer has been developed based on variable dispersion zoom optics. The system enables fixed collector cups with wider apertures that facilitate analysis of different elements as beams may be aligned by application of suitable potentials to deflection optics rather than mechanical movement of collectors. Further, wider collectors help in improvement of peak flatness from 500 ppm to

3000 ppm for Sr^{88}. The system design was optimized for analysis of U, Sr and Nd isotopic ratio analysis by simulation. The system enables improvement in both precision and accuracy of analysis. This has been demonstrated by analysis of $^{87}Sr/^{86}Sr$ ratio where precision and accuracy have been improved from 23 ppm to 8 ppm and 50 ppm to 10 ppm respectively.

Chapter-6

Faraday collector

Introduction

Faraday collectors are used in magnetic sector mass spectrometers for precise measurement of ion beam intensity. In chapter-5 results of studies carried out for improvement in the collector system using variable dispersion zoom optics [89] was discussed. This chapter presents results of various studies conducted to further improve the collector system by modifying the design of Faraday collectors. The Faraday collector has already been explained in chapter-2 whereby different parts of the collectors were explained in terms of their significance. Typical collectors use electrical suppressor for suppressing secondary electron current emitted on ions striking the collector. This has problem of inconsistent collection efficiency due to mechanical errors in the placement of electrical suppressor. To improve collector design for better mechanical strength and further reduce secondary electron contribution some approaches have been studied. These are: (a) use of magnetic field (instead of electric field) for secondary electron suppression, (b) graphite coating to reduce secondary electron emission and (c) inclination of collector end surface to 45° with respect to ion beam. As a result of these studies, a mechanically simpler design has been made and new collector shows improved performance in measurement of ^{87}Sr/^{86}Sr isotopic ratio.

Fig. 6.1 shows schematic of a Faraday collector employed with electrical secondary electron suppressor (SES) that has been used conventionally in a Faraday collector. In the present study, some alternate approaches for suppression of secondary electrons were investigated. As a result of these studies, collectors with reduced secondary electron emission have been developed. These have additional advantages of mechanical simplicity as there is no need to precisely place miniature stainless steel frame used as electric field based secondary electron suppressor. Use of magnetic field has additional advantages of suppressing secondary ions with positive and negative charge along with the secondary electrons emitted due to primary ion beam striking the main collector. This is in contrast to SES at negative potential that enhances positive secondary ion contribution. Improved Faraday collectors have been evaluated by measurement of ^{87}Sr/^{86}Sr isotopic ratio.

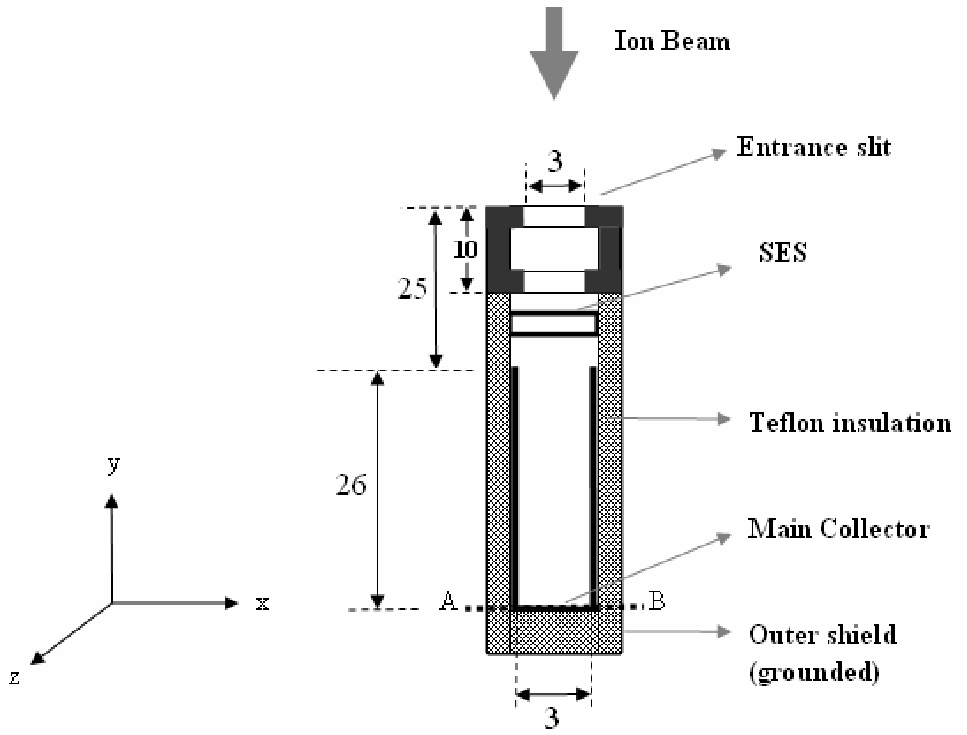

Fig. 6.1: Schematic diagram of the Faraday collectors, all dimensions are in mm, depth in z direction is 15 mm.

Many studies on improvement of Faraday collectors have been reported in the literature [1-2, 24-26, 90 -103]. To reduce effect of secondary positive ions, in one of the earlier studies [24], collector with an additional suppressor at positive potential has been used to suppress positive secondary ions but it increases the complexity of collector cup assembly. For ion collectors used for measurement of ion current in accelerators, weak magnetic field (10 gauss) has been used to suppress secondary electrons [92]. The field was generated using combination of curved permanent magnets placed alternately in terms of their magnetic polarity so that the field is normal to the incident ion beam and secondary electrons. In this case size of the collector is not critical. Due to large number of collectors, placed at small distances, this configuration of the magnets is not viable in case of magnetic sector mass spectrometers. Therefore, we have used magnetic field in horizontal direction (along *x* axis), orthogonal to the direction of analyte ions (along *y* axis) by placing set of magnets on either sides of the multiple collector system as shown in Fig. 6.2.

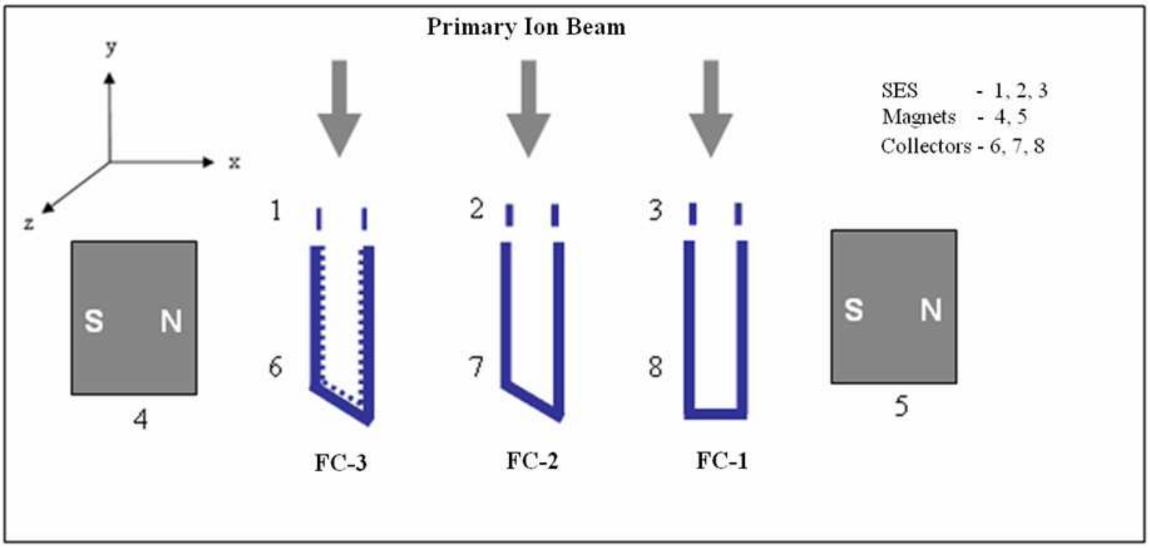

Fig. 6.2: Schematic diagram showing the experimental set up with collectors and magnets

Graphite is known to have lower secondary electron yield [90-91] compared to stainless steel used in conventional collectors. Therefore, solid carbon materials in tubular form [24] and solid graphite walls [25] have been used to reduce secondary emission. We show that a simple approach of coating the inner walls of the metal collector with graphite results in equally similar reduction in secondary electron emission. As secondary electrons are preferentially emitted normal to the surface, a surface inclined to ion beam should also yield reduced secondary electron yield and the same has been investigated.

6.1 Theory and design aspects

The conventional Faraday collector consists of a stainless steel main collector, a secondary electron suppressor (SES) frame and a grounded entry aperture [89] as shown in Fig. 6.1. The primary ions, after entry through the entry aperture (3 mm X 15 mm), collide with the end surface (A-B in Fig. 6.1) of the main collector and transfer their charge that is measured by an electrometer amplifier. The energetic primary ions, on collision with the surface of collector, lead to secondary electron emission as well as smaller number of secondary ions and reflected ions. Three approaches to reduce secondary electron emission and improve collector as mentioned in the introduction, are discussed in the following.

6.1.1 Coating with carbon

Secondary electron emission may be reduced by coating of inside surface of the Faraday cup by materials having low secondary electron emission. One of the important materials having low secondary electron emission is graphite [24-25, 90-91] and in some of the earlier reports solid graphite has been used to make Faraday cups [25]. However, this makes the cup size large as thick wall of graphite need be used compared to thin stainless steel cups. Therefore, we have coated thin layers graphite to improve cup design. The coating of graphite was carried out by dipping main collector in graphite slurry (20% by weight in alcohol medium) for a few seconds and drying it at room temperature in clean atmosphere. The graphite material used was ‘ROCOL METAFLO 20’ make, with particle size less than 10 μm and specific gravity 0.9 g/cc.

6.1.2 Orientation of the end face of collector

Secondary electrons from a surface are preferentially emitted normal to the surface and emission probability at angle Φ (with normal to surface) varies as CosΦ [104]. Therefore if end surface (A-B in Fig. 6.1) of the Faraday collector is inclined (instead of being normal to incident ions), most of the secondary electrons will strike wall of the collector and the probability of electron escape will be reduced. A very large inclination will also increase length of the collector and therefore, we have investigated possible reduction in secondary emission by using a collector with end surface inclined at 45° to the incident ion.

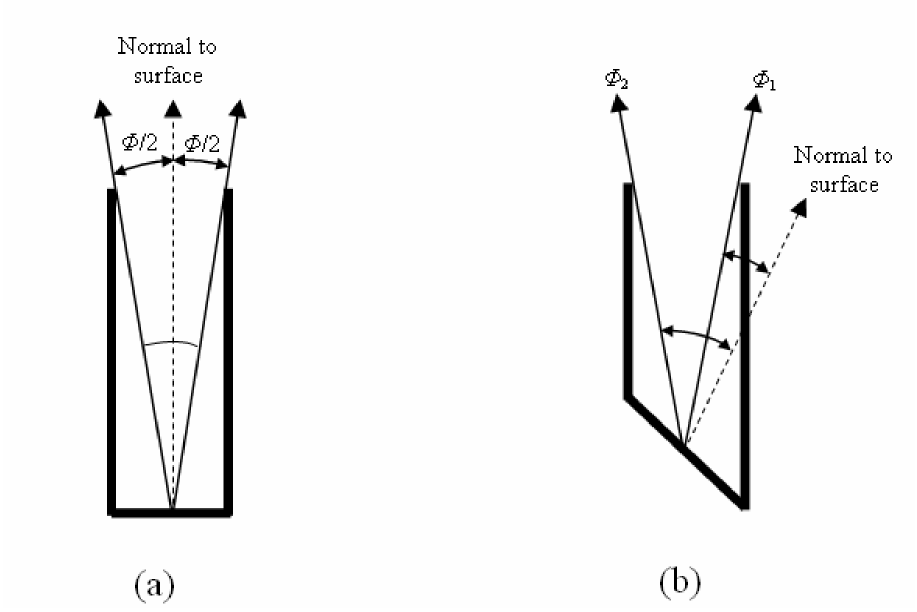

Fig. 6.3: Schematic showing the escape of electrons from Faraday collector with a) normal surface and b) surface inclined at 45°.

To estimate the effect of inclined surface on the escape of secondary electrons, calculations were carried out assuming cosine distribution [104] for the emission of electrons from the collector surface. The fraction (*f*) of total number of electrons escaping from the aperture of the collector was calculated in both the cases i.e. normal surface and the inclined surface (at 45°). In case of normal surface, the electrons within angle ± $\Phi/2$ with respect to normal to the surface were calculated. Here $\Phi = 6.9°$ is given by ratio of aperture width (*w*) to collector depth (*d*). In case of inclined surface, the secondary electrons emitted within $\Phi_1 = 41.5°$ to Φ_2

= 47.5° as shown in the Fig. 6.3 may escape. Using CosΦ distribution of emitted secondary electrons, ratio of probability of escape of electrons for normal and inclined incidence is = 1.43.

6.1.3 Suppression of secondary electrons by magnetic field

The magnetic field applied in direction normal to the charged particles makes them move in circular path with radius proportional to the mass of the particle. In case of electrons with kinetic energy (0.1 – 100 eV; as may be the case with secondary electrons), a small magnetic field of few gauss (~100 gauss) is enough to circulate them with a radius of 0.005 - 3.5 mm and will trap the electrons in the vicinity of the emitting surface [103]. The trapped electrons generate a negative space charge in the vicinity of the collection surface which inhibits further emission of secondary electrons. Hence by applying magnetic field the secondary emission from the collector surface can be reduced to a great extent. This will also take care of the secondary ions emitted from the surface to some extent. Moreover, the weak magnetic field will not have any significant effect on the path of the analyte ions having much higher energies (5 – 10 keV) and higher masses (masses Li to U) as compared to electrons.

Computer simulations were carried out using Simion 7.0 software [66] to determine effect of SES and magnetic field on secondary electrons emitted from two different types of collectors. These are: (1) conventional collector and (2) collector with end surface inclined at 45°. Initially, to see the effect of electric potential on SES, a group of electrons with energy range of 1-100 eV and angles between ± 90° in both the planes (*xy* and *zy*) was generated from end surface of collector. The magnetic field was set to zero and the effect of SES on secondary electrons was estimated by counting the number of electrons escaping out of the collector before and after the application of -150 volts on SES frame for both the collectors. The simulations showed that after the application of -150 volts, no electrons escaped out of any of the collectors as shown in Fig. 6.4.

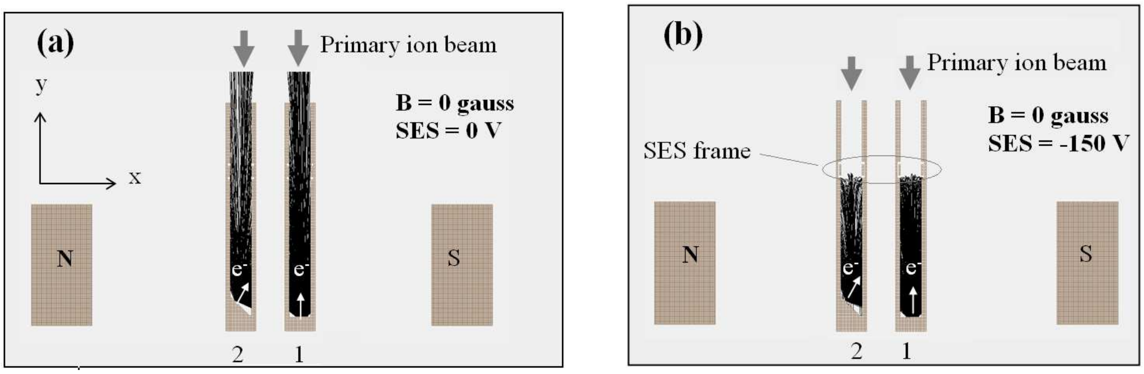

Fig. 6.4: Trajectories of electrons in *xy* plane cut view: a) electrons generated from the bottom surface of collector 1 and 2 escape out in the absence of magnetic field and voltage on SES, b) electrons blocked due to –ve voltage on SES frame.

In order to investigate the effect of magnetic field, the voltage on SES frame was set to 0 and the trajectories of electrons were recorded in the presence of magnetic field (applied along *x* axis) in the range of 0 to 200 gauss. Typical trajectories of electrons with energy 1-100 eV and a magnetic field of 100 gauss are shown in Fig. 6.5. Groups of electrons with energies 1 eV to 100 eV were considered with random emission angle within ± 90° from the surface of

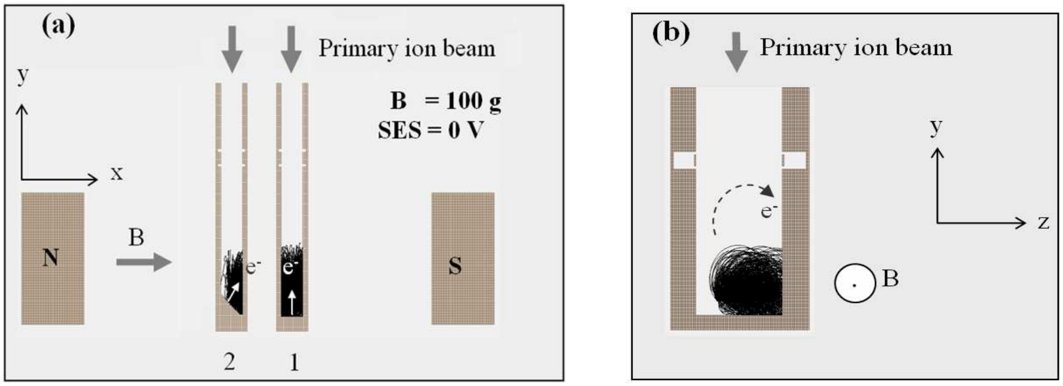

Fig. 6.5: Trajectories of electrons in the presence of magnetic field: a) cut view in *xy* plane with all the collectors, b) circular trajectories in *xz* plane in collector 1

Faraday collector in computer simulation. The magnetic field required to completely block the given group of electrons was estimated and plotted against the energy of electrons and the results are shown in Fig. 6.6. Now considering the energy distribution of secondary electrons [104] to be approximately Maxwell distribution with peak at 2 eV, probability of escape of electrons was calculated for different magnetic fields and results are shown in Fig. 6.7. It is seen that the escape probability reduces to almost zero above a magnetic field of 15 gauss.

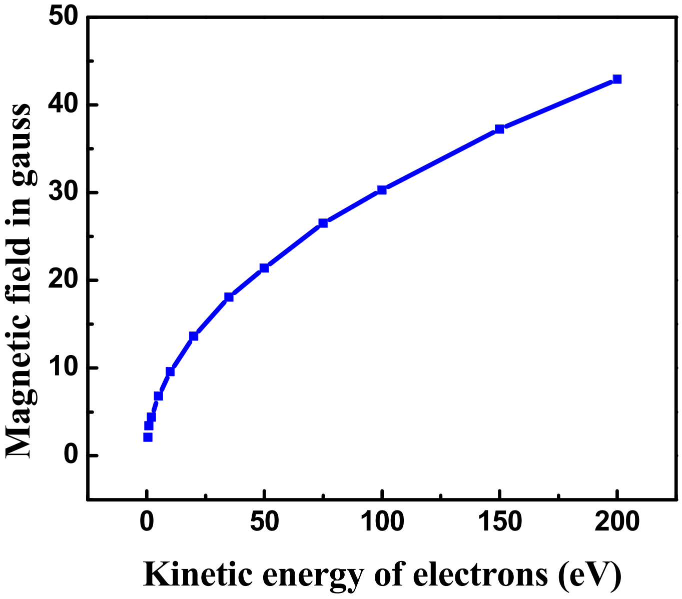

Fig. 6.6: Theoretical plot showing the magnetic field required to completely suppress the secondary electrons of given energy.

An undesirable effect of magnetic filed may be the deflection of primary ions in *z* direction (see Fig. 6.1) which may result in inaccurate measurement of the primary ions if the deflection experienced by some of the ions is more than the physical dimensions of the collector. The simulations showed that the maximum deflection by magnetic field for a primary ion of 3 keV energy at field strength of 200 gauss was 0.4 mm which can be well taken care by the extra margins used for the collector slit height (15 mm). An additional advantage of magnetic field over electrical suppression is its ability to partially suppress positive secondary ions that are not taken care by the electrical suppression.

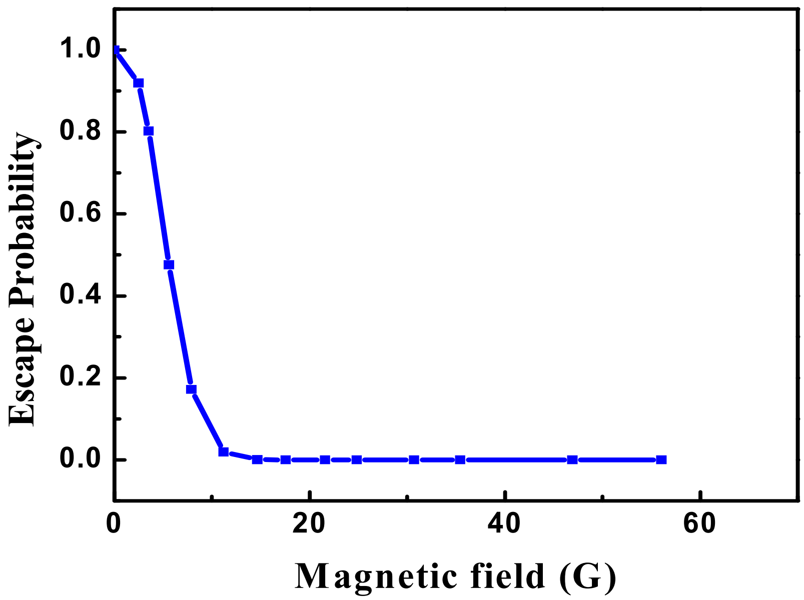

Fig. 6.7: Theoretical plot showing the effect of applied magnetic field on the escape of secondary electrons.

A quantitative study for the suppression of positive ions was carried out by using computer simulations. Since the surface of the actual collectors is to be coated with high purity graphite, the major contribution to the secondary emission will be from carbon ions. Therefore in simulations, only carbon positive ions were considered. The ions were generated in 10 groups with energy from 1 to 10 eV in steps of 1 eV and with number of ion in each group chosen in such a way that altogether they represent near Maxwell type of distribution within energy range of 1-10 eV with peak energy of 2 eV to match the distribution typically with secondary emission [104]. A total of 3995 ions were generated with angular divergence of ± 20° (with respect to normal to the surface) in horizontal and vertical plane. The trajectories of the ions were simulated and the number of ions escaping out of the collector (N_{esc}) was determined under different conditions and results are shown in the table 6.1. It is seen that a magnetic field of 100 gauss reduces the N_{esc} by 50 % as compared to the case when -150 volts on SES was used. The negative voltage on SES actually increases N_{esc} as data for V_{sec} = -150 and 0 volts indicates. This is because positive ions are being considered and negative voltage accelerates them increasing their escape probability. It may be noted that the effect of magnetic field on suppression of secondary ions is similar for both positive and negative ions.

Table 6.1: Variation of the number of escaped secondary ions with different values of the applied magnetic field and voltage on SES frame in computer simulations

	B =0 **V_{ses}= -150**	**B = 0** **V_{ses} = 0**	**B = 50** **V_{ses} = 0**	**B = 100** **V_{ses} = 0**	**B = 150** **V_{ses} = 0**	**B = 200** **V_{ses} = 0**
N_{esc}	560	352	351	278	232	162

B: magnetic field in gauss; **V_{ses}**: voltage on SES frame in volts; **N_{esc}**: Number of ions escaping out of collector.

6.2 **Experimental**

The experimental study was conducted in three parts. The first part comprised of studies on the effect of coating of graphite and inclination of end surface of collector on the secondary emission. In second part, the effect of magnetic field on the secondary emission of electrons was studied. This was followed by third part which incorporated testing and evaluation of a new collector system developed on the basis of studies in first two parts. The testing and evaluation was carried out by measurements of isotopic ratios (^{87}Sr /^{86}Sr) of Strontium standard SRM 987.

An experimental set up as shown in Fig. 6.2 was used to study the effect of graphite coating and inclination of end surface on the secondary emission. The set up consisted of three Faraday cups: (a) FC-1 as conventional collector, (b) FC-2 with end surface inclined at 45° and (c) FC-3 with graphite coating and end surface inclined at 45°. Each collector consisted of SES electrode which may be connected to a negative voltage supply of 150 volts through on/off switch. To study the effect of different parameters on escape of secondary electrons, we define escape factor F_s as relative change in ion current with SES voltage on and off. This provides a relative measure of number of secondary electrons escaping under different conditions.

Ten repeated measurements of F_s were carried out on each collector using primary ion beam of $^{88}Sr^+$ and average value was calculated. The integration time of the ion current amplifier during these measurements was 10 s and sufficiently long settling time (30 s) was given for amplifier to stabilize while switching from 'ON' to 'OFF' and vice versa. The data on F_s was collected for primary ion energy in the range of 4-6 keV. The measurements were also repeated with another set of three collectors and results obtained were similar in both cases.

To study effect of magnetic field, an electromagnet was placed across the collectors to generate a magnetic field in the range up to 200 gauss. Data on F_s was collected under different magnetic fields in 0-200 gauss range.

Effect of improvement in Faraday cup design, was investigated by measurement of ^{87}Sr /^{86}Sr ratio of Strontium standard (SRM 987) in dynamic mode of operation [1]. A set of three collectors with graphite coated surfaces and end surface inclined at 45° were used with magnetic field of 100 gauss applied using a pair of rare earth permanent magnets. A triple filament assembly was used on which 3 μg strontium (SRM 987) was loaded on side filaments. The isotopic ratio data for ^{87}Sr /^{86}Sr was collected in a set of 100 measurements and the average value with relative standard error (precision) was calculated. The average values for ten such sets (taken over a period of around 10 days) are presented in table 6.2 with relative standard error. For comparison, measurements on a set of conventional collectors were also carried out similarly, and results are shown in Table 6.2.

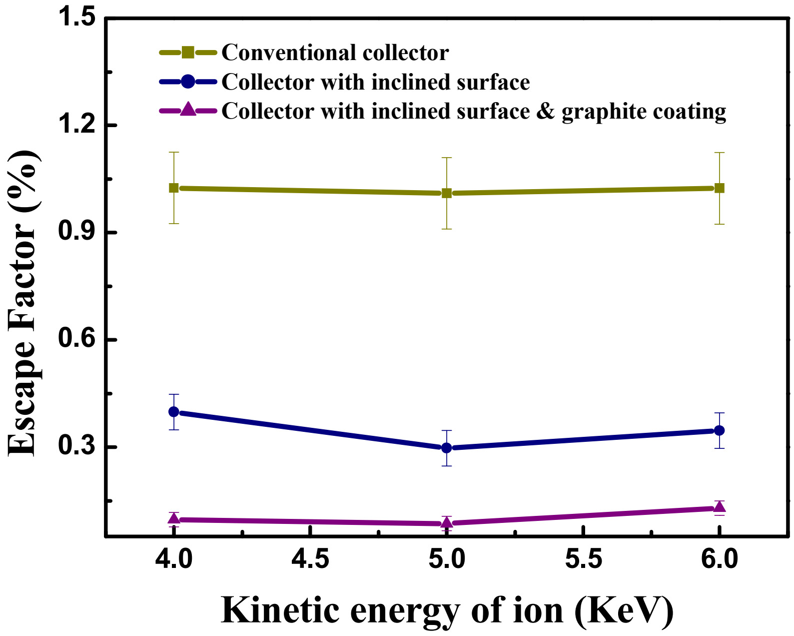

Fig. 6.8: Variation of escape factor of secondary electrons with variation in primary ion energy for different collectors.

6.3 Results and discussion

The plot of F_s for primary ions with different energies (acceleration potential) for various collectors is shown in Fig. 6.8. The value of F_s reduces from ~1% on FC-1 to 0.3% - 0.4% on FC-2. The reduction in secondary emission is attributed to the inclined surface of FC-2. To rule out any effect due to differences in surface conditions of the collectors, the results were confirmed using a different set of collectors. Improvement by factor of 3 on using inclined surface is much higher than factor of 1.43 expected theoretically. This is not fully understood and could be due to difference in secondary electrons emitted in forward and reverse directions with respect to incident ion direction. We may add that angular dependence of secondary electrons (with ions incident at an angle) and difference in secondary emission in forward and reverse directions has not been reported in literature. A further reduction of F_s (to ~ 0.1%) is observed on FC-3 due to reduced secondary emission from graphite. This is in agreement with reported secondary yield of graphite with respect to stainless steel surface to be ~ 0.5 [104 -

106]. It may also be noted that F_s is independent of energy of primary ions in the range of 3- 6 kV (typical range of accelerating potential in magnetic sector mass spectrometers). Effect of magnetic field on suppression of secondary electron contribution by measurement of F_s is presented in Fig. 6.9 for three collectors. The results show that a field of 50 gauss is sufficient to fully suppress secondary electron contribution.

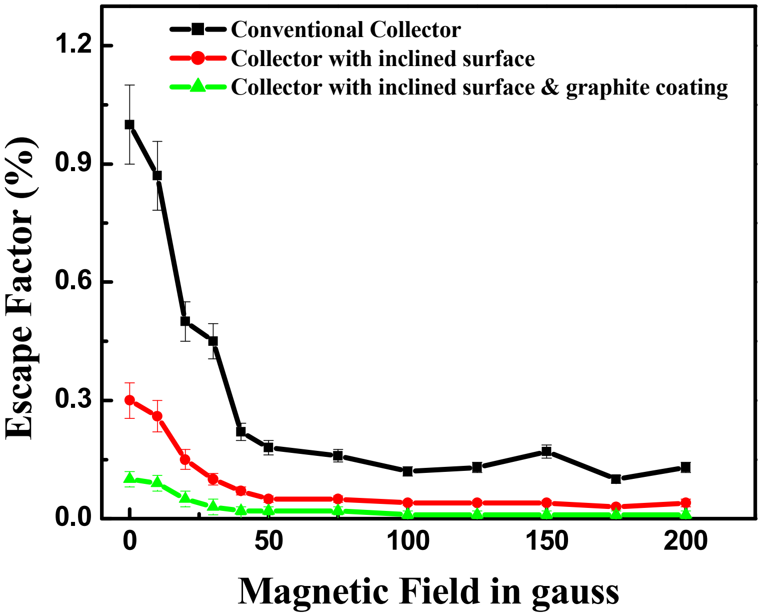

Fig. 6.9: Effect of magnetic field on the escape factor of secondary electrons for different collectors.

Isotopic ratio data for ^{87}Sr / ^{86}Sr measured on improved collectors with magnetic suppression and conventional collectors with electric SES is given in Table 6.2. It shows a precision of ~5 ppm for each data set as compared to a precision of 9 ppm for conventional collectors. This clearly shows improved performance of new Faraday collector system.

A reason of concern for using graphite coating is that the carbon can get sputtered due to the impact of energetic primary ions which can cause the erosion of the coating resulting in deterioration of the performance of collector [25]. To address this concern, we have calculated

Table 6.2: Data on the isotopic ratio ($^{87}Sr/^{86}Sr$) measurement for standard strontium sample SRM-987; average $^{87}Sr/^{86}Sr$ ratio with relative standard error (internal precision; in parenthesis)$^{\#}$ has been given for each run

S.No.	**$^{87}Sr/^{86}Sr$ $^{\#}$ (with modified collectors)**	**$^{87}Sr/^{86}Sr$ $^{\#}$ (with conventional collectors)**
1.	0.710243 (4)	0.710229 (6)
2.	0.710233 (4)	0.710221 (5)
3.	0.710237 (3)	0.710230 (6)
4.	0.710234 (4)	0.710237 (7)
5.	0.710237 (4)	0.710245 (7)
6.	0.710243 (5)	0.710231 (7)
7.	0.710227 (4)	0.710238 (7)
8.	0.710231 (4)	0.710231 (7)
9.	0.710246 (3)	0.710240 (6)
10.	0.710230 (4)	0.710228 (7)

($^{\#}$ the value in parenthesis is the variation in the last significant digit of the data)

the time taken for complete erosion of the graphite coating. For a coating thickness of 10 μm and for the primary ion beam cross section of 1 mm x 10 mm, the number of carbon atoms present in the interaction volume of ions with graphite is around 4.5×10^{18} atoms. For a primary ion current in the range of 10^{-10} A (typical ion current in a magnetic sector MS for isotopic ratio measurement), the rate of impact of ions is $\sim 10^{9}$ ions/s. With a reasonable assumption of sputtering yield to be one, an erosion rate of graphite is 10^{9} atoms/s. This leads to a time scale of 10^9 seconds (~30 years with continuous operation) for the complete removal of the graphite material. It can be clearly inferred that the life of collector coated with graphite is sufficient.

6.4 Conclusion

A new Faraday collector system for thermal ionization mass spectrometers has been developed with a simpler and sturdier design. It is seen that secondary electron contribution is reduced by factor of 3 if collector with 45% inclination is used and a further factor of ~3 reduction is observed on coating stainless steel surface with graphite. It is also seen that magnetic field of nearly 50 gauss may be used in place of electric field based secondary electron suppressor resulting in better mechanical design and consistent collection efficiency. The new collector system enabled improvement in the internal precision of $^{87}Sr/^{86}Sr$ ratio measurement in comparison to conventional collectors.

Chapter-7

Summary

The magnetic sector mass spectrometry is highly important tool to investigate various analytes useful to nuclear field among other fields. Owing to its importance for the nuclear programme of DAE and to become self reliant in this technology, the development of magnetic sector based mass spectrometers was taken up in BARC. The mass spectrometer is mainly characterized by sensitivity and precision. In the field of nuclear technology the requirement of high sensitivity becomes more important because of possible radiation hazard from the nuclear materials. The precision of isotopic ratio is important to control the various processes in different stages of nuclear technology. In thermal ionization mass spectrometers (TIMS) developed in Technical Physics Division, various areas were identified where scope of improvement was seen in terms of sensitivity and precision.

The work reported in the thesis is based on studies for improvement and further development of TIMS. The studies have been carried out on ion source, analyzer and collector system, to improve the overall performance of system in terms of sensitivity and precision. The ion source is one of the main sub-systems of any mass spectrometer which converts neutral analyte molecules into ions. The sensitivity of the TIMS is dependent on the ionization efficiency of ion source and its transmission that in turn depends on filament assembly and the electrostatic lens. The study incorporated computer simulations followed by the experimental validation of the modified design. The study on electrostatic lens resulted into a modified lens with higher transmission (by a factor of ~2) than the conventional design. It also exhibited better electrical insulation than the conventional design which enabled application of higher accelerating potential on ion source thereby further increasing the transmission. The higher accelerating potential also helps in reducing the relative energy spread of the ions thereby improving the focusing of ion on collector and hence helps in getting better precision for the measurement of isotopic ratios. The new filament assembly with ceramic base ensures stable signal for long durations thereby improving the precision. The combined effect of modified filament assembly and the electrostatic lens has resulted into an ion source which requires only ~2 μg of uranium sample for the isotopic ratio analysis compared to 5 μg in case of conventional ion source.

The inclined focal plane of a conventional magnetic analyzer results in complicated mechanical assembly of the collector system. It also makes the collector system very bulky and unwieldy particularly in case of large number of collectors. Improved analyzer has been made by rotating the plane along a line normal to the principal beam axis by using curved shims on the entry and exit boundaries of the magnetic sector analyzer. The study incorporated optimizing the radius of curvature of shims using computer simulation and theoretical calculations. Subsequently, experimental study was carried out to optimize the radius of curvature of the shims. Optimum radii of curvature of 130 mm for exit side and 100 mm for entry side of the magnetic sector analyzer were found. This facilitated compactness of collector chamber and easy location of the collectors resulting in design of TIMS with seven collectors required for geochronological applications.

The placement of the collectors which are movable along the focal plane using rotary motion feed through in the conventional collector system also increases complexity of the system leading to mechanical errors in the placement of collectors and limiting the performance of TIMS in terms of precision and accuracy. A variable dispersion zoom optics was developed that resulted in a collector system consisting of fixed collectors with wider entry apertures due to the higher dispersion produced by the design of the system. The system also permitted adjustment in the dispersion of ion beams making it versatile for the analysis of elements covering wider mass range as compared with the conventional system. The performance of this system was compared with the conventional system, designed &

developed at BARC, using isotopic ratio measurement of Sr standard (SRM 987) and an improvement in the external precision and accuracy to better than 10 ppm was observed from more than 20 ppm with conventional system. A precision < 10 ppm is desirable for analysis of samples (Sr, Nd etc.) pertaining to geochronology work and the newly developed collector system with variable dispersion zoom optics will be highly useful for the analysis of these samples.

In conventional Faraday collectors employed in TIMS, a secondary electron suppressor (SES) is used to suppress the secondary electrons generated from the surface of main collector due to the impact of primary ions. Mechanical errors in placing SES are source of non uniformity of the collection efficiency and increased complexity in the mechanical assembly of the collectors. An alternate approach of secondary electron suppression using magnetic field was investigated by computer simulation followed by experimental studies. The studies also included (a) the reduction of secondary emission from the collector surface by employing graphite coated surfaces instead of bare stainless steel surface and (b) inclination of the collector end surface to reduce effect of secondary emission. It was seen that graphite coating along with the inclined collector reduces the escape of secondary electrons by a factor of 10 and a magnetic field ~ 50 gauss effectively suppresses the secondary electrons and hence can be considered a fair alternate to electrical suppression. The studies resulted in a collector exhibiting reduced secondary emission of 0.1% as compared to ~1 % and improvement in internal precision to ~ 5 ppm from ~ 9 ppm.

As discussed above, the studies have resulted in significant improvement of TIMS characteristics. However, there is scope for further improvements that may form part of further studies. The source slit employed in the ion source of TIMS plays a vital role in determining the transmission of the ions. The width of source slit is ascertained on the basis of obtaining ion beam width (at collector) to be smaller than the collector aperture to ensure flat top peak of magnetic scan across the collector. A smaller source slit width leads to peak with larger flat region but at the cost of transmission of the ion source and hence the sensitivity of TIMS. Therefore, the source slit width was optimized to 0.3 mm in conventional TIMS and the same has been employed even after implementation of modified collector system with variable dispersion zoom optics (VDZO). Since the VDZO enables the use of Faraday collectors with wider apertures of 3 mm (instead of 1 mm), it generates further scopes of increasing the source slit to higher value. In this regard, further studies can be undertaken for the optimization of source slit width of the ion source.

The VDZO also enables higher dispersion as compared with the conventional collector system. This can be exploited to develop a magnetic sector mass spectrometer with sector radius lower than that employed in the present mass spectrometers reducing cost and footprint of the mass spectrometer. The compact geometry will exhibit lower transmission losses that can lead to a higher sensitivity and may result in better vacuum. Studies can be undertaken to develop a compact magnetic sector mass spectrometer particularly for Uranium.

In the studies related to Faraday collectors, orientation of end surface was fixed to 45° to reduce the escape of secondary electrons from the collector. However the comparison between the theoretical calculations and the experimental data for 45° showed inconsistency. Investigation may be carried out to obtain the angular distribution of secondary electrons from the collector surface and optimize the orientation of the end surface. Further, coating the collector surface with graphite was found to reduce secondary electron emission. Other materials may be investigated to minimize secondary emission.

References

[1] I.T.Platzner "Modern isotope ratio mass spectrometry" John Wiley & Sons, 1997

[2] John Roboz "Introduction to mass spectrometry" John Wiley & Sons,1968

[3] Jurgen H. Gross "Mass spectrometry" Springer

[4] S.K.Aggarwal, H.C.Jain "Introduction to mass spectrometery" Indian Society for Mass spectrometry, 1997

[5] Douglas A. Skoog, Donal M. West, F.James Holler and Stanley R. Crouch "Fundamental of analytical chemistry" Brooks Cole, 2013

[6] Simon Maher, Fred P.M.Jjunju and Stephen Taylor, Reviews of Modern Physics, Vol. 87, Jan –March 2015

[7] J. Sabine Becker, J. Anal. At. Spectrom. 20 (2005) 1173 – 1184

[8] A. Benninghoven, F.G.Rudenauer and H.W.Werner, Secondary Ion Mass Spectrometry, Wiley, New York (1987)

[9] Laure F.Marvin, Matthew A.Roberts, Laurent B.Fay, Clinica Chimica Acta 337 (2003) 11-21

[10] Shibdas Banerjee and Shyamalava Mazumdar, International Journal of Analytical Chemistry, Vol. 2012, Artical ID 282574

[11] Andries P. Bruins, Journal of Chromatography A, 794 (1998) 345-357

[12] Peter H. Dawson, "Quadrupole Mass Spectrometer and its application" Elsevier Scientific Publishing Company, Amsterdam (Netherland), 1976

[13] Robert J.Cotter, Analytical Chemistry News & Features, July 1, 1999, 445 -451

[14] Raymond E.March, Journal of Mass Spectrometry, 32, 351-369

[15] V.V.K.Rama Rao et.al., International Journal of Mass Spectrometry and Ion Physics, 52 (1983) 289 - 298

[16] F.L.Kind, J.Teng and R.E.Steiner, Journal of Mass Spectrometry, 30, 1061-1075 (1995)

[17] Christopher Geppert and Klaus D A Wendt, Journal of Physics, Indian Academy of Sciences, 75,6, Dec. 2010, 1057-1064

[18] Klaus Wendt and Norbert Trautmann, International Journal of Mass Spectrometry, 242 (2005) 161-168

[19] Harald A. Enge, "Deflecting Magnets", pp. 203-263, from Septier, A., The Focusing of Charged Particles, Academic Press, New York, 1967

[20] H.Hintenberger and L.A.König, Advances in Mass Spectrometry, Pergamon Press, New York, 1959, p. 16-35

[21] H.H.Tuithof and A.J.H.Boerboom, International Journal of Mass Spectrometry and Ion Physics, 20 (1976), 107-121

[22] Konig, L.A. and Hinterberger, H., Nuclear Instruments, 3, (1958), 133

[23] V.V.K. Rama Rao, International Journal of Mass Spectrometry, Vol. 145, Issue 1-2, 1995, p.45

[24] Patrick James Turner, Raymond Clive Haines, Kelsall, United States Patent, Patent no. 5903002

[25] Johannes Schwieters, United States Patent, Patent no. US 6452165 B1

[26] Michael E. Wieser, Johannes B. Schwieters, International Journal of Mass Spectrometry 242 (2005) 97–115

[27] G.W.Goodrich and W.C.Wiley, Review of Scientific Instruments 33, 761 (1962); doi: 10.1063/1.1717958

[28] Joseph Ladislas Wiza, Nuclear Instruments and Methods, 162 (1979) 587-601

[29] N.R.Daly, Review of Scientific Instruments, 31, 264 (1960); doi: 10.1063/1.1716953

[30] C.L. Harper, S.B. Jacobsen, Nature 360 (1992) 728.

[31] M. Sharma, D.A. Papanastassiou, G.J. Wasserburg, R.F. Dymek, Geochim. Cosmochim. Acta 60 (1996) 2037

[32] G. Caro, B. Bourdon, J.-L. Birck, S. Moorbath, Nature 423 (2003) 428

[33] G. Caro, B. Bourdon, J.-L. Birck, S. Moorbath, Geochim. Cosmochim Acta 68 (Suppl. 1) (2004) A746.

[34] E.Ravisankar et.al. Proceedings of 11th ISMAS-TRICON-2009, 419-421

[35] Arkadip Bhasak et.al., Proceeding of 28th ISMAS-WS 2014, 161-165

[36] Albert Septier, "Focusing of charged particles" Academic Press, Vol.1, 1967

[37] John Jacob Livingood, "The optics of dipole magnets" Academic Press, 1969

[38] R.K.Bhatia et.al., Prodeedings of *9th ISMAS Symposium 2003*

[39] K.G.Bhushan, "Introduction to Vacuum Technology" Indian Vacuum Society

[40] J.F.O'Hanlon, "A user's guide to Vacuum Technology", 2nd. Ed., Wiley, Ny, 1989

[41] A.Roth, "Vacuum Technology", North Holland, Amsterdam, 1976

[42] K.L. Ramakumar, P.S. Khodade, A.R. Parab, S.A. Chitambar, H.C. Jain, J. Radioanal. Nucl. Chem. 107 (1985) 215

[43] S.K.Aggarwal, A.I.Almaula, P.S.Khodade, A.R.Parab, R.K.Duggal, C.P.Singh, A.S.Rawat, G.Chourasiya, S.A.Chitambar and H.C.Jain, J. Radioanal.Nucl.Chem.-Letters, 87, (1984) , p.169-178.

[44] S.K.Aggarwal, D.Alamelu, International Journal of Mass Spectrometry, 241 (2005) 83 - 88

[45] D.Alamelu, A.R.Parab,K.SasiBhushan, Raju V.Shah, S.Jagdish Kumar, Radhika M.Rao, S.K.Aggarwal, R.K.Bhatia, V.K.Yadav, Madhavi P.Shrma, Puneet Tulsyan, Pradip Chavda, P.Sriniwasan, "Performance evaluation of indigenous Thermal Ionization Mass Spectrometer for determination of ^{235}U/^{238}U atom ratios" Report No. BARC/2014/E/004

[46] R.K.Bhatia, V.K.Yadav, M.M.Gulhane, Rabi Datta, K.D.Joshi, A.M.Kasbekar, Madhavei Sharma, Meera Murali, M.M.Vilas, E.Ravisankar, M.Gopalakrishna, T.K.Saha, V.Nataraju and S.K.Gupta, "" BARC Newsletter, Issue no. 332, May-June 2013, p. 19

[47] A.E.Fallick, International Journal of Mass spectrometry and Ion Physics, 46 (1983) 59-62

[48] V.A.Pavlenko et.al., International Journal of Mass Spectrometry and Ion Physics, 46(1983) 55-58

[49] F.G.Ruedenauer, Review of Scientific Instruments, Vol. 41, Oct 1970, p.1487

[50] Peter van Calsteren, et.al., Internataional Journal of Mass Spectrometry and Ion Processes, 146/147 (1995) 119-129

[51] A.Eberhardt, R.Deiwiche and J.Geiss, Z, Naturforsch., Teil A, 19A, 736 (1964)

[52] H.Kanno, Bull. Chemical Society of Japan., 44, 1808 (1971)

[53] K.Habfast, International Journal of Mass Spectrometry and Ion Physics, 51, 165 (1983)

[54] G.P.Russ, III and J.M.Bazan, Spectrochemica Acta, Bart B, 42, 49 (1987)

[55] Rajender K. Bhatia, Yogesh Kumar, K. Prathap Reddy, V. K. Yadav, E. Ravisankar, T. K. Saha, V. Nataraju, V.K. Handu, International Journal of Mass Spectrometry 313 (2012) 36– 40

[56] R. K. Bhatia, V. K. Yadav, V. M. Mahadeshwar, M. M. Gulhane, E. Ravisankar, T. K. Saha, V. Nataraju, S. K. Gupta, International Journal of Mass Spectrometry 339– 340 (2013) 39– 44

[57] S. N. Bindal, R.K.Bhatia, E.Ravisankar and V.K.Handu, Proceedings of 10th ISMAS Symposium-2006, 155 - 157

[58] F. Hintenberger, "Ion optic with electrostatic lenses" Proceedings of 2005 CAS, CERN 2006-012, 2006, p.27

[59] F. H. Read, J. Phy. E: Sci. Instrum., Vol. 2, 1969, 165-169

[60] A. Adams, F. H. Read, J. Phys. E: Sci. Instrum., 1972, 5, 150 - 155

[61] A. Adams, F. H. Read, J. Phys. E: Sci. Instrum., 1972, 5, 156 - 160

[62] J. N. H. Brunt, F. H. Read, J. Phys. E: Sci. Instrum., 1975, 8, 1015 - 1020

[63] G. Martinez, M. Sancho, J. Phys. E: Sci. Instrum., 1983, 16, 625 - 630

[64] O. Sise, M. Ulu, M. Dogan, Nuc. Instrum. and Methods in Physics Research A, 554 (2005) 114 – 131

[65] Omer Sise, Melike Ulu, Mevlut Dogan, Nuc. Instrum. and Methods in Physics Research A 573 (2007) 329 - 339

[66] D. A. Dahl, "SIMION version 7.0", Idaho National Engineering Laboratory, 2000

[67] R.K.Bhatia, R.Datta, R. Chandak, M.M.Gulhane, P.R.Kasina, A.M.Kasbekar, N.Ved, V.k.Yadav, M.Gopalakrishna, E.Ravisankar, R.K.Saha, V.Nataraju and V.K.Handu, 11th ISMAS-TRICON-2009, 493-495

[68] John S. Cottrell, Patrick J. Turner, J. David K., United State Patent no. 4524275

[69] Konig, L.A. and Hinterberger, H., Nuclear Instruments, 3, (1958), 133

[70] H.Hintenberger, L.A.Konig, Z. Naturforsch, 11a, (1956), 1039

[71] L.A.Konig, H.Hintenberger, Z. Naturforsch, 12a, (1957), 377

[72] I.Chavet, Nuclear Instruments and Methods 99(1972), 115-119

[73] S.I.Warshaw, Nucl. Instr. And Meth.72, (1969), 5

[74] P.Bounin, Rev. Sci. Instr. 38, (1967), 1305

[75] H.Liebl, Optik 16, (1959), 19

[76] H.Wollnik, Nucl. Instr. And Meth. 53, (1967), 197

[77] Herald A. Enge, The Review of Scientific Instruments, 35, (1964), 278-288

[78] H. Wollnik, H. Ewald, Nucl. Instr. And Meth. 36, (1965) ,93

[79] Mario Ishihara, United states patent, Patent no. 4998015

[80] Mario Ishihara, United states patent, Patent no. 5118939

[81] Freedman, Philip, Antony, European patent no. EP 0857353B1

[82] Matthew A. Coble et al., Chemical Geology 290 (2011) 75-87

[83] Xiaoping Xia, J. Anal. At. Spectrom. 26 (2011) 1868

[84] J.M. Saxton, International Journal of Mass Spectrometry and Ion Processes 154 (1996) 99-131

[85] N.S. Belshaw et al., International Journal of Mass Spectrometry 181 (1998) 51–58

[86] Simon Turner et al, J. Anal. At. Spectrom. 16 (2001) 612-615

[87] R.M. Rao, A.R. Parab, K. Sasibhushan, S.K. Aggarwal, International Journal of Mass Spectrometry 273 (2008) 105–110

[88] A.J. Spivack, J.M. Edmond, Anal. Chem. 58 (1986) 31

[89] R.K. Bhatia, V.K. Yadav, V.M. Mahadeshwar, M.M. Gulhane, E. Ravisankar, T.K. Saha, V. Nataraju, S.K. Gupta, International Journal of Mass Spectrometry 339– 340 (2013) 39– 44

[90] C.E.Kuyatt, Methods of experimental Physics 7a (1968) 1-43

[91] Paul Marmet and Larkin Kerwin, Canadian Journal of Physics 38 (1960) 787-796

[92] Tokoro, Nobuhiro, Japanese Patent, Patent no. JP63249079

[93] G. Stupakov and M. Pivi, Linear Collider Collaboration Tech Notes, LCC-0145, SLAC-TN-04-045, June 2004

[94] Ing Hwie Tan, Mario Ueda, Renato S. Dallaqua, and Jose O. Rossi, Applied Physics Letters 86, 023509 (2005)

[95] Mohammad Reza Babapour, GhadikolaeeEbad Talebi Ghadikolaee, J Fusion Energ 31 (2012) 569–572

[96] Kashefian Naieni, F. Bahrami, N. Yasrebi, B. Rashidian, Vacuum 83 (2009) 1095–1099

[97] J.J. Scholtz, D. Dijkkamp and R.W.A. Schmitz, Philips J. Res. 50 (1996) 375-389

[98] Jacques Cazaux, Journal of Applied Physics 85 (1999) 1137

[99] Kenneth L. Busch, Spectroscopy 26(11) 2011, 12-18

[100] V. Baglin, J. Bojko1, O. Gröbner, B. Henrist, N. Hilleret, C. Scheuerlein, M. Taborelli, Proceedings of EPAC 2000, Vienna, Austria

[101] T. Iyasu and R. Shimizu, Journal of Surface Analysis, 13 (2) (2006) 200 - 205

[102] E. R. Cawthron, Australian Journal of Physics 24 (1971) 859-69

[103] A. Shih , J. Yater, C. Hor, R. Abrams, Applied Surface Science 111 (1997) 251-258

[104] S.*Y.*Lai, D.Briggs, A.Brown and J.C.Vickerman, Surface and Interface Analysis, Vol. 8, 93-111 (1986)

[105] S. G. Walton, J. C. Tucek and R. L. Champion, Journal of Applied Physics, Vol . 85 (3), 1832-1837 (1999)

[106] R.E.Kirby and F.K.Kind, SLAC-PUB-8212, October,2000